July 1984
oulder, Colorado

U.S. DEPARTMENT OF COMMERCE
NOAA/ERL Wave Propagation Laboratory

AN EVALUATION OF WIND MEASUREMENTS BY FOUR DOPPLER SODARS

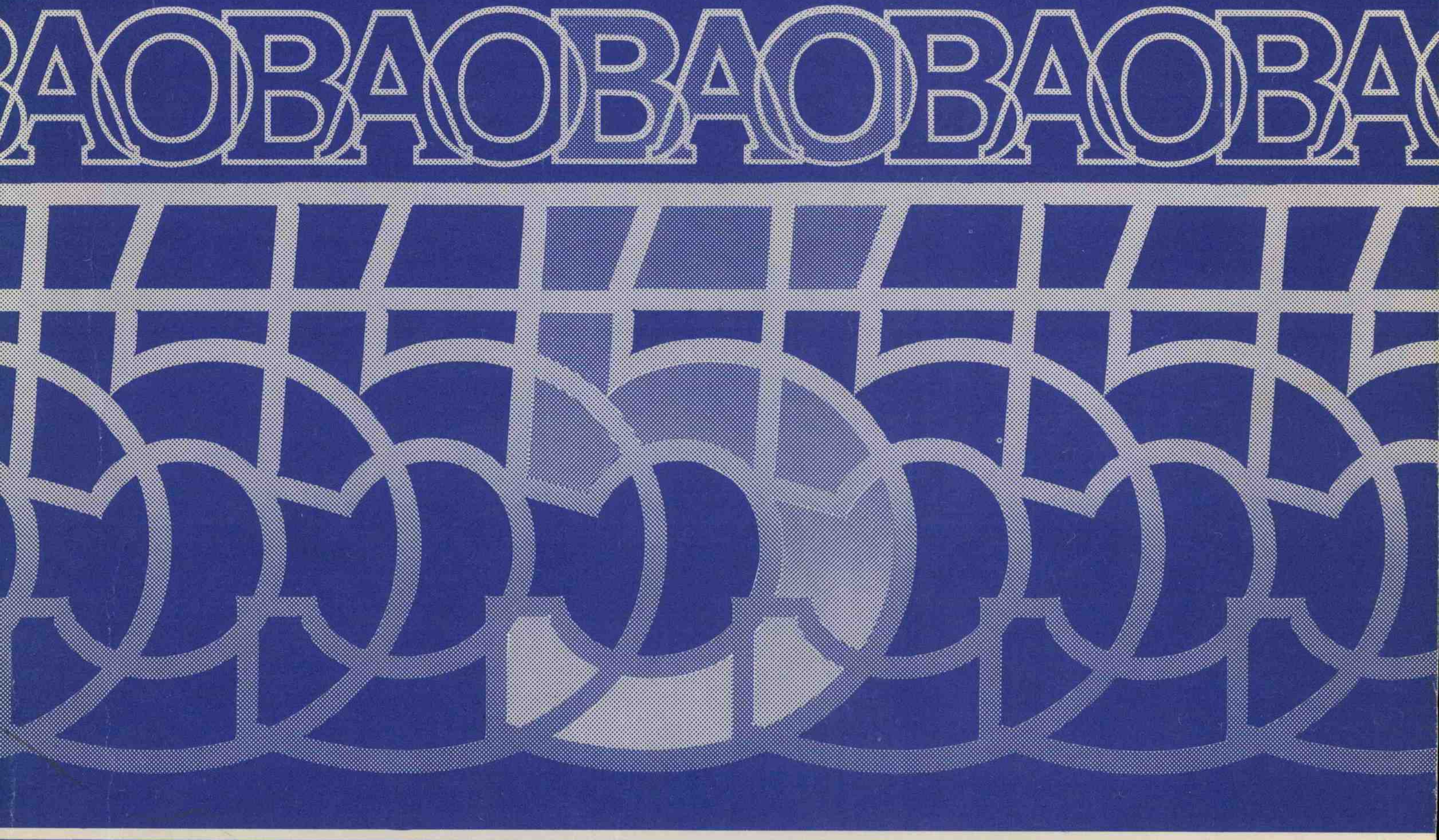

AN EVALUATION OF WIND MEASUREMENTS BY FOUR DOPPLER SODARS

J. C. Kaimal
J. E. Gaynor
P. L. Finkelstein
M. E. Graves
T. J. Lockhart

Report Number Five
July 1984

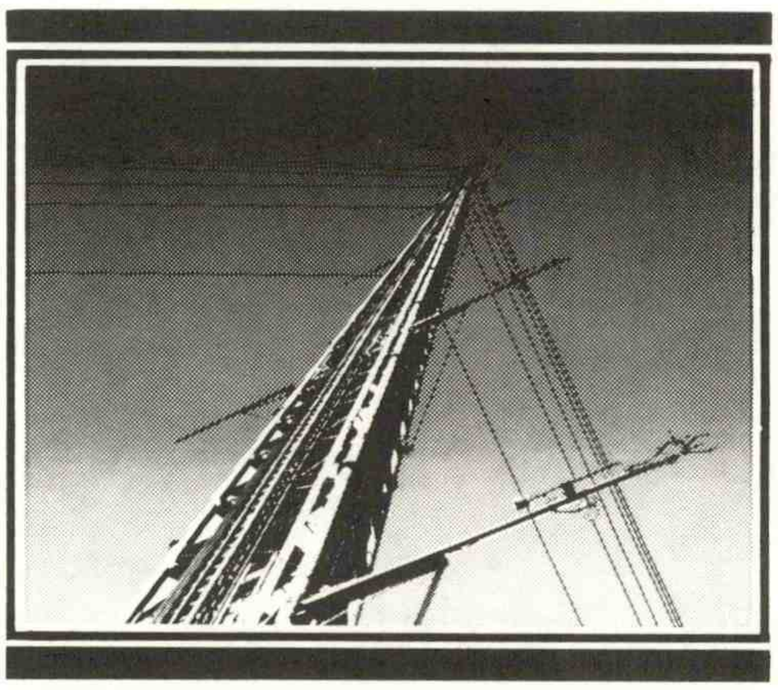

NOAA
Boulder Atmospheric Observatory

U.S. Department of Commerce
National Oceanic and Atmospheric Administration
Environmental Research Laboratories

A NOAA publication available from NOAA/ERL, Boulder, CO 80303.

AN EVALUATION OF WIND MEASUREMENTS BY FOUR DOPPLER SODARS

by

J. C. Kaimal and J. E. Gaynor
NOAA/ERL/Wave Propagation Laboratory
Boulder, Colorado 80303

P. L. Finkelstein*
Environmental Protection Agency
Research Triangle Park, North Carolina 27711

M. E. Graves
Northrop Services, Inc.
Research Triangle Park, North Carolina 27709

T. J. Lockhart**
Meteorology Research, Inc.
Altadena, California 91001

This study was conducted for
U.S. Environmental Protection Agency
under Interagency Agreement No. DW1-3F2A059

Wave Propagation Laboratory
Environmental Research Laboratory
U.S. Department of Commerce
Boulder, Colorado 80303

---

* On assignment from National Oceanic and Atmospheric Administration

** Present Affiliation: Meteorological Standards Institute
Fox Island, Washington 98333

NOTICE

Acquisition of the information provided in this document was funded in part by the United States Environmental Protection Agency under Interagency Agreement No. DW1-3F2A059. This study was conducted jointly by NOAA/ Environmental Research Laboratory and the Environmental Protection Agency.

CONTENTS

Abstract vii
Figures viii
Tables xii
Acknowledgments xiii

1. Introduction 1
2. Description of Instrumentation 3
3. Description of Field Program 9
4. Measurement of the Standard Deviation of w 17
5. Measurement of Wind Speed 47
6. Measurement of Wind Direction 65
7. Sodar Rawinsonde Comparisons 81
8. Characteristics of Sodar w Spectra 87
9. Concluding Remarks 97

References 99
Appendix 101

ABSTRACT

Measurements of wind speed, wind direction, and the vertical component of turbulence, from four different commercially available Doppler sodars, are compared with similar measurements from in situ sensors on a 300 m instrumented tower. Results indicate that the four sodars measure wind speed and direction accurately and with reasonably high precision. The sodars tended to overestimate the vertical component of turbulence at night and to underestimate it during the day. Precision in those measurements was considerably poorer than for the averaged speeds and directions. Analysis of the vertical wind from the sodars indicates that the measurement inaccuracies arise from a combination of aliasing and spatial averaging.

FIGURES

Number		Page
1	Plot plan showing sodar antenna deployment in the BAO test area....	10
2	Contour map of the immediate BAO terrain showing location of the tower and the sodar test area.....	11
3	(a) View of the sodar test area looking north from County Road 8...	12
	(b) Instrumentation on the BAO 300 m tower.....	13
4	Comparison of 100 m σ_w values from the AV sodar and the BAO sensor.....	26
5	Comparison of 100 m σ_w values from the RAD sodar and the BAO sensor.....	27
6	Comparison of 100 m σ_w values from the REM sodar and the BAO sensor.....	28
7	Comparison of 100 m σ_w values from the XON sodar and the BAO sensor.....	29
8	Comparison of 200 m σ_w values from the AV sodar and the BAO sensor.....	30
9	Comparison of 200 m σ_w values from the RAD sodar and the BAO sensor.....	31
10	Comparison of 200 m σ_w values from the REM sodar and the BAO sensor.....	32
11	Comparison of 200 m σ_w values from the XON sodar and the BAO sensor.....	33
12	Comparison of 300 m σ_w values from the AV sodar and the BAO sensor.....	34
13	Comparison of 300 m σ_w values from the RAD sodar and the BAO sensor.....	35
14	Comparison of 300 m σ_w values from the REM sodar and the BAO sensor.....	36
15	Comparison of 300 m σ_w values from the XON sodar and the BAO sensor.....	37

16 Comparison of 100 σ_w values from RAD (mode: BI) sodar and the BAO sensor..... 38

17 Comparison of 200 m σ_w values from RAD (mode: BI) sodar and the BAO sensor..... 39

18 Comparison of 300 m σ_w values from RAD (mode: BI) sodar and the BAO sensor..... 40

19 Comparison of 100 m σ_w values from RAD (mode: MONO) sodar and the BAO sensor..... 41

20 Comparison of 200 m σ_w values from RAD (mode: MONO) sodar and the BAO sensor..... 42

21 Comparison of 300 m σ_w values from RAD (mode: MONO) sodar and the BAO sensor..... 43

22 Comparison of 100 m σ_w values from RAD (mode: MULTI) sodar and the BAO sensor..... 44

23 Comparison of 200 m σ_w values from RAD (mode: MULTI) sodar and the BAO sensor..... 45

24 Comparison of 300 m σ_w values from RAD (mode: MULTI) sodar and the BAO sensor..... 46

25 Comparison of 100 m wind speeds from AV sodar and BAO sensors..... 53

26 Comparison of 100 m wind speeds from RAD sodar and BAO sensors.... 54

27 Comparison of 100 m wind speeds from REM sodar and BAO sensors.... 55

28 Comparison of 100 m wind speeds from XON sodar and BAO sensors.... 56

29 Comparison of 200 m wind speeds from AV sodar and BAO sensors..... 57

30 Comparison of 200 m wind speeds from RAD sodar and BAO sensors.... 58

31 Comparison of 200 m wind speeds from REM sodar and BAO sensors.... 59

32 Comparison of 200 m wind speeds from XON sodar and BAO sensors.... 60

33 Comparison of 300 m wind speeds from AV sodar and BAO sensors..... 61

34 Comparison of 300 m wind speeds from RAD sodar and BAO sensors.... 62

35 Comparison of 300 m wind speeds from REM sodar and BAO sensors.... 63

36 Comparison of 300 m wind speeds from XON sodar and BAO sensors.... 64

37 Comparison of 100 m wind directions from AV sodar and BAO sensors..... 69

38 Comparison of 100 m wind directions from RAD sodar and BAO sensors..... 70

39 Comparison of 100 m wind directions from REM sodar and BAO sensors..... 71

40 Comparison of 100 m wind directions from XON sodar and BAO sensors..... 72

41 Comparison of 200 m wind directions from AV sodar and BAO sensors..... 73

42 Comparison of 200 m wind directions from RAD sodar and BAO sensors..... 74

43 Comparison of 200 m wind directions from REM sodar and BAO sensors..... 75

44 Comparison of 200 m wind directions from XON sodar and BAO sensors..... 76

45 Comparison of 300 m wind directions from AV sodar and BAO sensors..... 77

46 Comparison of 300 m wind directions from RAD sodar and BAO sensors..... 78

47 Comparison of 300 m wind directions from REM sodar and BAO sensors..... 79

48 Comparison of 300 m wind directions from XON sodar and BAO sensors..... 80

49 Comparison of wind speeds and wind directions from rawinsonde and sodar measurements..... 83

50 Wind speed and wind direction profiles from sodar (AV), rawinsonde, and tower measurements in a stable boundary layer.... 84

51 Wind speed and wind direction profiles from sodar (AV), rawinsonde, and tower measurements in a convective boundary layer..... 85

52 (a) Schematic representation of distortions introduced in the w spectrum from attenuation due to spatial averaging and from aliasing.
(b) Shift in spectral behavior with height and its implications for sampling and aliasing errors..... 89

53 Sodar and sonic anemometer w spectra at (a) 150 m and (b) 200 m compared for morning conditions..... 91

54 Sodar and sonic anemometer w spectra at 300 m compared for (a) morning and (b) nighttime conditions..... 92

55 Time series of w corresponding to spectral forms shown in Fig. 54(b) in the frequency range 0<n<0.02 Hz..... 95

TABLES

Number		Page
1	Sodar σ_w compared with sonic σ_w	19
2	Separation of Table 1 into daytime and nighttime categories	20
3	Regression analysis for σ_w	22
4	Radian modal σ_w compared with sonic σ_w	25
5	Sodar wind speed compared with reference wind speed	50
6	Regression analysis for wind speed	51
7	Radian modes: Accuracies and precision for wind speed	52
8	Sodar wind direction compared with sonic wind direction	67
9	Test of day versus night wind direction bias	68
10	Regression analysis for wind direction	68
11	Sodar wind speeds and directions for all heights compared with rawinsonde speeds and directions	82
12	Variances of w measured by the sodar and the sonic anemometers for the cases illustrated in Figs. 53 and 54	93
13	Fraction of total variance sensed by the sodar and the sonic anemometers over bandwidth $0<n<0.02$ Hz	93

ACKNOWLEDGMENTS

The authors acknowledge the valuable contributions made by David McSorley, Janet Lockhart, Joan Hart, Jim Newman, Daniel Wolfe, Norbert Szczepcynski, Leslie Mosley, and Mary Sue Phillips to the field experiment and to the analysis of the data. They are also grateful for the spirit of cooperation and dedication shown by the vendors and their representatives throughout the experiment. The experiment and the data analysis were sponsored by the U.S. Environmental Protection Agency under Interagency Agreement No. DW1-3F2A059.

1. INTRODUCTION

During the first three weeks of September 1982, an experiment was conducted at the Boulder Atmospheric Observatory (BAO), under the sponsorship of the Environmental Protection Agency (EPA), to assess the ability of in situ and remote sensors to measure the mean and turbulent properties of the lower atmosphere. The experiment was conducted in response to the need for comparative data from which scientists could evaluate the accuracy, precision, and general performance of some of the more commonly used meteorological instruments that measure atmospheric turbulence.

Recent advances in modeling transport and diffusion of pollutants, achieved largely through theoretical insights gained from field experiments, point to the site-specific nature of turbulence. Attention is therefore being directed to better on-site characterization of turbulence and to the development of techniques for measuring the mean and turbulent wind variables needed for input into the models. This experiment was designed to provide information needed to formulate a monitoring strategy for developing site-specific dispersion meteorology.

The Boulder Atmospheric Observatory (BAO) was chosen as the site for the experiment because of the availability of precise profile and turbulence data from sensors on a 300 m tower. Facilities for launching rawinsondes and for processing the data received from them were added benefits. Two categories of sensors were tested against measurements on the tower. One category consisted

of a set of lightweight in situ sensors selected for this study. The other category consisted of four commercially available Doppler sodars with the capability to measure variances in the vertical wind component in addition to the mean three-dimensional wind field. This report deals only with the sodar comparisons. The in situ sensor comparisons will be described in a separate report. The question addressed here is whether the sodars can measure the mean and turbulent properties of the flow at heights that are above the reach of conventional 10 m meteorological towers.

2. DESCRIPTION OF INSTRUMENTATION

Four Doppler sodar manufacturers who currently market their products in the United States were invited by EPA to participate in the experiment. Under arrangements made through EPA's principal contractor, Meteorology Research, Inc., the sodars were installed and operated by personnel from the participating firms. The four systems differ significantly in their physical configuration and approach to signal processing. Two of the systems used monostatic three-axis arrays, one used a bistatic array, and the other a colocated monostatic/bistatic array.

2.1 AeroVironment Three-Axis Monostatic System (AV)

The system consisted of three acoustic transceivers mounted on a trailer. Doppler shifts in the backscattered signals received on each axis were interpreted as wind components in the radial directions. Wind components thus measured were transformed into components along the N-S, E-W, and vertical directions. Since, in this configuration, sampling volumes are separated by large distances the assumption of horizontal homogeneity in the mean wind field is essential to justify using wind components measured along the different axes for the coordinate transformation.

The AeroVironment system transmitted a sound pulse (150-200 watts) at a frequency of 1500 Hz (duration 0.18 s) sequentially from each of three adja-

cent pencil-beam antennas. One tilts south 30° from the vertical to be sensitive to the N-S component, one tilts west 30° from vertical to be sensitive to the E-W component, and one points straight up to be sensitive to the vertical component. The receiver echo is heterodyned and then passed through an electronic comb filter with 31 teeth to yield the full spectral distribution in the return signal. For each 33.3 m altitude range gate, the spectrum is examined according to several criteria to obtain a best estimate of Doppler shift along with an estimated reliability factor. The pulse repetition interval was 8 s.

2.2 Remtech Three-Axis Monostatic System (REM)

The Remtech system (developed originally at Bertin et Cie) also uses a trailer-mounted array of three transceivers. They are operated in sequence as monostatic systems; the same assumption of horizontal homogeneity is invoked for wind measurements. In this system the horizontal wind-sensing antennas are tilted 18° from the vertical; the transmitted pulse is a 1600 Hz signal of 0.08 s duration. The received signals are digitized after appropriate band-pass filtering, and the Doppler frequency shift extracted by using Fast Fourier Transform (FFT) techniques. The pulse repetition interval was 5 s.

2.3 Radian Corporation Colocated Monostatic/Bistatic System (RAD)

Radian's antenna configuration permitted both monostatic and bistatic operation. Both systems shared the central, vertically pointing, pencil-beam transceiver. The two tilted (18° from vertical) monostatic transceivers were not located close to the vertical transceiver as on the AV and REM systems but aimed to intersect at a height of 150 m. In the bistatic mode, two fan-beam

transmitters (located 250 m to the south and to the west) illuminated the vertical beam of the central transceiver. The movement of the sound pulse up the vertical beam was followed by time gating of the receiver signal. Doppler frequency shifts in each gated segment are converted to wind velocity components to produce a wind profile. For details of this approach see Kaimal and Haugen (1977).

In both configurations, the vertical transceiver was operated in the monostatic mode to measure the vertical wind component. Since the three monostatic beams were not divergent, the assumption of homogeneity is not as critical here. The RAD system transmitted 120 watt pulses at 2.0 kHz (0.1 s duration) and computed Doppler shifts using the Complex Covariance method. RAD operated in three modes, monostatic, bistatic, and multistatic (alternating in time, one series of monostatic and one series of bistatic pulses). Pulse repetition interval for all systems was 5 s.

2.4 Xontech Three-Axis Bistatic System (XON)

This bistatic system consisted of a vertical pencil-beam transceiver and two fan-beam receivers aimed at a central vertical common volume. Therefore, the geometry in this system is exactly the reverse of the RAD bistatic system. The transmitted frequency was 2.0 kHz (0.08 and 0.16 s duration under computer control). Its bistatic baseline was 350 m long. The fan-beam antennas receive signals scattered from the vertical transceiver beam, so the winds are computed along a vertical column above the transceiver (Balser et al., 1976) as in the RAD bistatic system. A microcomputer determined the Doppler frequency shift with an FFT detection scheme powerful enough to sense small frequency variations in the presence of high ambient noise levels. The wind

data are, therefore, presented without qualifiers, but if the program cannot detect a consistent signal for the entire averaging period, no data are printed for that height range. The pulse repetition interval was 5 s.

2.5 BAO Instrumented Tower

The 300 m tower at BAO is instrumented at eight levels: 10, 22, 50, 100, 150, 200, 250, and 300 m. Sonic anemometers installed at each level measured the three-dimensional wind field. R.M. Young propeller-vane anemometers are mounted on the side of the tower opposite the sonic anemometers to serve as backup wind sensors when the tower is shadowing the sonic anemometers. For this experiment, the sonic anemometers were mounted on the booms pointing SSW, and the propeller-vane anemometers were on booms pointing NNE. These booms also supported sensors for measuring mean and fluctuating air temperatures and the dewpoint temperature. Data from the sonic anemometer and other fast-response sensors were sampled 10 times per second; the propeller-vane anemometer, like other slow-response sensors, was sampled only once per second.

Data from the BAO are recorded in one of two modes. In the "regular" mode, only the 10 s averaged data points and 10 s grab samples (last point in a 10 s data block) of the time series are retained. In the "raw data" mode all data points are recorded. In both modes the software computes and lists once every 20 min the means, variances, and fluxes for the preceding 20 min period. These listings became the common reference for comparing the performance of the different sodars. The raw data mode is employed only when the full time series is needed for special analyses or for the details in the structure of the flow. Such recordings were made for three relatively brief periods during this experiment for the purpose of comparing the spectral

responses of the sodars and examining the limitations imposed by sampling volumes and sampling rates.

2.6 Rawinsonde

The rawinsonde station located near the base of the tower was operated daily during this experiment to obtain wind data above 300 m. In addition to providing basic meteorological information, the data were needed to assess the range limitations of the monostatic sodars under different atmospheric conditions. Standard ground monitoring equipment and radiosonde packages of the type used by the National Weather Service were deployed. The procedure followed was to schedule a release at about sunrise and about midday, such that a release coincided with the observing period of a different sodar system each day. The purpose was to provide a near-equal distribution of radiosonde comparisons for each type. For two 4 h periods during the experiment, hourly ascents were made covering sunrise to late morning and late afternoon to sunset.

3. DESCRIPTION OF THE FIELD PROGRAM

The sodar measurements were centered over an area 0.5 × 0.3 km, about 0.65 km southwest of the BAO tower. The bistatic arrays were laid out to provide a height range of at least 300 m, hence the requirement for such a large test area. The deployment of the antennas for the four systems is shown in the plot plan of Fig. 1. The electronic equipment associated with the Doppler systems was housed in trailers located within the visitors' area. A larger trailer in the same area served as the control center for the experiment.

The terrain in the vicinity of the tower, including the area covered in Fig. 1, is reasonably flat. There is a gentle slope to the north, east, and west (see Fig. 2), but the steepest grade (7%) is toward the small hill south of the tower. Except for the trailers and the fence surrounding the visitors' area, the site is free of small-scale surface obstructions. The photographs in Figs. 3(a) and (b) show the characteristics of the test site. For a more detailed description of the site and its effect on flow over the area see Kaimal et al. (1982).

Procedures for data collecting and reporting were established to ensure against unfair bias for any of the participants. All systems were assumed capable of unattended continuous operation. All systems were to provide data in the form of wind speeds, wind directions, vertical wind components, and standard deviations of vertical wind averaged over 20 min periods coincident with the BAO averaging periods. The three comparison levels would be 100,

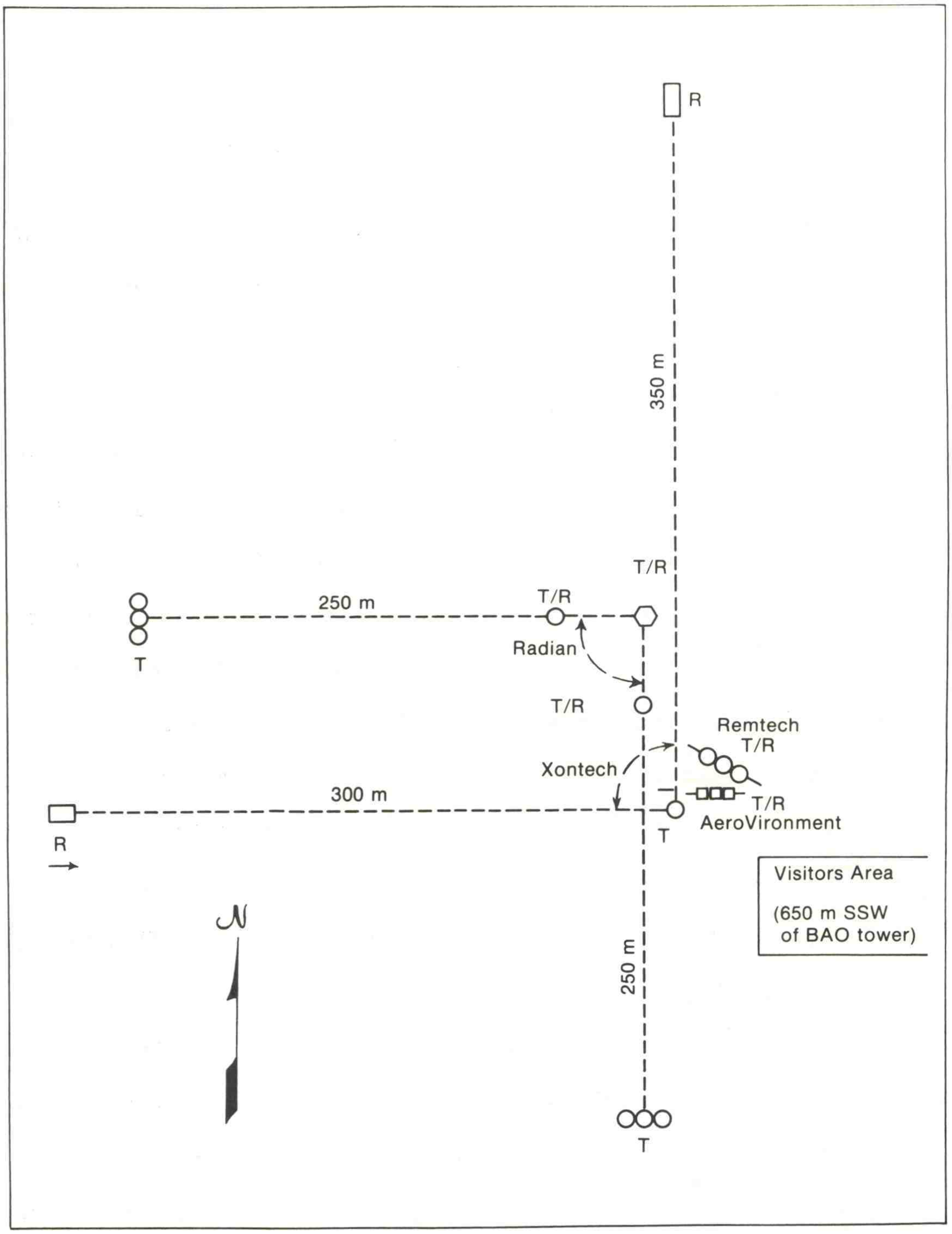

Figure 1. Plot plan showing sodar antenna deployment in the BAO test area.

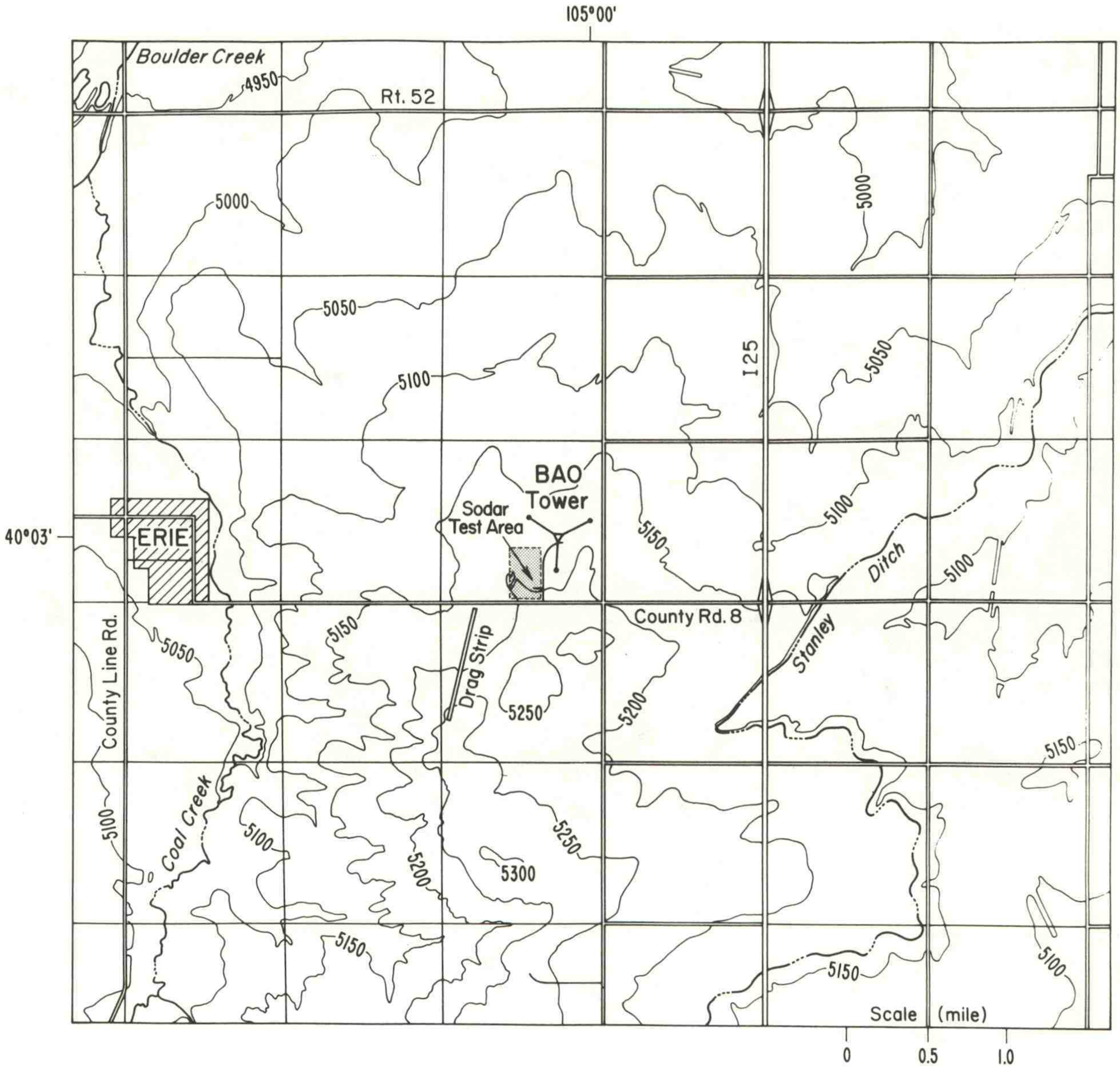

Figure 2. Contour map of the immediate BAO terrain showing location of the tower and the sodar test area.

Figure 3. (a) View of the sodar test area looking north from County Road 8.

(b) Instrumentation on the BAO 300 m tower.

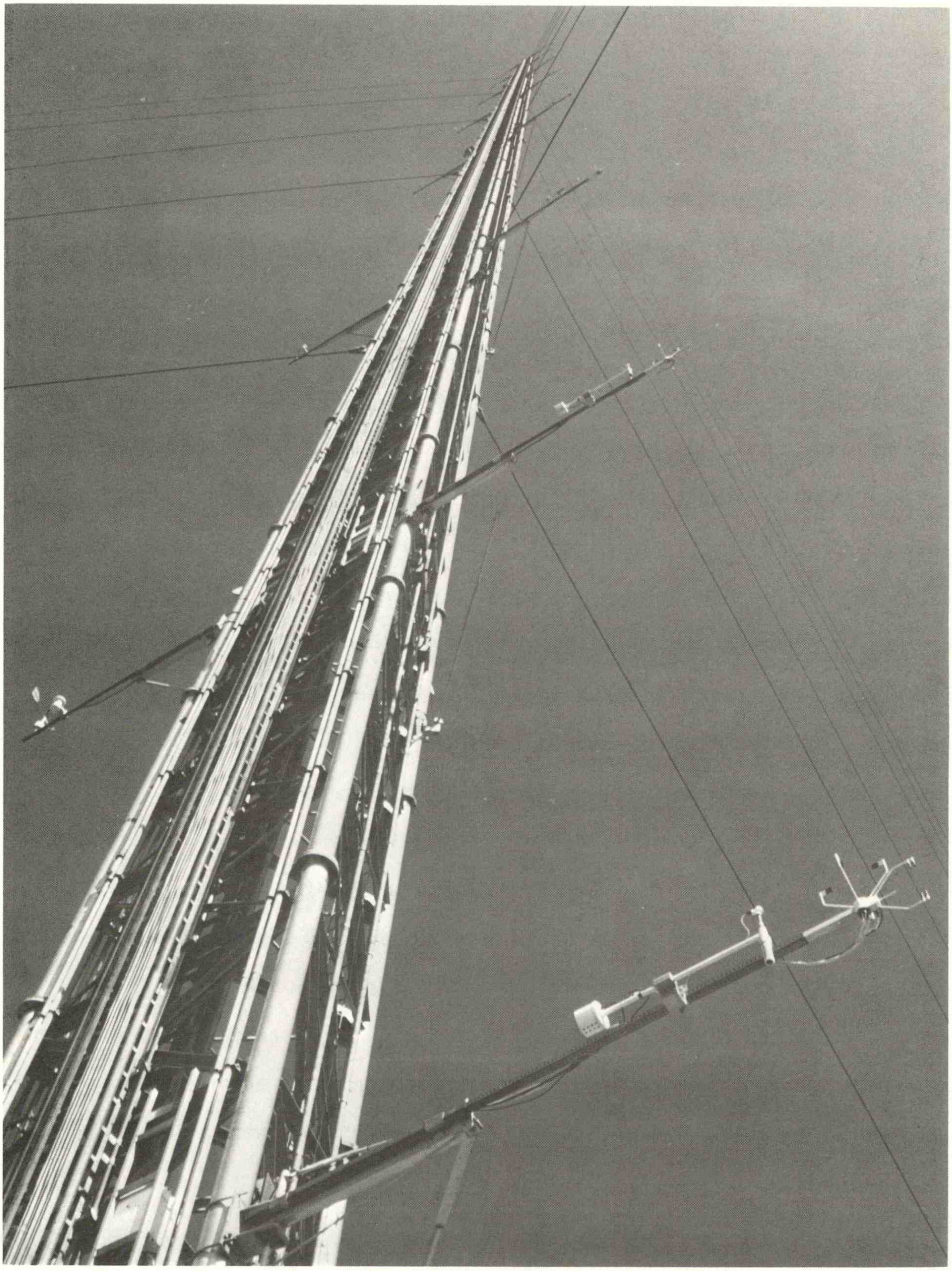

200, and 300 m. Every morning at 0800 MST the data collected over the previous 24 h period were submitted to EPA personnel directing the experiment in exchange for tower data covering the same period.

Concurrent operation of some of the sodars was considered at one time, but quickly ruled out because of cross-contamination, even between systems operating at different frequencies. The sodars were therefore operated in sequence, the switch-over from one system to the other being controlled by a central timer switch. The assigned observing period was one 20 min period each cycle. The experiment took place between 1 and 21 September. On three different occasions, the observing period was extended to 120 min (9 September) and to 80 minutes (16/17 and 18/19 September) in order to obtain long enough records for spectrum analysis. The BAO data were recorded in the raw data mode on these occasions. The three occasions were: 0800-1600, 9 September; 1520-0800, 16/17 September and 1600-0140, 18/19 September. The two 4 h periods, when rawinsonde measurements were made hourly, occurred on 8 September (0400-0800) and 18 September (1200-1600).

AV, REM, and RAD computed σ_w, the standard deviation of w (the vertical wind component), from their time series. Missing data points were not filled in by interpolation, but the number of points missed (or accepted) was displayed. REM used four-point block averages instead of the original time series. XON computed its standard deviation from the width of its 2 min w spectra, estimated for each level. Successive 2 min standard deviations were averaged to obtain the 20 min values. Each spectrum was automatically examined for level and shape of background noise, and steps were taken to remove their effects.

AV, REM, and RAD reported standard deviations of the wind direction, σ_D. REM and RAD calculated theirs from the wind direction time series; AV used the relationship

$$\sigma_D = \sigma_v/U \ ,$$

where U is mean horizontal wind vector. XON reported the standard deviations of the longitudinal and lateral wind components. These were obtained through coordinate transformation of horizontal wind components measured by the sodar.

No attempt is made in this report to present the results of our σ_D comparisons. The azimuth direction standard deviations show very large scatter. The data are withheld pending a better understanding of the reasons for the scatter. Meanwhile, we can only suggest caution in using σ_D for diffusion predictions.

During the experiment, the sodars encountered a wide range of weather conditions: from clear skies to heavy rain, and winds ranging from very light to well over 10 m/s. A summary of daily weather conditions for the duration of the experiment is given in the Appendix. As the manufacturers were asked to submit only data they believed were correct, all submitted data were used in our comparison study.

AV, REM, and XON maintained a consistent operating pattern throughout the experiment. However, RAD changed its operating mode every 24 h, switching from multimode to bistatic and monostatic, back to multimode and so on. For the extended observing periods, RAD operated in the monostatic mode on 9 September, in the bistatic mode on 16/17 September, and multimode on 18/19 September.

4. MEASUREMENT OF THE STANDARD DEVIATION OF w

At the three heights under consideration (100 m, 200 m, 300 m), only AV attained a complete data record. The other three manufacturers had these ranges of completeness at the three heights: RAD, 70% to 95%; REM, 55% to 72%; XON, 77% to 94%. However, wind shadow effects depleted the sonic records so that the final outcome regarding completeness shows composite sonic/sodar percentages of 47% at 100 m, 41% at 200 m, and 47% at 300 m for the sodar versus sonic comparison.

4.1 Sodar Reference Differences

Since the sonic measurements of vertical wind speed standard deviation provide reference values, the accuracy and precision of each sodar system can be determined from the collections of 20 min average differences. The two input variables for these computations are σ_w for the sodar instruments and $\sqrt{\overline{ww}}$ for the sonic vertical wind speed. The comparative statistics used to estimate accuracy and precision then become the average difference, or sample bias (b), and the standard deviation of the differences (s). In addition, the root mean square difference, or comparability (c), is computed; this statistic was defined by Hoehne (1971, 1977), and it characterizes the repeatability of a system. Finally, the precision is also represented as a percentage (s') of the average value of sonic σ_w, i.e., a coefficient of variation.

Expressions for b, c, s, and s' are given in Eqs. (1) to (4).

$$b = \frac{1}{N} \sum_{i=1}^{N} [(\sigma_w)_i - \sqrt{ww}_i] \tag{1}$$

$$c = \{\frac{1}{N} \sum_{i=1}^{N} [(\sigma_w)_i - \sqrt{ww}_i]^2\}^{1/2} \tag{2}$$

$$s = (c^2 - b^2)^{1/2} \tag{3}$$

$$s' = s/\bar{\sigma}_w \times 100. \tag{4}$$

Values of b, c, s, and s' are presented in Table 1 for the combined sodar observations at each of three heights, as well as for the individual vendor data subsets.

The sample bias (b) in Table 1 shows a large range of values around nearly constant composite values of 0.08 to 0.09 m/s. At 100 m the spread is greatest, REM having the only negative bias value (i.e., sodar < sonic) and XON having a sizable 0.23 m/s bias. AV is well below the composite bias amount; RAD is above it. At 200 m the REM value is slightly negative, AV remains small, XON approximates the composite value, but RAD is in excess of 0.2 m/s. At 300 m the RAD bias continues to be relatively large, but the other vendors are grouped between 0.04 and 0.07 m/s.

From Table 1 it is clear that there is much scatter in c and s' about the true value in all systems. There is no statistical difference between s and s' values for AV and REM at any of the levels. The division of Table 1 into daytime and nighttime categories is displayed in Table 2. The bias columns show that all sodar systems tend to overestimate σ_w at night.

Table 1. Sodar σ_w compared with sonic σ_w

Height	Vendor	b (m/s)	c (m/s)	s (m/s)	s'(%)	N
100 m	All	0.08	0.24	0.22	50	678
	RAD	0.12	0.25	0.21	47	178
	REM	-0.05	0.18	0.17	38	139
	AV	0.01	0.16	0.16	35	190
	XON	0.23	0.34	0.24	53	171
200 m	All	0.08	0.27	0.26	54	576
	RAD	0.22	0.39	0.32	65	144
	REM	0.00	0.19	0.19	39	119
	AV	0.03	0.20	0.20	43	167
	XON	0.08	0.25	0.24	51	146
300 m	All	0.09	0.27	0.26	54	665
	RAD	0.23	0.38	0.30	62	158
	REM	0.07	0.23	0.22	47	136
	AV	0.04	0.25	0.25	53	214
	XON	0.04	0.19	0.18	38	157

b = bias (accuracy) (sodar-sonic)
c = comparability
s = standard deviation of differences (precision)
s' = s expressed as a percentage of average value of sonic standard deviation
N = number of observations

AV = Aerovironment
RAD = Radian
REM = Remtech
XON = Xontech

Table 2. Separation of Table 1 into daytime and nighttime categories

Height	Vendor	b_d	b_n	c_d	c_n	s_d	s_n	s'_d	s'_n	N_d	N_n
100 m	All	0.02	0.17	0.21	0.27	0.21	0.21	34	99	389	288
	RAD	0.08	0.18	0.23	0.26	0.22	0.20	34	88	100	78
	REM	-0.10	0.22	0.21	0.24	0.19	0.11	28	58	77	62
	AV	-0.03	0.08	0.16	0.15	0.16	0.13	27	57	115	75
	XON	0.13	0.37	0.25	0.43	0.21	0.22	33	99	97	73
200 m	All	0.04	0.14	0.30	0.23	0.30	0.19	43	78	306	269
	RAD	0.21	0.23	0.43	0.33	0.38	0.24	54	93	78	66
	REM	-0.06	0.06	0.21	0.17	0.20	0.16	27	72	62	57
	AV	-0.02	0.09	0.23	0.18	0.23	0.15	34	62	90	77
	XON	0.00	0.17	0.28	0.23	0.28	0.15	42	62	76	69
300 m	All	0.06	0.12	0.28	0.27	0.27	0.24	41	89	359	304
	RAD	0.21	0.24	0.39	0.36	0.33	0.27	49	98	87	71
	REM	0.03	0.11	0.25	0.22	0.25	0.19	36	78	70	66
	AV	-0.00	0.09	0.23	0.29	0.23	0.27	36	100	121	93
	XON	0.03	0.06	0.22	0.15	0.22	0.14	33	52	81	74

Subscript d: daytime (0600-1800 hours)
Subscript n: nighttime (0000-0600 and 1800-2400 hours)

4.2 Individual 20 Minute Average Values

Additional information about the effectiveness of sodar measurements of σ_w can be sought in the scatter plots of their 20 min average values against the sonic standard deviation of vertical wind speed. Such plots are presented by height and vendor in Figs. 4-15; daytime observations (0600-1800 MST) are distinguished from nighttime observations.

Each chart has a broken line at 45° from the origin to represent a slope of 1. The estimates of the correlation coefficient based upon the 20 day sample are given in Table 3.

Each chart also has a line for sodar regressed linearly upon reference according to the following model:

$$Y_i = \beta_0 + \beta_1 X_i + \varepsilon_i \ ,$$

where

Y_i = ith sodar measurement,

X_i = ith reference measurement,

β_0 = Y-intercept,

β_1 = slope,

ε_i = error term,

In all cases, the regression line misses the origin on the upper side and has a slope less than 1. Both characteristics are significant at the 0.05 level.

As is readily seen in Figs. 4-15, the sodar systems are all consistently recording too high when σ_w < 0.5 m/s and too low when σ_w > 1.0 m/s.

Table 3. Regression analysis for σ_w.

Height	Vendor	ρ	β_0	β_1	N
100 m	RAD	0.85	0.28	0.67	178
	REM	0.89	0.10	0.68	139
	AV	0.89	0.18	0.63	190
	XON	0.67	0.46	0.51	171
200 m	RAD	0.77	0.39	0.67	144
	REM	0.88	0.12	0.75	119
	AV	0.84	0.20	0.64	167
	XON	0.83	0.26	0.63	146
300 m	RAD	0.72	0.39	0.69	158
	REM	0.84	0.17	0.79	136
	AV	0.70	0.19	0.68	214
	XON	0.82	0.13	0.80	157

ρ = estimate of correlation coefficient
β_0 = intercept term
β_1 = slope term
N = number of observations

4.3 Sodar Modes

The sodar systems had two distinct operational modes: monostatic (MONO) and bistatic (BI). AV and REM employed the former mode; XON represented the latter mode; RAD rotated daily among MONO, BI, and a combination of the two modes called multistatic (MULTI).

A comparison of RAD modal data with simultaneous sonic standard deviation values yields the b, c, and s results of Table 4. The sample bias (b) is significantly nonzero in all modes at all heights. It is equivalent among modes at each height at a probability level of 0.05, except for a significant difference between MONO and MULTI biases at 200 m.

Comparability (c) and standard deviation (s) do not show a uniform ranking of modes with height. The large c-value for MONO at 200 m is partly due to the large bias and the presence of two σ_w values slightly greater than 2 m/s in the subset. The s-values are inconsistent in their equivalence from height to height, possibly because of the sparseness of the data.

Scatter diagrams of individual 20 min average values of sodar σ_w versus sonic σ_w are shown by height and by mode in Figs. 16-24. The BI mode has the largest departures from the 1:1 line. Figures 16-18 do not include sonic σ_w > 1.0 m/s. Thus the plots involving BI mode are not strictly comparable with the others.

In summary, there is a consistent tendency in all sodar systems to overestimate σ_w at low sonic readings (in stable conditions). Conversely, the sodar systems underestimated σ_w when the true value was higher (unstable conditions). In all cases the regression lines had positive y-intercepts and slopes less than unity.

On average, sample biases were generally significantly positive, but AV did not show a significant bias at 100 m and was marginally biased at 200 m and 300 m. REM was the only vendor with a negative bias at 100 m, but at 300 m, REM had a positive bias, as did all the others.

REM performed very well with respect to c and s at 200 m, but results for these statistics were not consistent with height. In fact, a different vendor emerged with the lowest, i.e., best, values of c and s at each level.

Mode switching in the RAD system revealed a significant amount of bias in each mode (BI, MONO, MULTI) at 100 m, 200 m, and 300 m. However, as Table 4 indicates, there was little difference among modes.

Table 4. Radian modal σ_w compared with sonic σ_w

Height	Mode	b (m/s)	c (m/s)	s (m/s)	N
100 m	MONO	0.14	0.28	0.24	68
	BI	0.14	0.24	0.19	44
	MULTI	0.10	0.22	0.20	66
200 m	MONO	0.30	0.50	0.40	58
	BI	0.19	0.35	0.29	30
	MULTI	0.15	0.26	0.21	56
300 m	MONO	0.25	0.36	0.25	57
	BI	0.23	0.40	0.32	48
	MULTI	0.19	0.39	0.34	53

b = bias (accuracy)
c = comparability
s = standard deviation of differences (precision)
N = number of observations

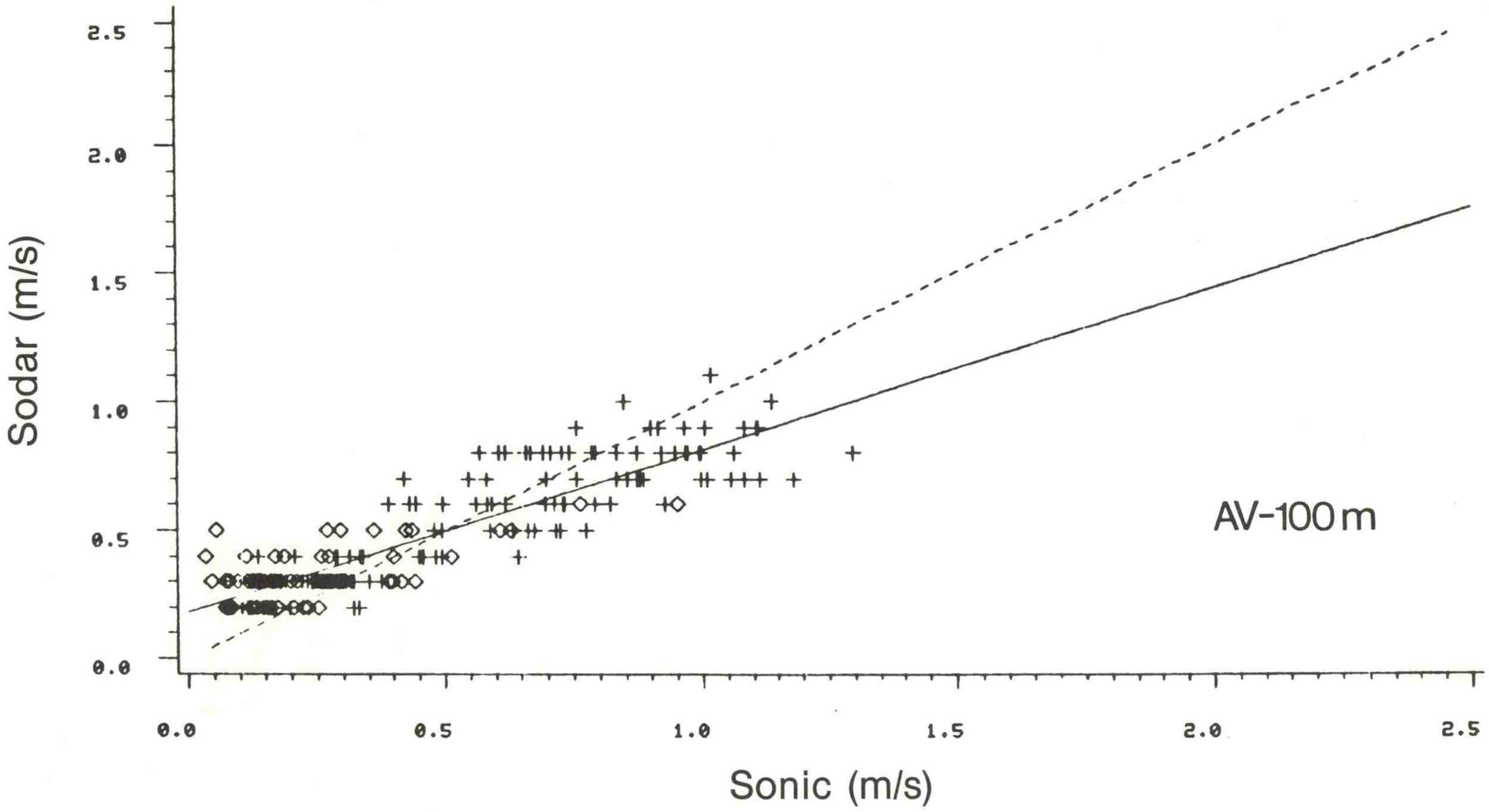

REGRESSION LINE ————————————

DAY TIME OBSERVATIONS +

NIGHT TIME OBSERVATIONS ◇

INTERCEPT=0 AND SLOPE=1 (45° ANGLE) LINE -------

Figure 4. Comparison of 100 m σ_w values from the AV sodar and the BAO sensor.

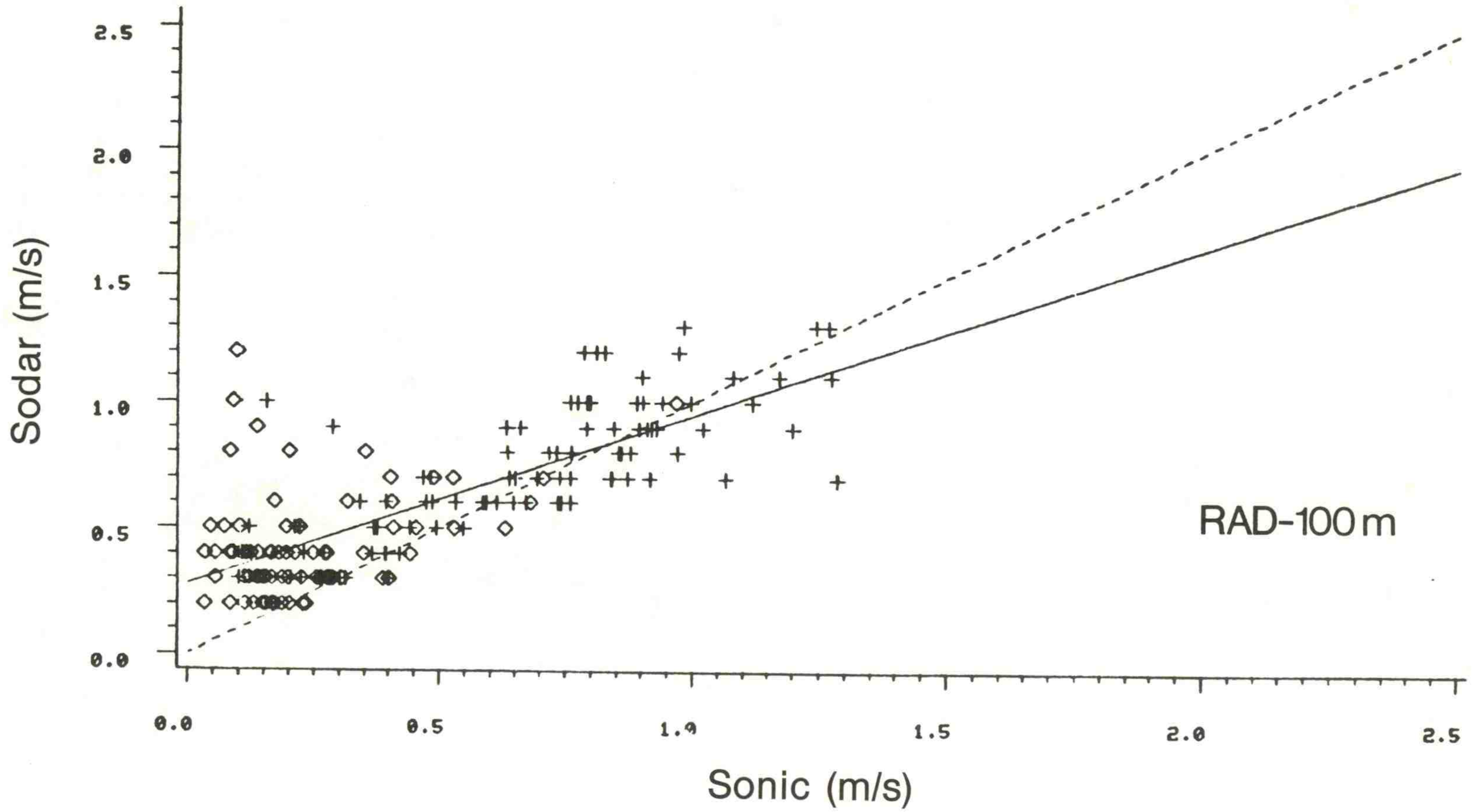

REGRESSION LINE ————————

DAY TIME OBSERVATIONS +

NIGHT TIME OBSERVATIONS ◇

INTERCEPT=0 AND SLOPE=1 (45° ANGLE) LINE -------

Figure 5. Comparison of 100 m σ_w values from the RAD sodar and the sensor.

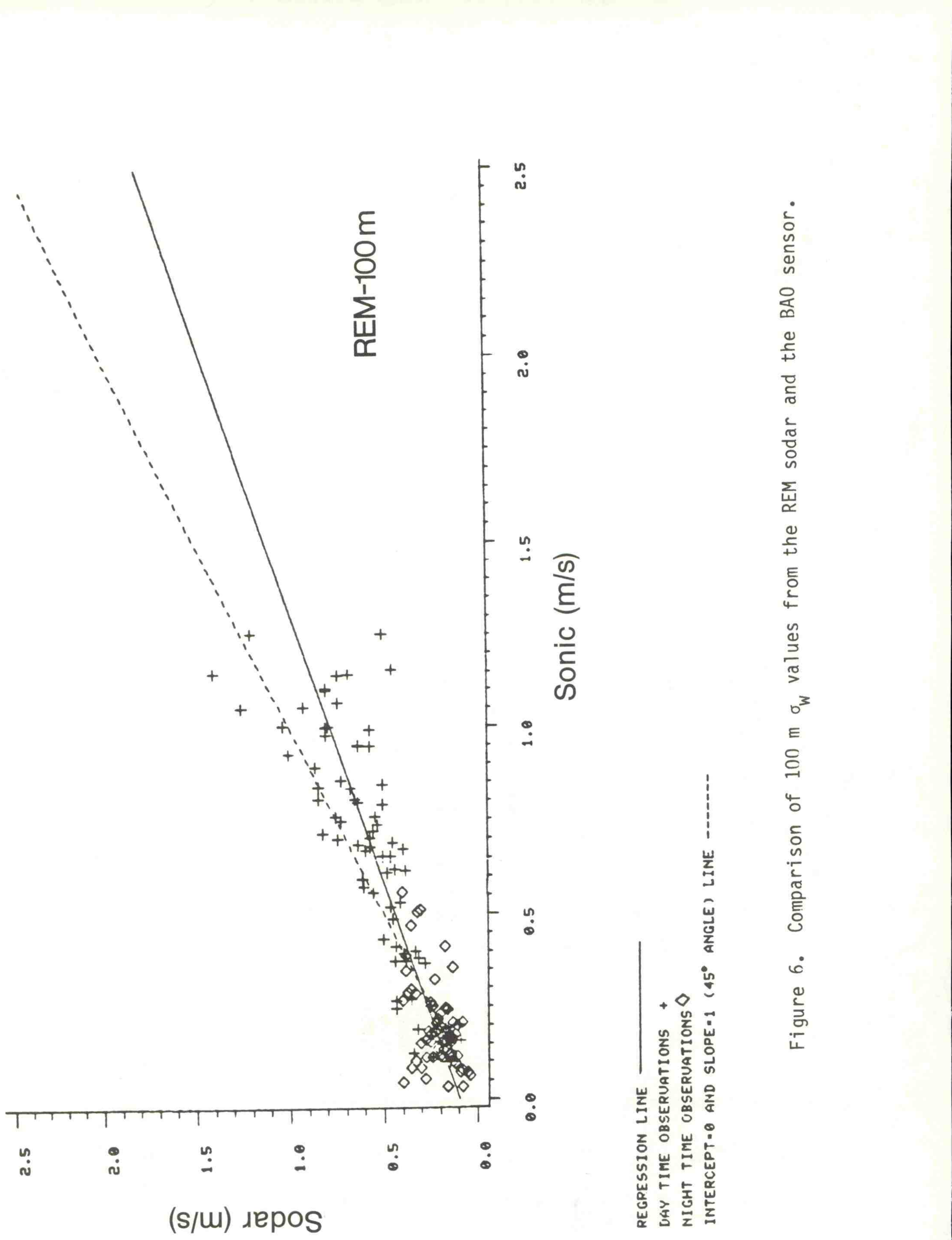

Figure 6. Comparison of 100 m σ_w values from the REM sodar and the BAO sensor.

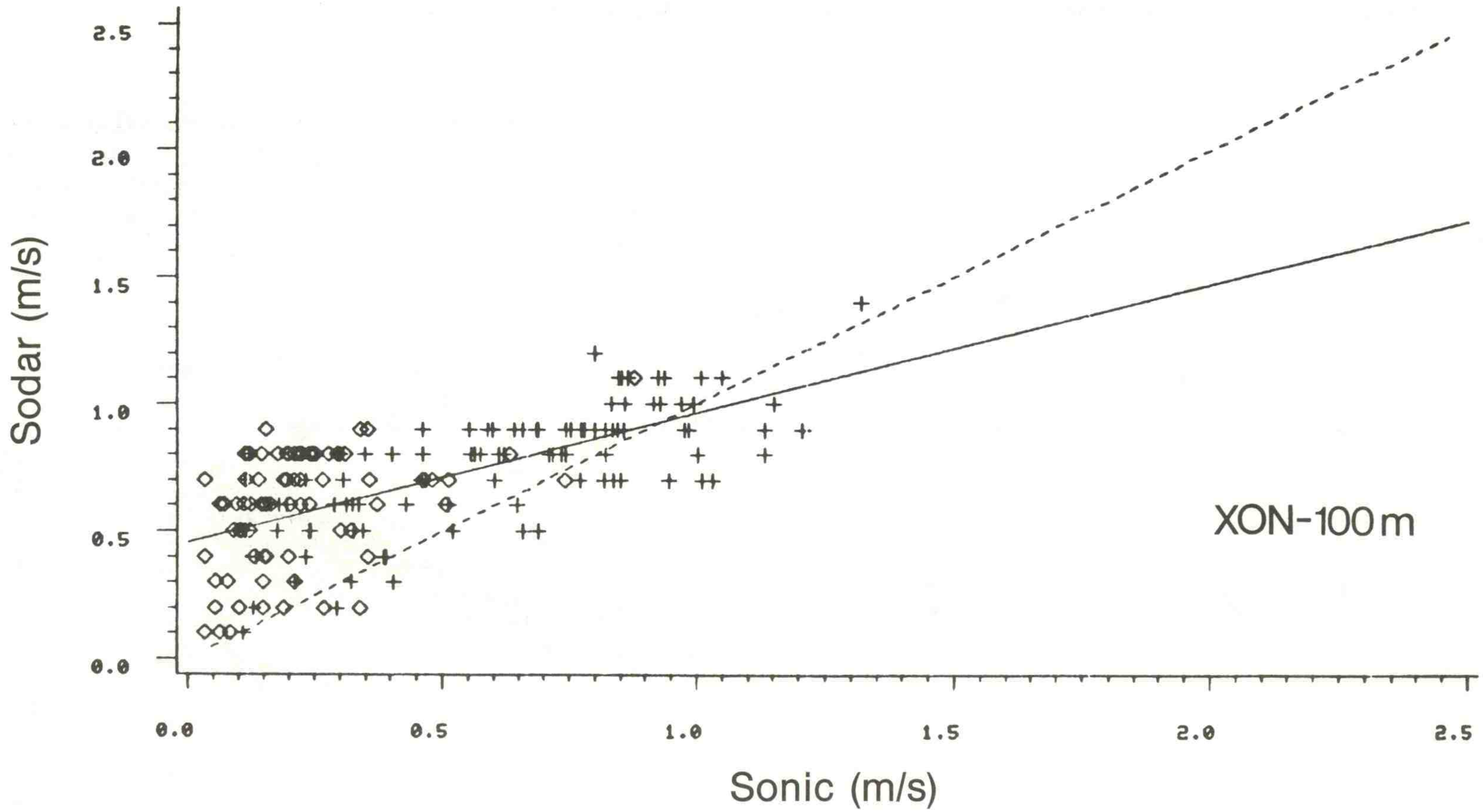

REGRESSION LINE ————————

DAY TIME OBSERVATIONS +

NIGHT TIME OBSERVATIONS ◇

INTERCEPT=0 AND SLOPE=1 (45° ANGLE) LINE -------

Figure 7. Comparison of 100 m σ_w values from the XON sodar and the BAO sensor.

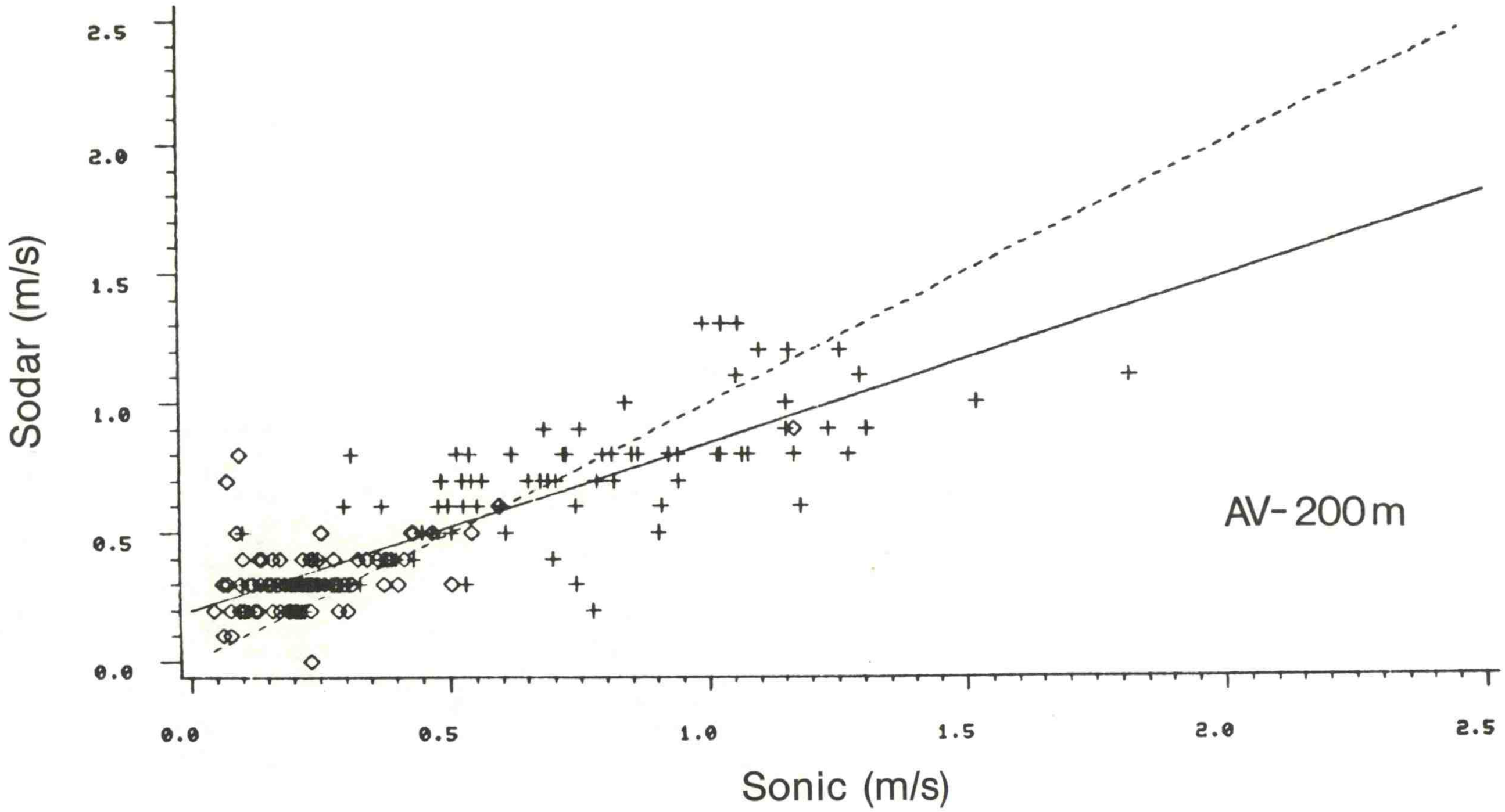

REGRESSION LINE ————————————

DAY TIME OBSERVATIONS +

NIGHT TIME OBSERVATIONS ◇

INTERCEPT=0 AND SLOPE=1 (45° ANGLE) LINE -------

Figure 8. Comparison of 200 m σ_w values from the AV sodar and the BAO sensor.

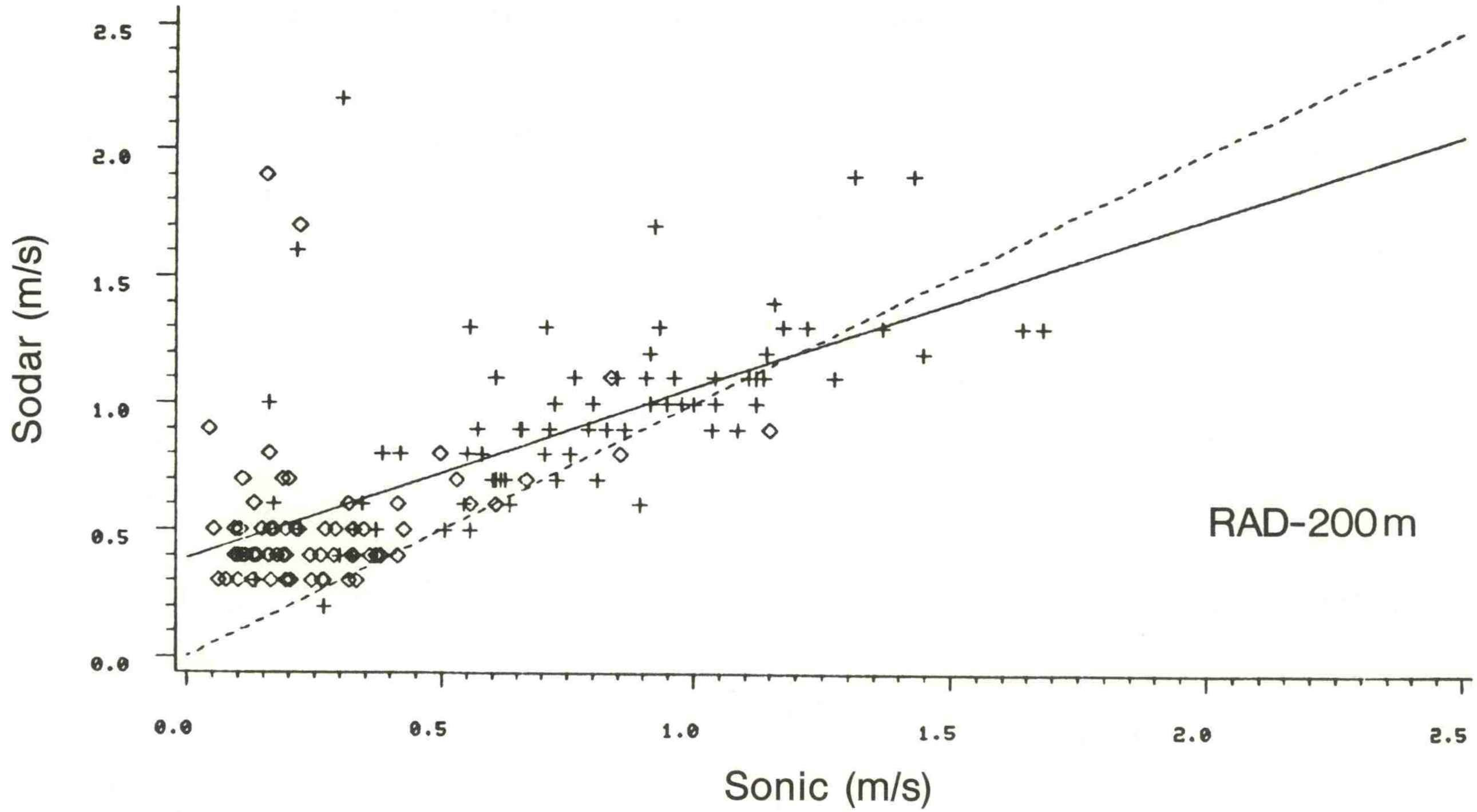

Figure 9. Comparison of 200 m σ_w values from the RAD sodar and the BAO sensor.

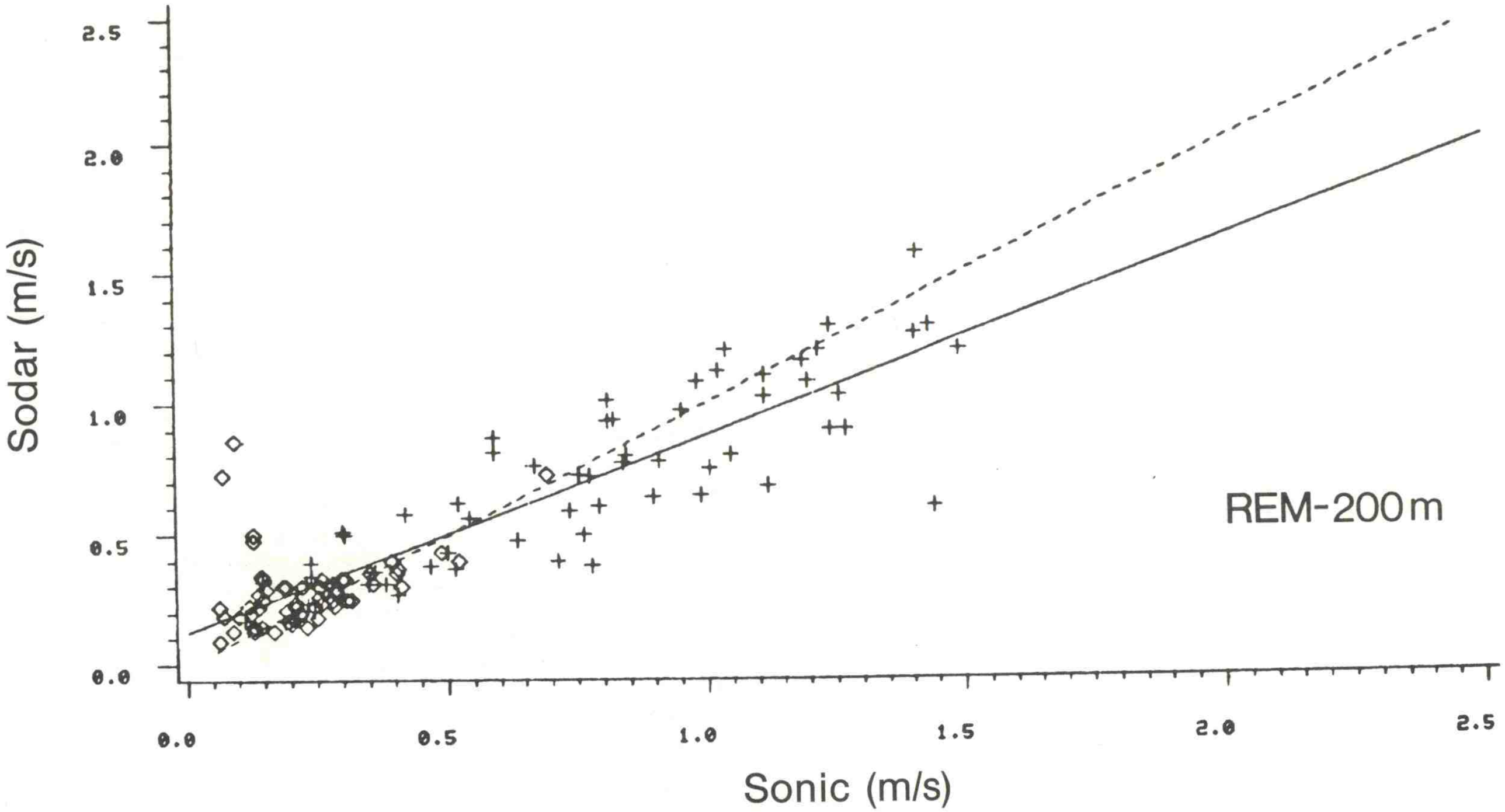

REGRESSION LINE ————————

DAY TIME OBSERVATIONS +

NIGHT TIME OBSERVATIONS ◇

INTERCEPT=0 AND SLOPE=1 (45° ANGLE) LINE -------

Figure 10. Comparison of 200 m σ_w values from the REM sodar and the BAO sensor.

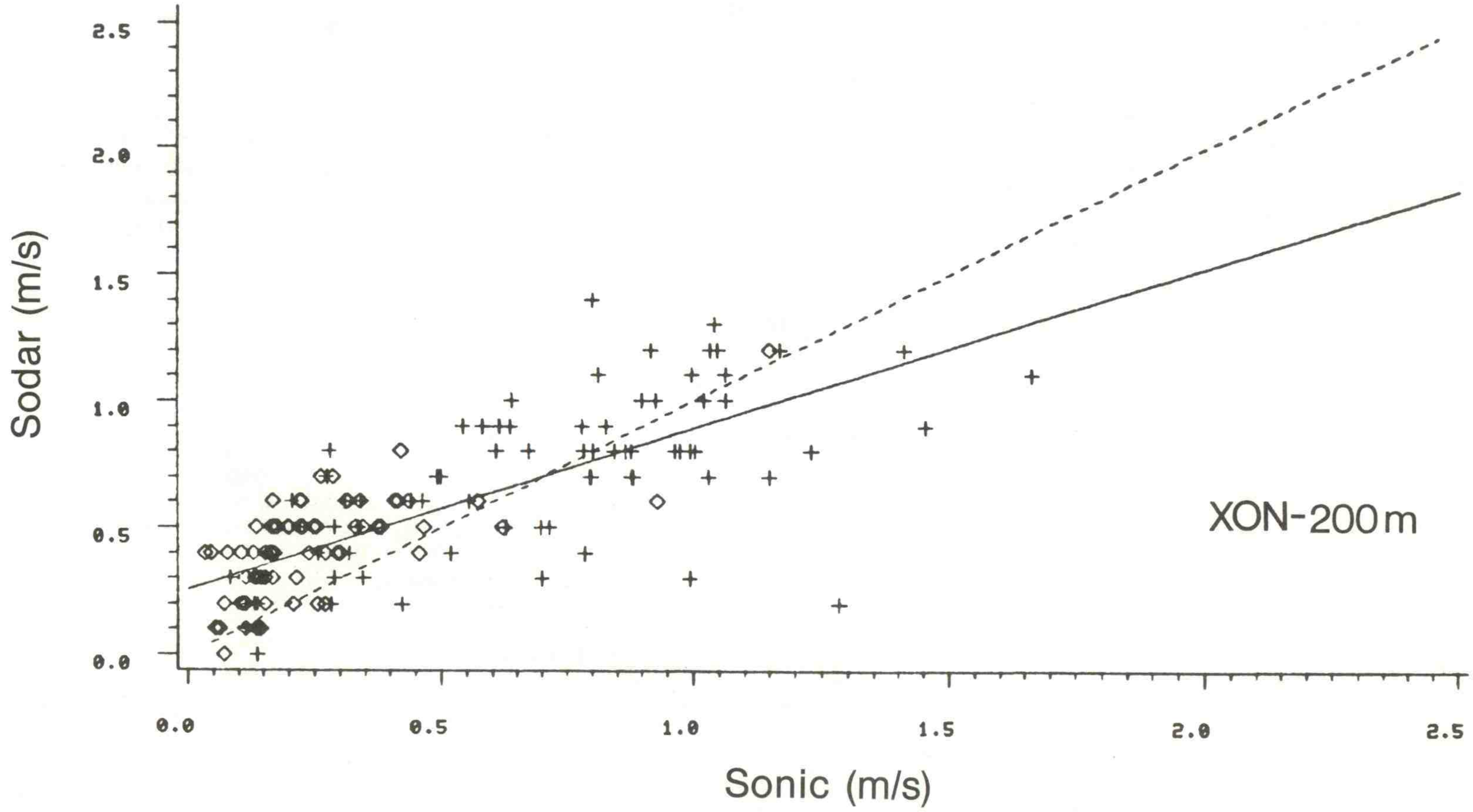

REGRESSION LINE ————————

DAY TIME OBSERVATIONS +

NIGHT TIME OBSERVATIONS ◇

INTERCEPT=0 AND SLOPE=1 (45° ANGLE) LINE -------

Figure 11. Comparison of 200 m σ_w values from the XON sodar and the BAO sensor.

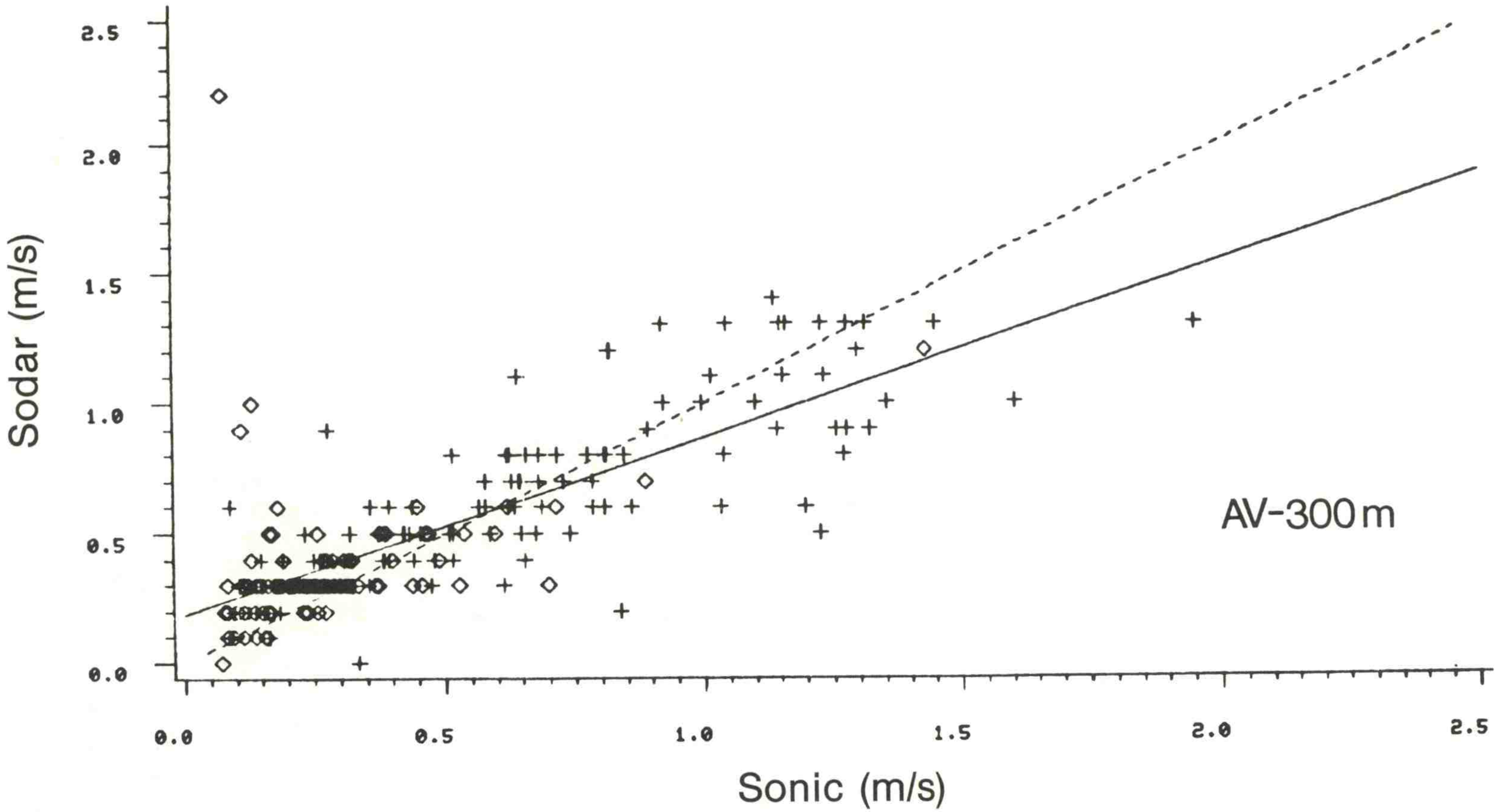

REGRESSION LINE ————————

DAY TIME OBSERVATIONS +

NIGHT TIME OBSERVATIONS◇

INTERCEPT=0 AND SLOPE=1 (45° ANGLE) LINE -------

Figure 12. Comparison of 300 m σ_w values from the AV sodar and the BAO sensor.

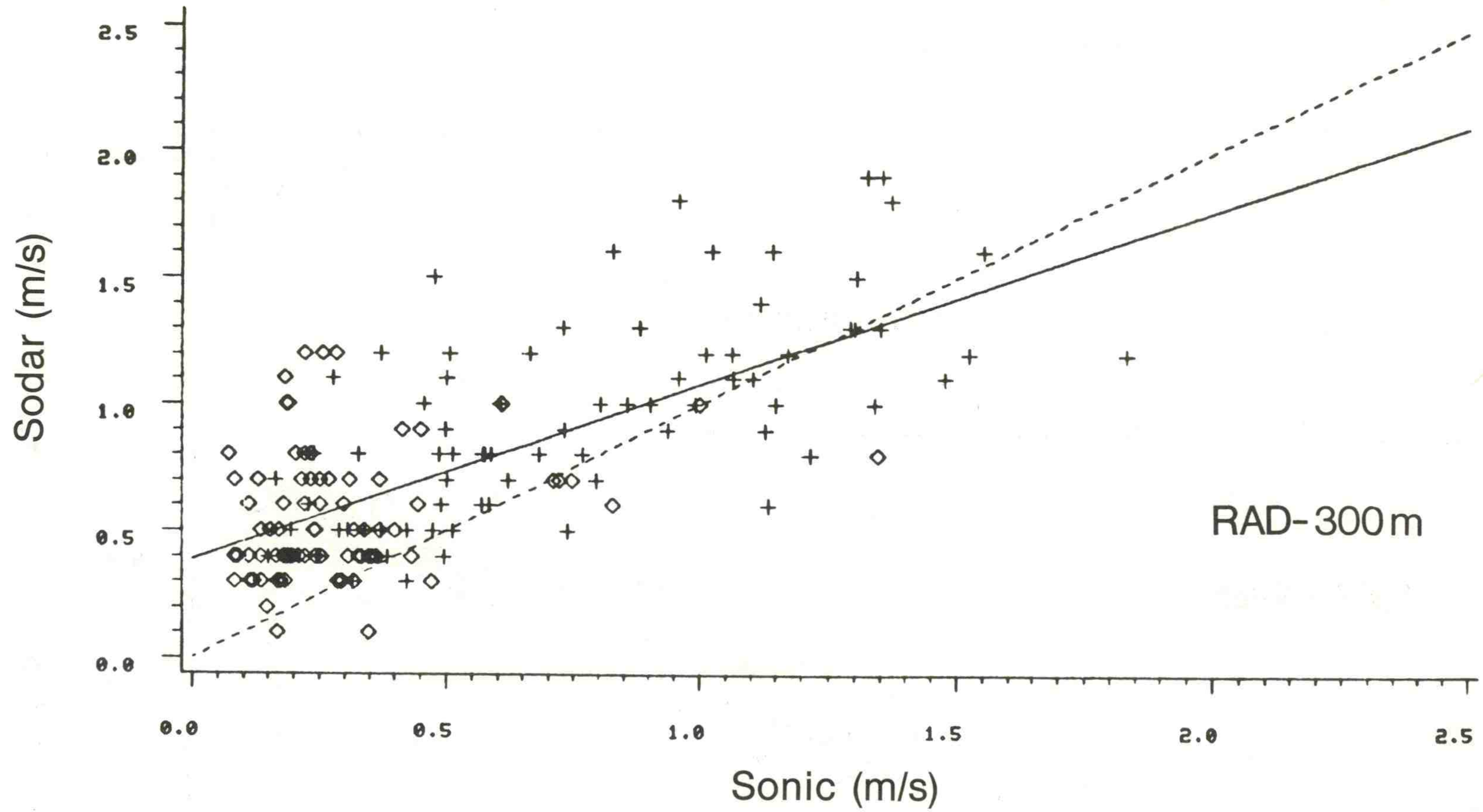

REGRESSION LINE ————————
DAY TIME OBSERVATIONS +
NIGHT TIME OBSERVATIONS ◇
INTERCEPT=0 AND SLOPE=1 (45° ANGLE) LINE -------

Figure 13. Comparison of 300 m σ_w values from the RAD sodar and the BAO sensor.

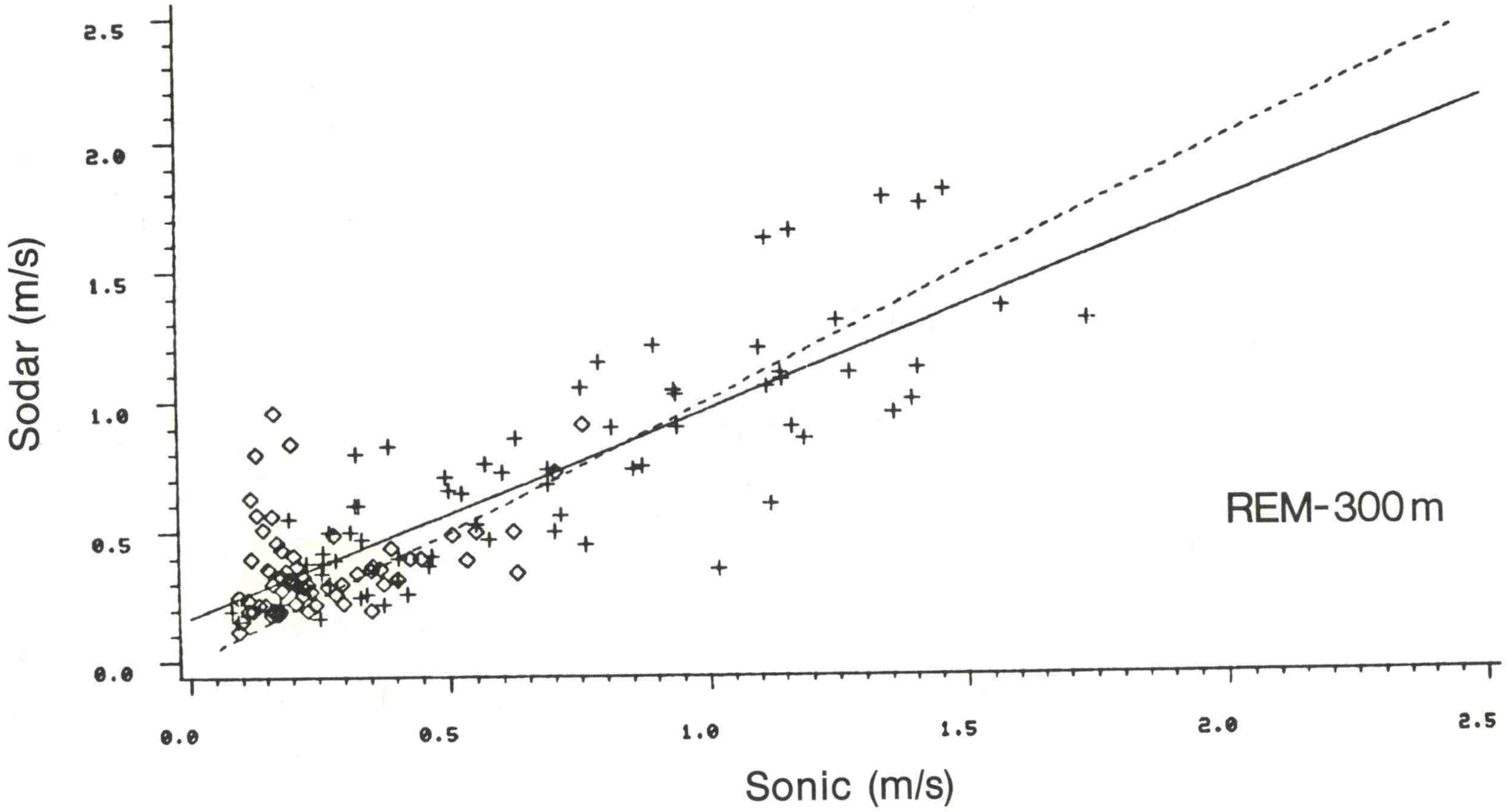

REGRESSION LINE ————————
DAY TIME OBSERVATIONS +
NIGHT TIME OBSERVATIONS ◇
INTERCEPT=0 AND SLOPE=1 (45° ANGLE) LINE -------

Figure 14. Comparison of 300 m σ_w values from the REM sodar and the BAO sensor.

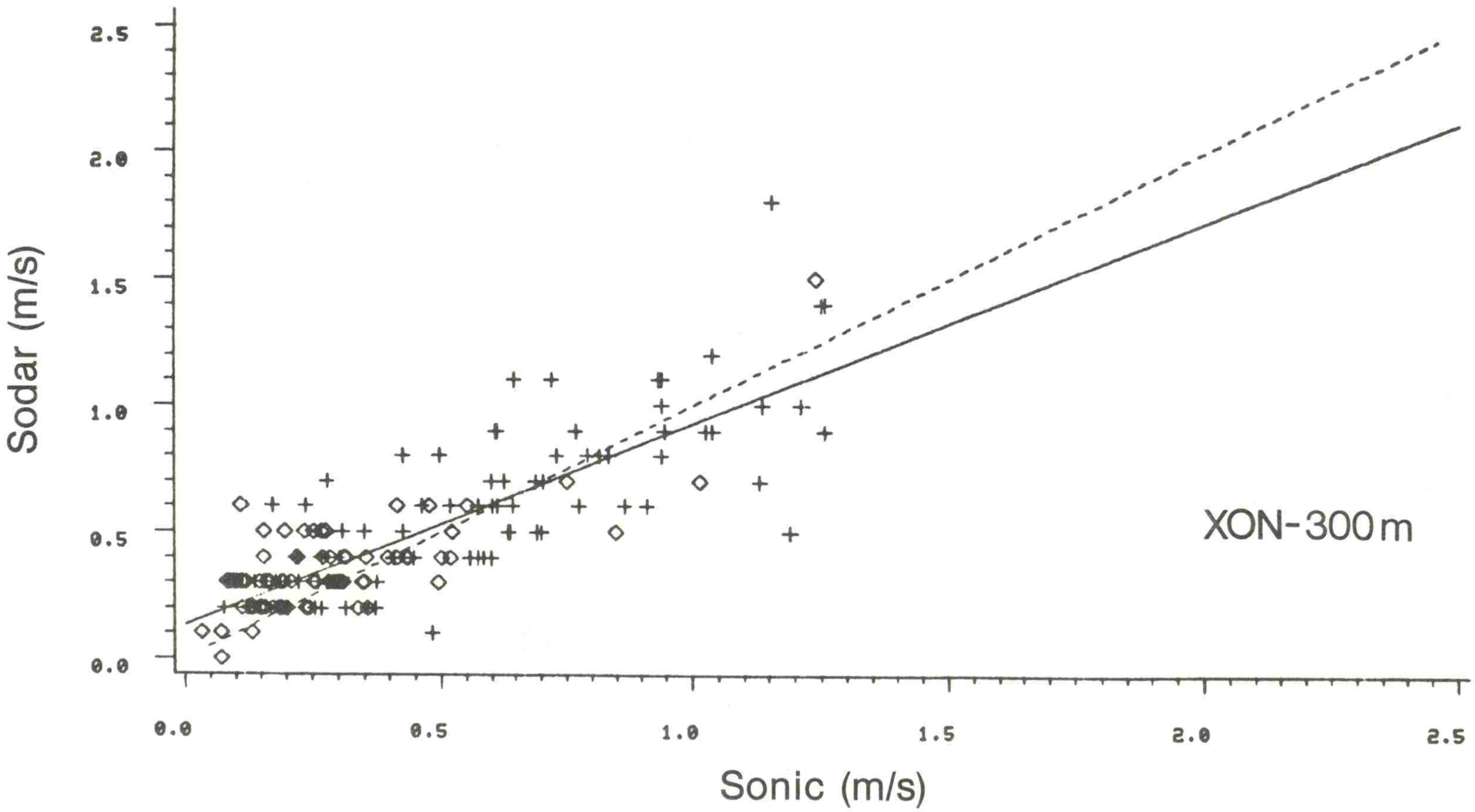

REGRESSION LINE ————————
DAY TIME OBSERVATIONS +
NIGHT TIME OBSERVATIONS ◇
INTERCEPT=0 AND SLOPE=1 (45° ANGLE) LINE -------

Figure 15. Comparison of 300 m σ_w values from the XON sodar and the BAO sensor.

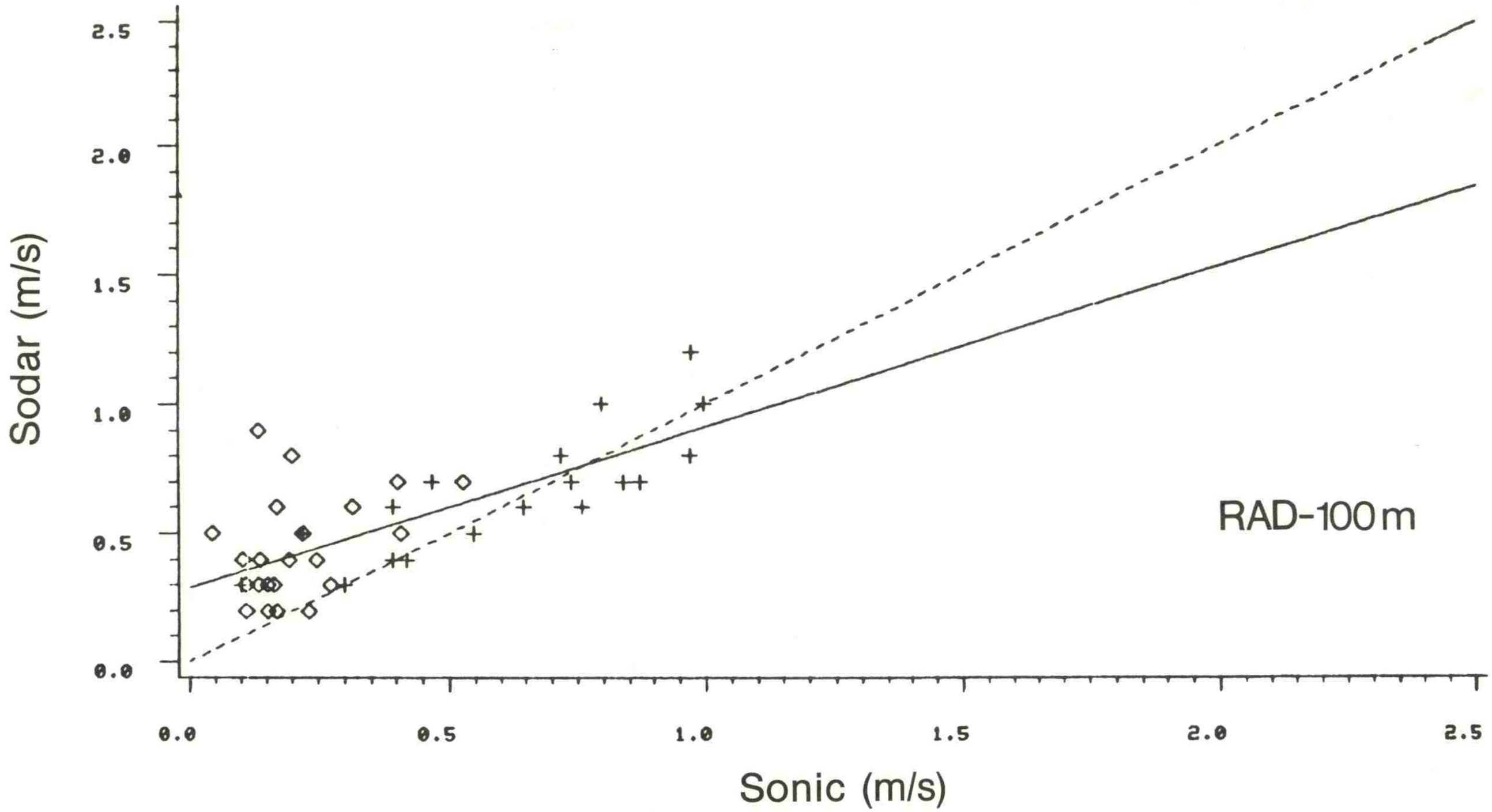

REGRESSION LINE ————————

DAY TIME OBSERVATIONS +

NIGHT TIME OBSERVATIONS ◇

INTERCEPT=0 AND SLOPE=1 (45° ANGLE) LINE -------

Figure 16. Comparison of 100 σ_w values from RAD (mode: BI) sodar and the BAO sensor.

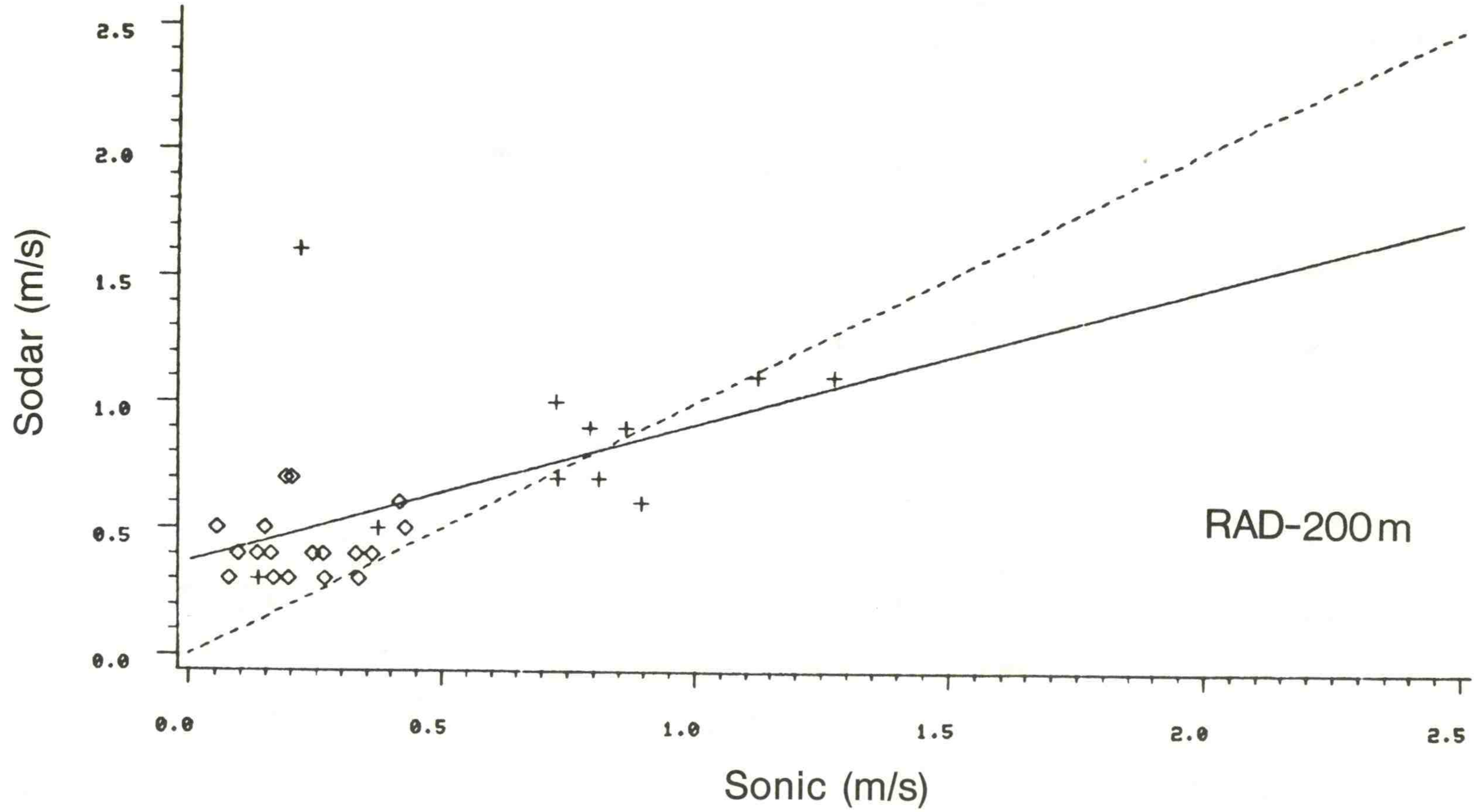

Figure 17. Comparison of 200 m σ_w values from RAD (mode: BI) sodar and the BAO sensor.

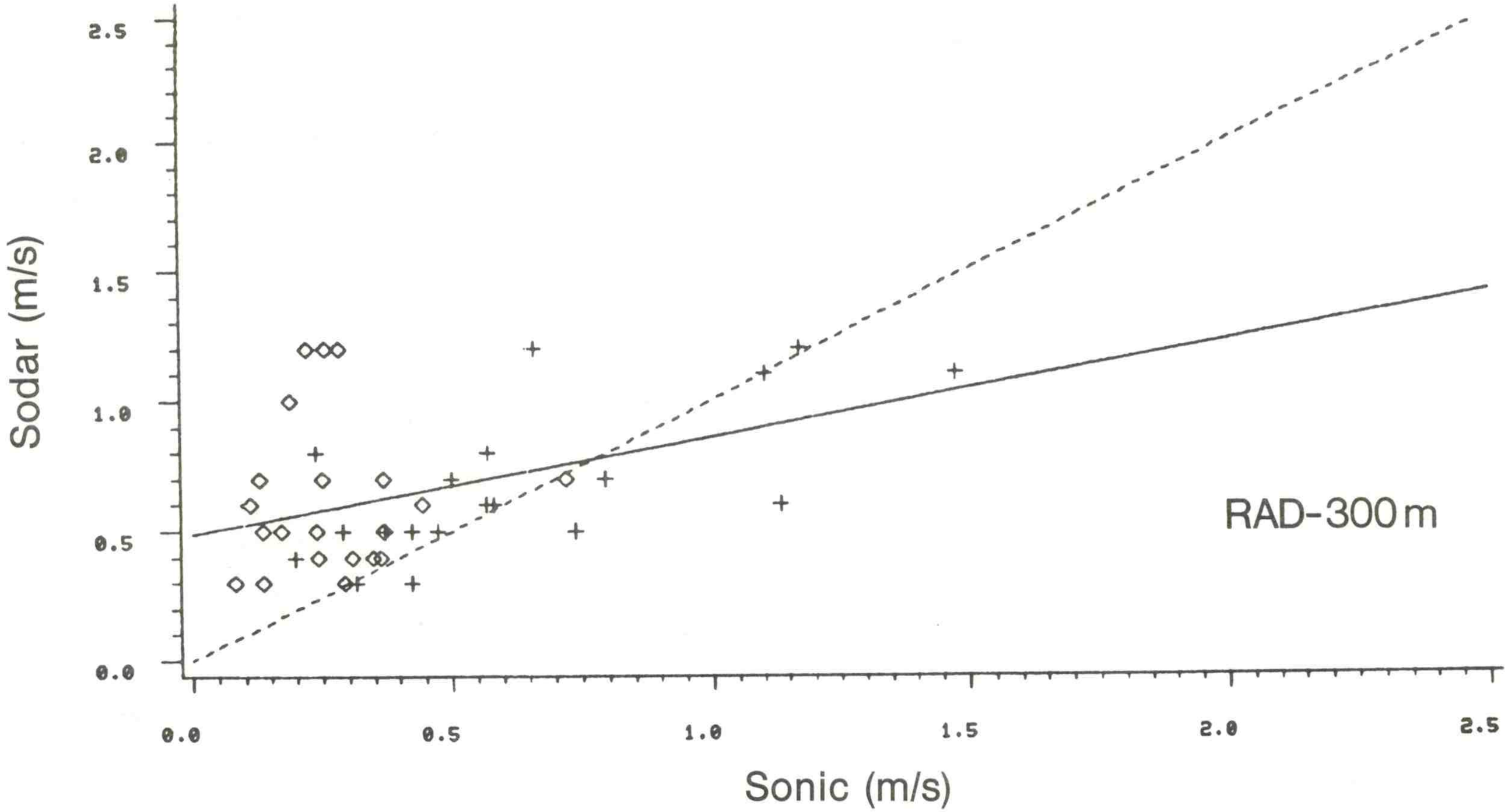

REGRESSION LINE ————————————

DAY TIME OBSERVATIONS +

NIGHT TIME OBSERVATIONS ◇

INTERCEPT=0 AND SLOPE=1 (45° ANGLE) LINE -------

Figure 18. Comparison of 300 m σ_w values from RAD (mode: BI) sodar and the BAO sensor.

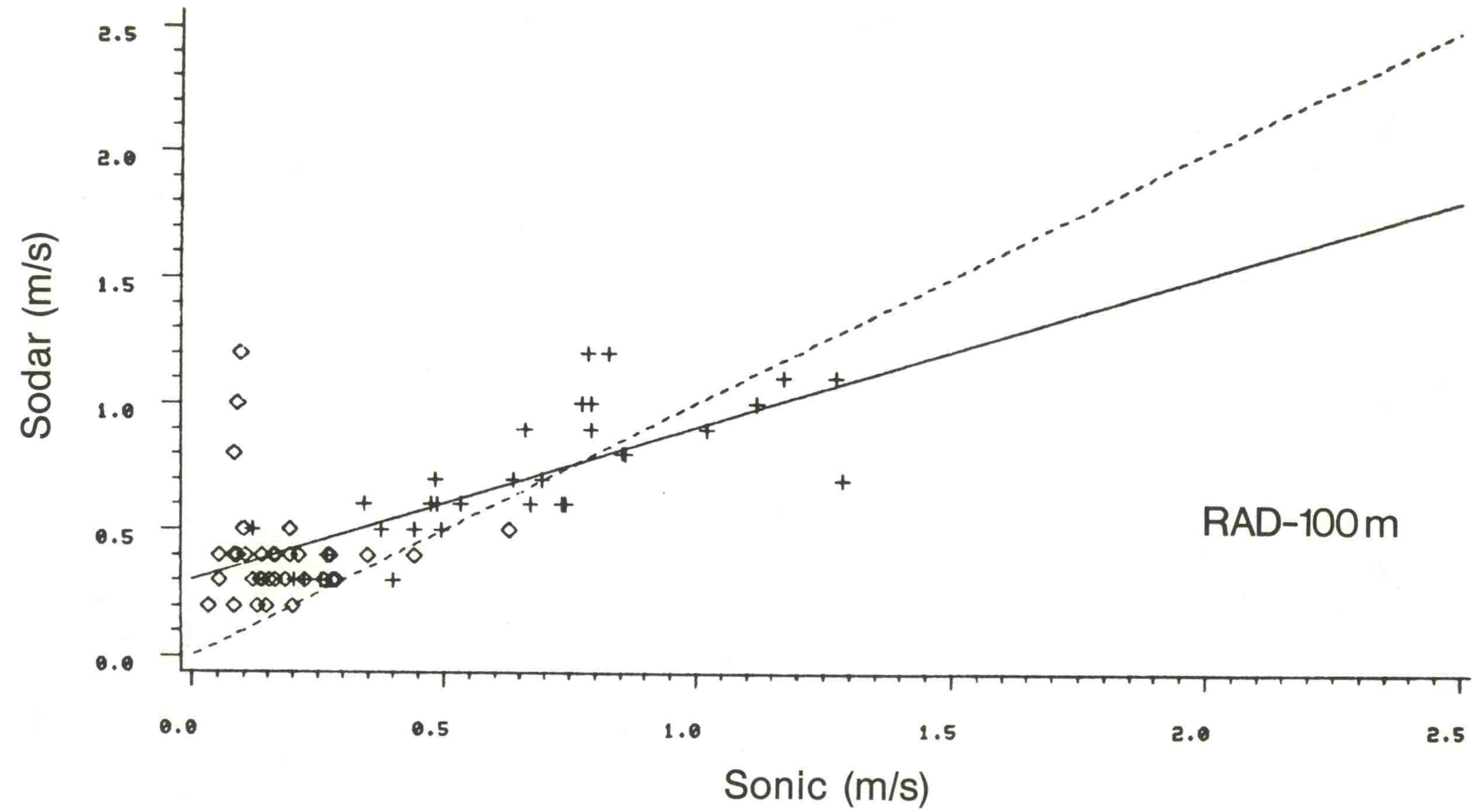

Figure 19. Comparison of 100 m σ_w values from RAD (mode: MONO) sodar and the BAO sensor.

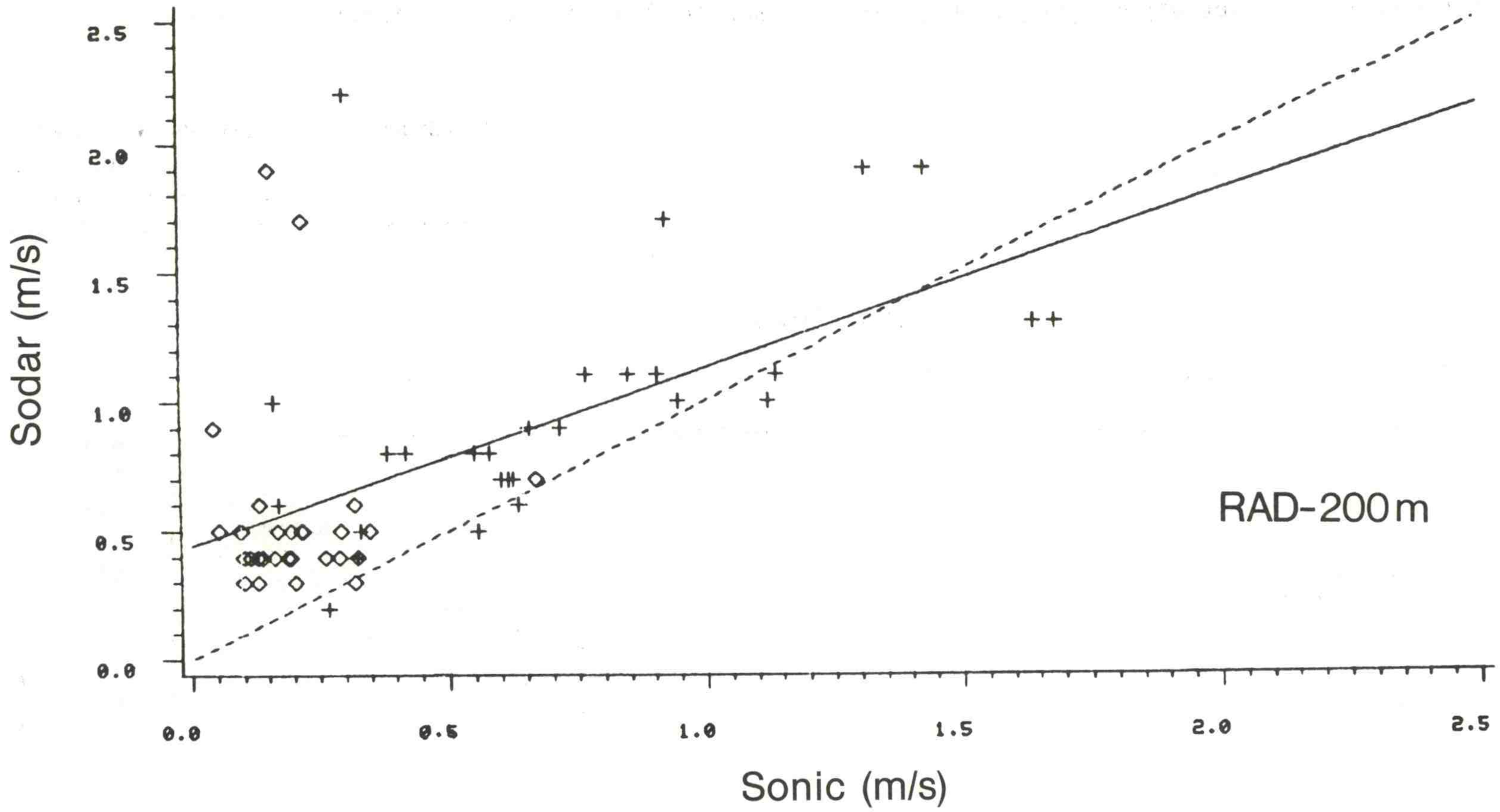

REGRESSION LINE ————————————
DAY TIME OBSERVATIONS +
NIGHT TIME OBSERVATIONS ◇
INTERCEPT=0 AND SLOPE=1 (45° ANGLE) LINE -------

Figure 20. Comparison of 200 m σ_w values from RAD (mode: MONO) sodar and the BAO sensor.

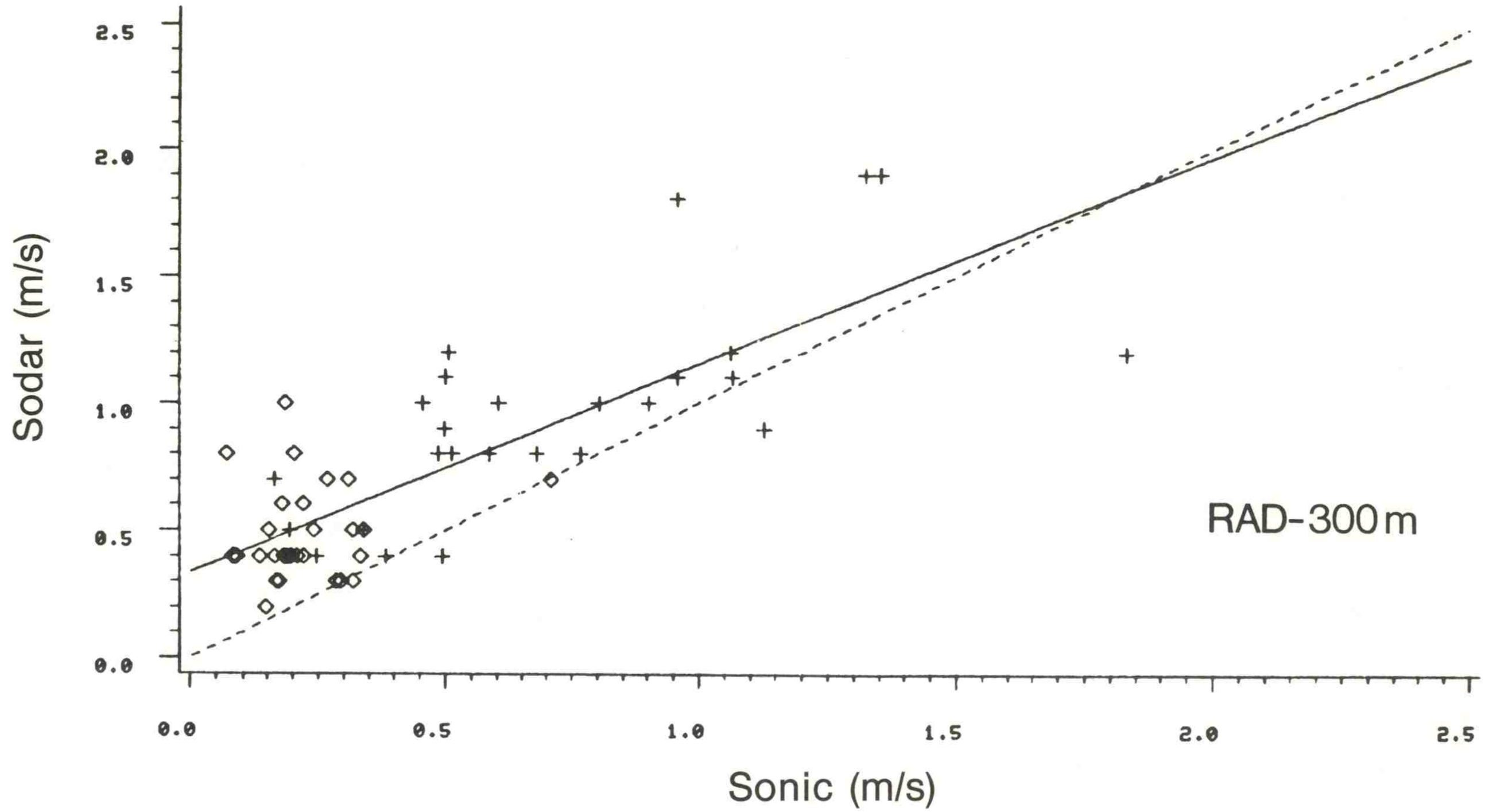

REGRESSION LINE ————————
DAY TIME OBSERVATIONS +
NIGHT TIME OBSERVATIONS ◇
INTERCEPT=0 AND SLOPE=1 (45° ANGLE) LINE -------

Figure 21. Comparison of 300 m σ_w values from RAD (mode: MONO) sodar and the BAO sensor.

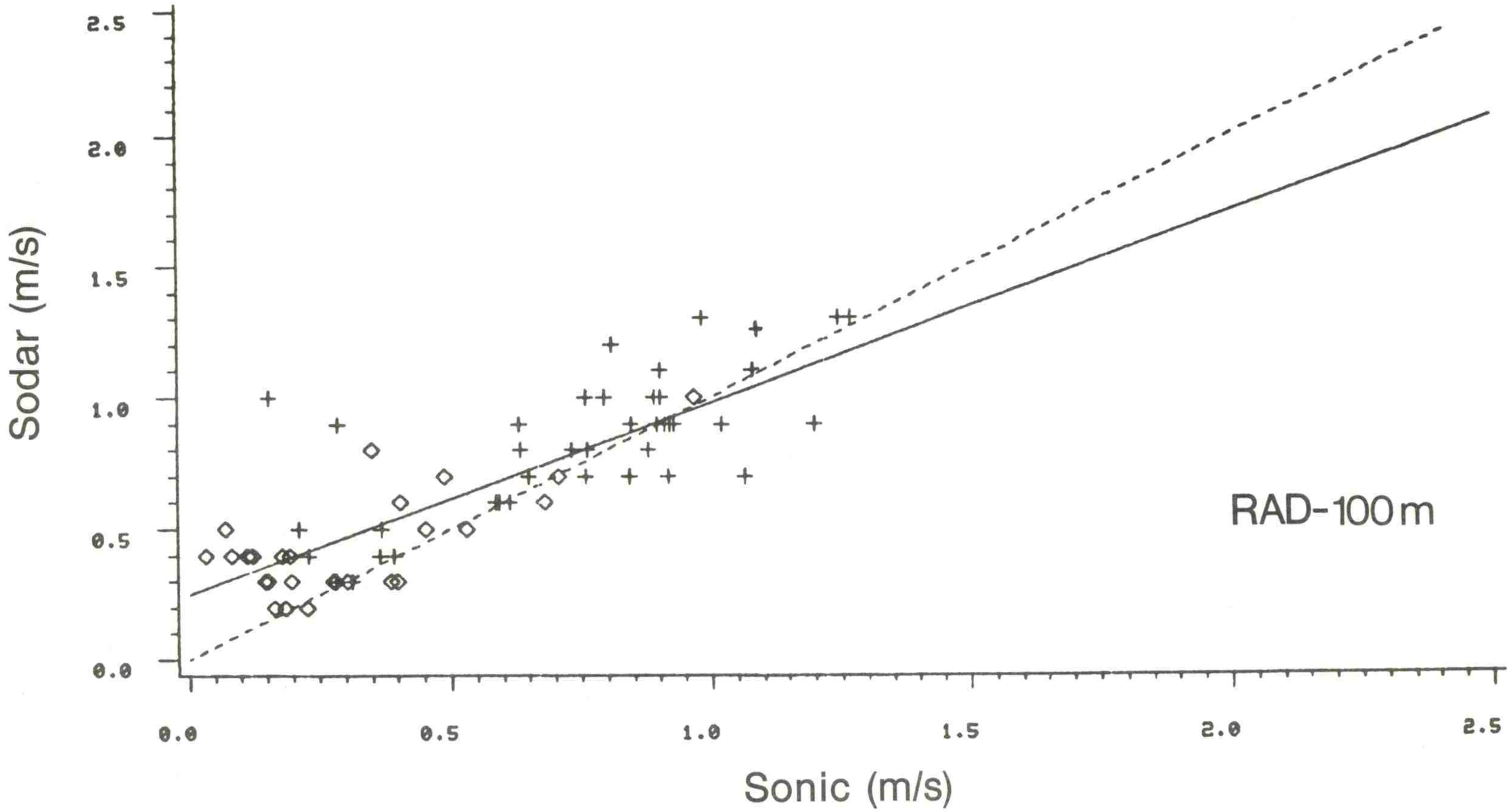

REGRESSION LINE ————————

DAY TIME OBSERVATIONS +

NIGHT TIME OBSERVATIONS ◇

INTERCEPT=0 AND SLOPE=1 (45° ANGLE) LINE -------

Figure 22. Comparison of 100 m σ_w values from RAD (mode: MULTI) sodar and the BAO sensor.

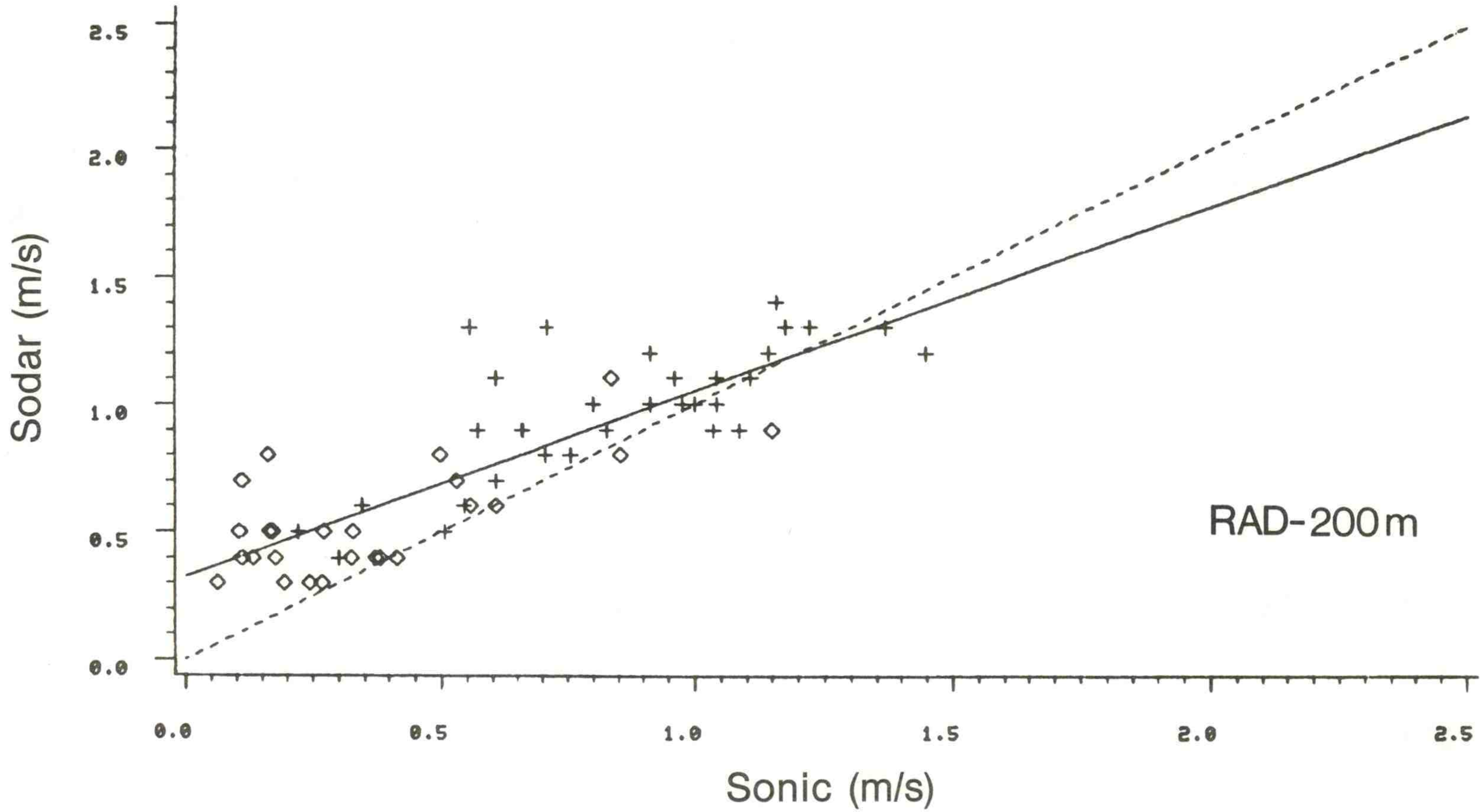

REGRESSION LINE ————————————
DAY TIME OBSERVATIONS +
NIGHT TIME OBSERVATIONS ◇
INTERCEPT=0 AND SLOPE=1 (45° ANGLE) LINE -------

Figure 23. Comparison of 200 m σ_w values from RAD (mode: MULTI) sodar and the BAO sensor.

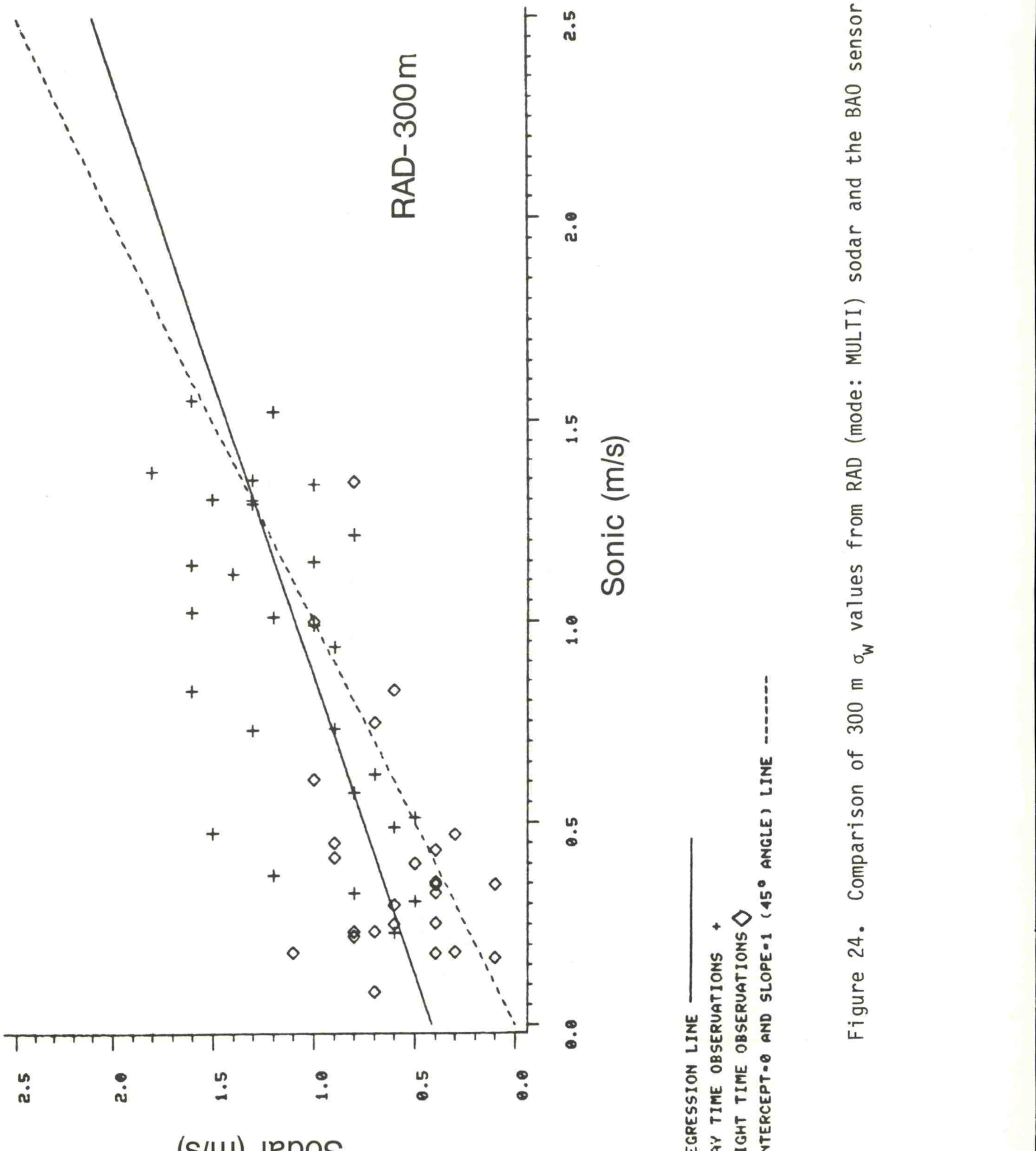

Figure 24. Comparison of 300 m σ_w values from RAD (mode: MULTI) sodar and the BAO sensor.

5. MEASUREMENT OF WIND SPEED

Measurements of wind speed (S) were obtained at sampling rates of 1 datum/15 s (REM, RAD, XON) and 1 datum/24 s (AV), and average S was computed in the field over 20 min intervals. The four sodars cycled in sequence, so that a maximum of about 1440/4, or 360, values could be obtained by each vendor in the 20 days of the experiment. At the three heights under consideration (100 m, 200 m, 300 m), AV had complete data and the other manufacturers ranged in completeness as follows: RAD, 60% to 96%, REM, 55% to 72%; XON, 91% to 92%, depending on the variable.

To examine the accuracy and precision of the sodars, simultaneous observations of wind speed were recorded from sonic anemometers at the same three heights on a tower that was about 600 m from the sodar systems. The sonic systems had a sampling rate of 10 Hz, and they are regarded as the reference instruments in the evaluation. However, owing to a wind shadow zone created by the tower, extending ±40° from north for the sonic instruments, reference data in this sector were obtained by the propeller-vane at the BAO tower. A comparison of sonic and propeller wind speed measurements on the tower showed that the instruments were approximately equivalent. The resulting sonic and propeller data sets are about equal in size at 200 m, but the sonic set has one-third more data at 100 m and four-thirds more data at 300 m. Considering omissions in the reference data, these completeness percentages resulted: AV, 83% to 91%; RAD, 55% to 88%; REM, 51% to 66%; XON, 75% to 84%.

5.1 Sodar Reference Differences

Values of sample bias (b), comparability (c), and standard deviation (s) and coefficient of variation (s') for the differences between sodar and reference values are presented in Table 5 for combined sodar observations at each height as well as for the sodar record of each vendor. Propeller wind speeds were excluded when the wind speed was less than 1 m/s.

The estimates of bias in Table 5 show mostly negative values at 100 m and a composite value near -0.4 m/s. Since the difference is taken as (sodar - reference), this means that the sodar systems tend to register too low. An exception is RAD, which does not have a significant bias at 100 m.

At 200 m, the vendors all record too high, and at 300 m, RAD and XON again record too high whereas AV is slightly negative and REM unbiased. Biases were computed for day (0600-1800 hours) and night (1800-0600 hours) values. Most differences between day and night are insignificant.

The comparability (c) of sodar wind speeds with reference values is also given in Table 5. Precision is represented by standard deviation (s) and percentage deviation (s'). The s' values range from about 15% to 35% around composite values near 25%.

5.2 Individual 20 Minute Average Values

Additional information about the characteristics of sodar measurements of S can be sought in the scatter diagrams of sodar 20 min average values plotted against reference values. Such plots are presented by height and by vendor in Figs. 25-36.

Each chart has a broken line at 45° from the origin representing a slope

of 1. The estimates of the correlation coefficient, slope, and intercept are given in Table 6.

The agreement between sodar and tower wind speed measurements is obviously quite good. Differences between manufacturers can be deduced by the reader.

5.3 Sodar Modes

A comparison between RAD modal data and corresponding 20 min reference averages yields the b, c, and s results of Table 7. The monostatic mode had significantly higher bias than the other two modes at all heights.

The comparability and standard deviation show a distinct advantage to the bistatic mode; MONO has the greatest magnitudes of c at 200 m and 300 m, and MULTI has the greatest magnitudes of s at 100 m and 300 m.

Table 5. Sodar wind speed compared with reference wind speed

Height	Vendor	b (m/s)	c (m/s)	s (m/s)	s'(%)	N
100 m	All	-0.42	1.28	1.21	28	1179
	AV	-0.50	1.03	0.90	21	327
	RAD	0.02	1.18	1.18	28	315
	REM	-0.12	0.62	0.60	14	236
	XON	-1.04	1.88	1.56	37	301
200 m	All	0.14	0.98	0.96	23	1019
	AV	0.05	0.72	0.72	17	298
	RAD	0.31	1.00	1.47	35	258
	REM	0.12	0.73	0.72	17	194
	XON	0.09	0.71	0.70	17	269
300 m	All	0.16	1.24	1.23	27	1005
	AV	-0.10	1.15	1.15	25	328
	RAD	0.29	1.71	1.69	37	198
	REM	0.02	0.74	0.74	17	183
	XON	0.44	1.20	1.12	25	296

b = bias (accuracy)
c = comparability
s = standard deviation of differences (precision)
s' = s expressed as a percentage of average value of reference wind speed
N = number of observations

AV = Aerovironment
RAD = Radian
REM = Remtech
XON = Xontech

Table 6. Regression analysis for wind speed

Height	Vendor	ρ	β_0	β_1	N
100 m	AV	0.94	-0.03	0.89	327
	RAD	0.90	0.41	0.91	315
	REM	0.97	-0.22	1.02	236
	XON	0.82	-0.07	0.77	301
200 m	AV	0.96	-0.02	1.02	298
	RAD	0.87	0.04	1.07	258
	REM	0.96	0.34	0.95	194
	XON	0.96	0.02	1.01	269
300 m	AV	0.93	0.45	0.88	328
	RAD	0.85	1.02	0.84	198
	REM	0.96	0.18	0.96	183
	XON	0.93	0.46	0.97	296

ρ = estimate of correlation coefficient
β_0 = intercept term
β_1 = slope term
N = number of observations

Table 7. Sodar Radian modes: Accuracy and precision for wind speed

Height	Mode	b (m/s)	c (m/s)	s (m/s)	N
100 m	BI	-0.15	0.56	0.54	90
	MULTI	-0.10	1.54	1.53	128
	MONO	0.31	1.18	1.04	97
200 m	BI	-0.01	0.90	0.90	78
	MULTI	0.27	1.64	1.62	110
	MONO	0.74	1.79	1.63	70
300 m	BI	0.08	1.26	1.26	66
	MULTI	0.12	1.89	1.88	92
	MONO	1.01	1.96	1.68	40

b = bias (accuracy)
c = comparability
s = standard deviation of differences (precision)
N = number of observations

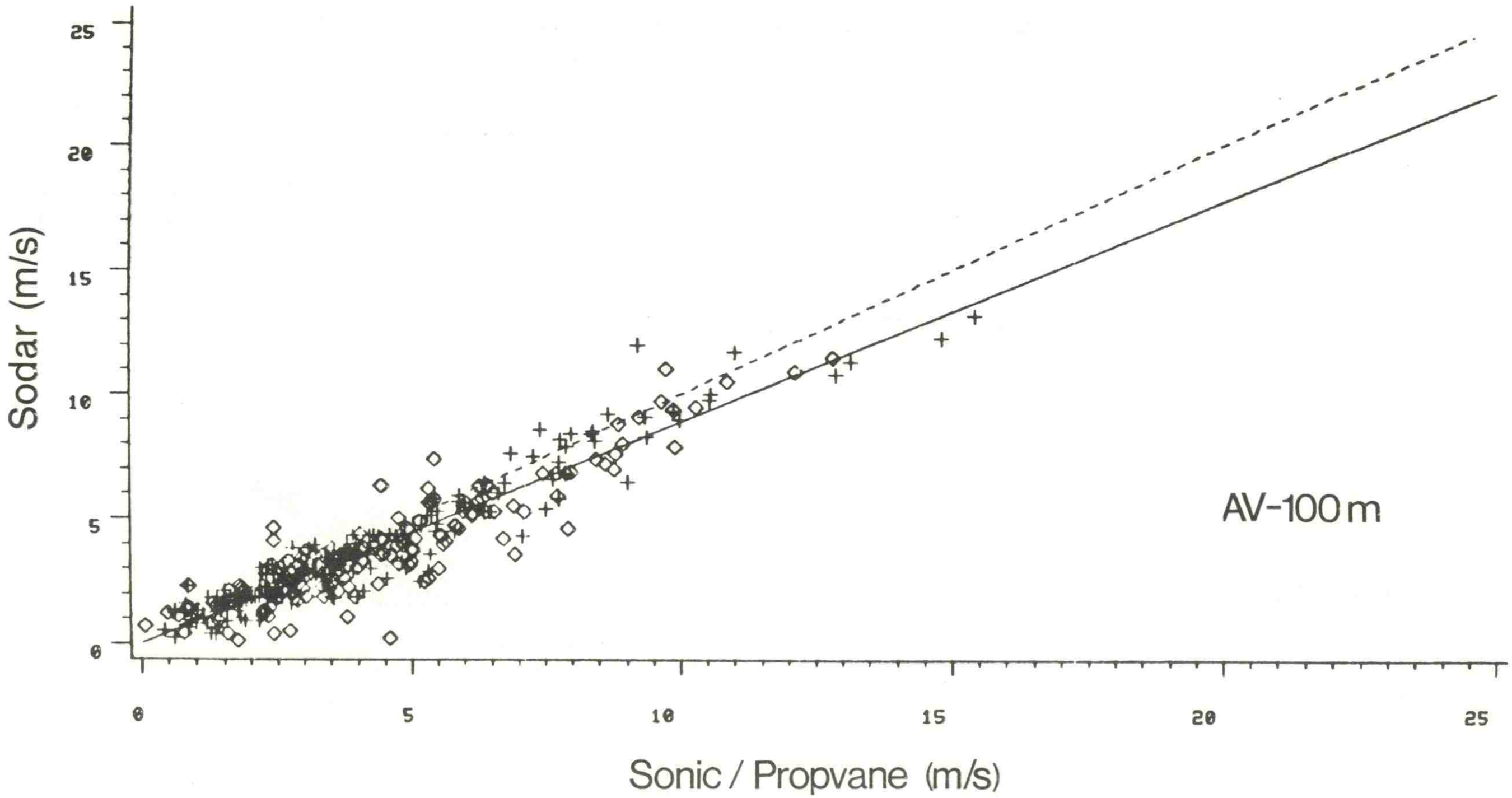

Figure 25. Comparison of 100 m wind speeds from AV sodar and BAO sensors.

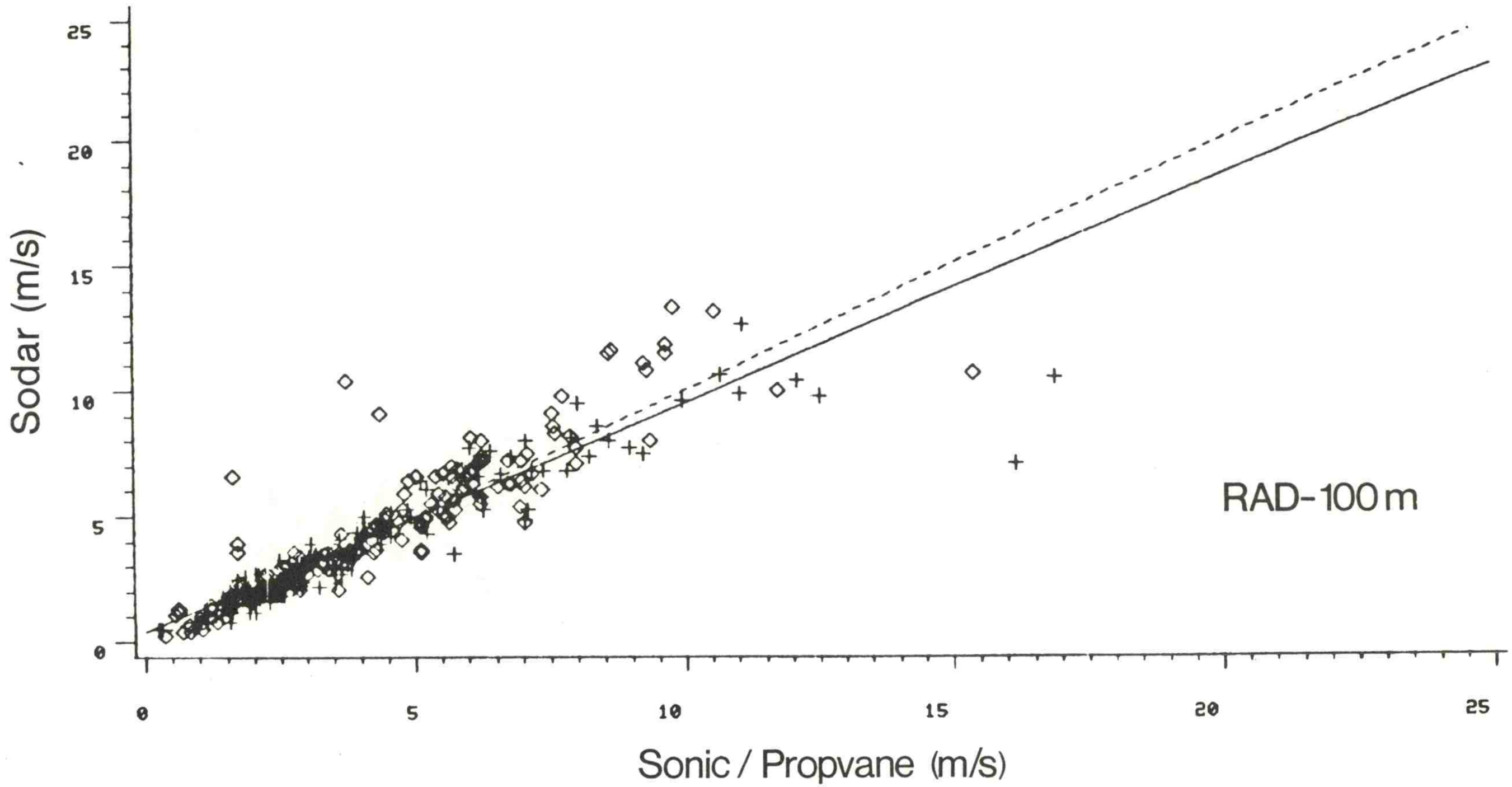

REGRESSION LINE ————————
DAY TIME OBSERVATIONS +
NIGHT TIME OBSERVATIONS ◇
INTERCEPT=0 AND SLOPE=1 (45 ANGLE) LINE -------

Figure 26. Comparison of 100 m wind speeds from RAD sodar and BAO sensors.

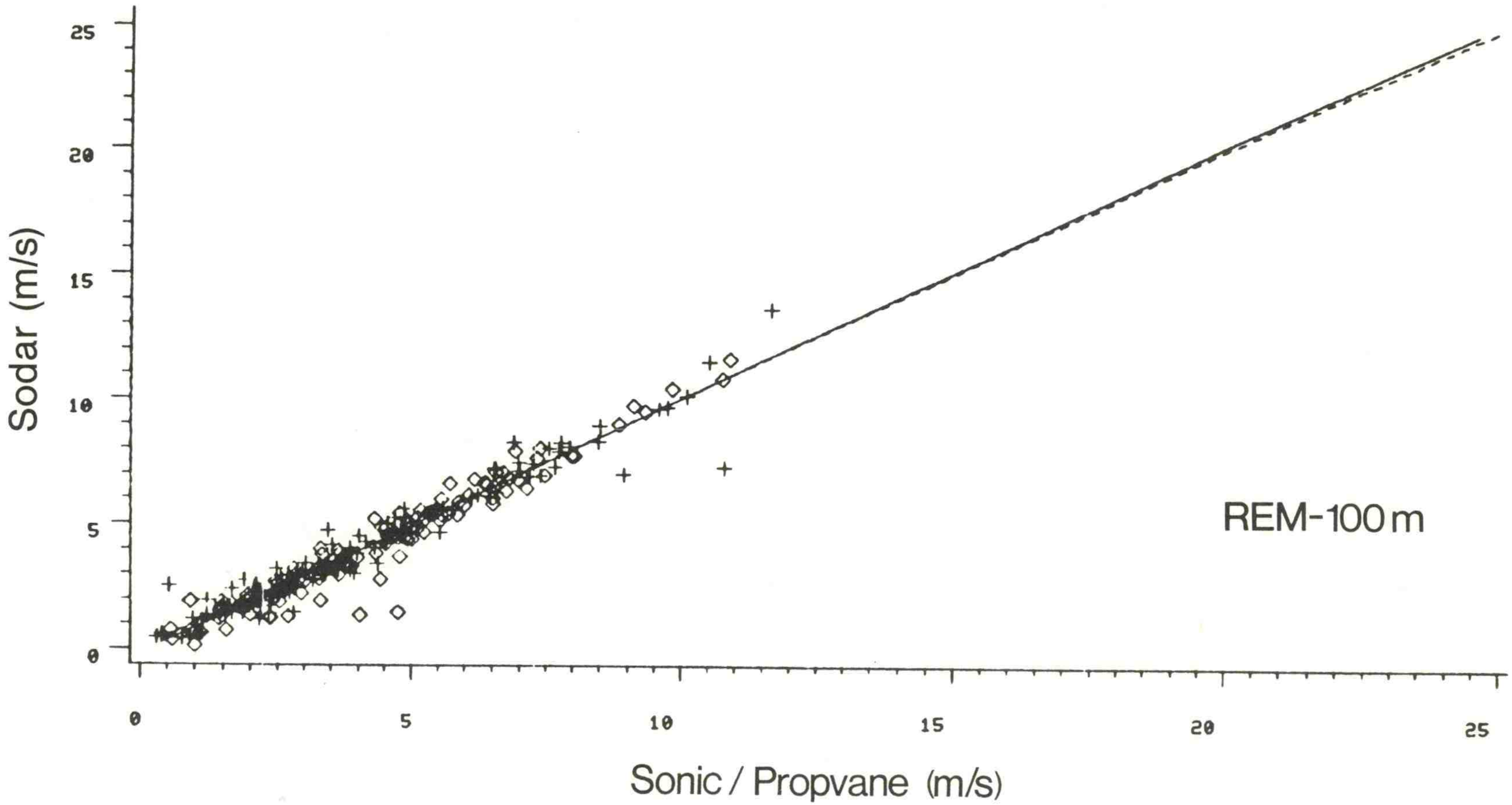

Figure 27. Comparison of 100 m wind speeds from REM sodar and sensors.

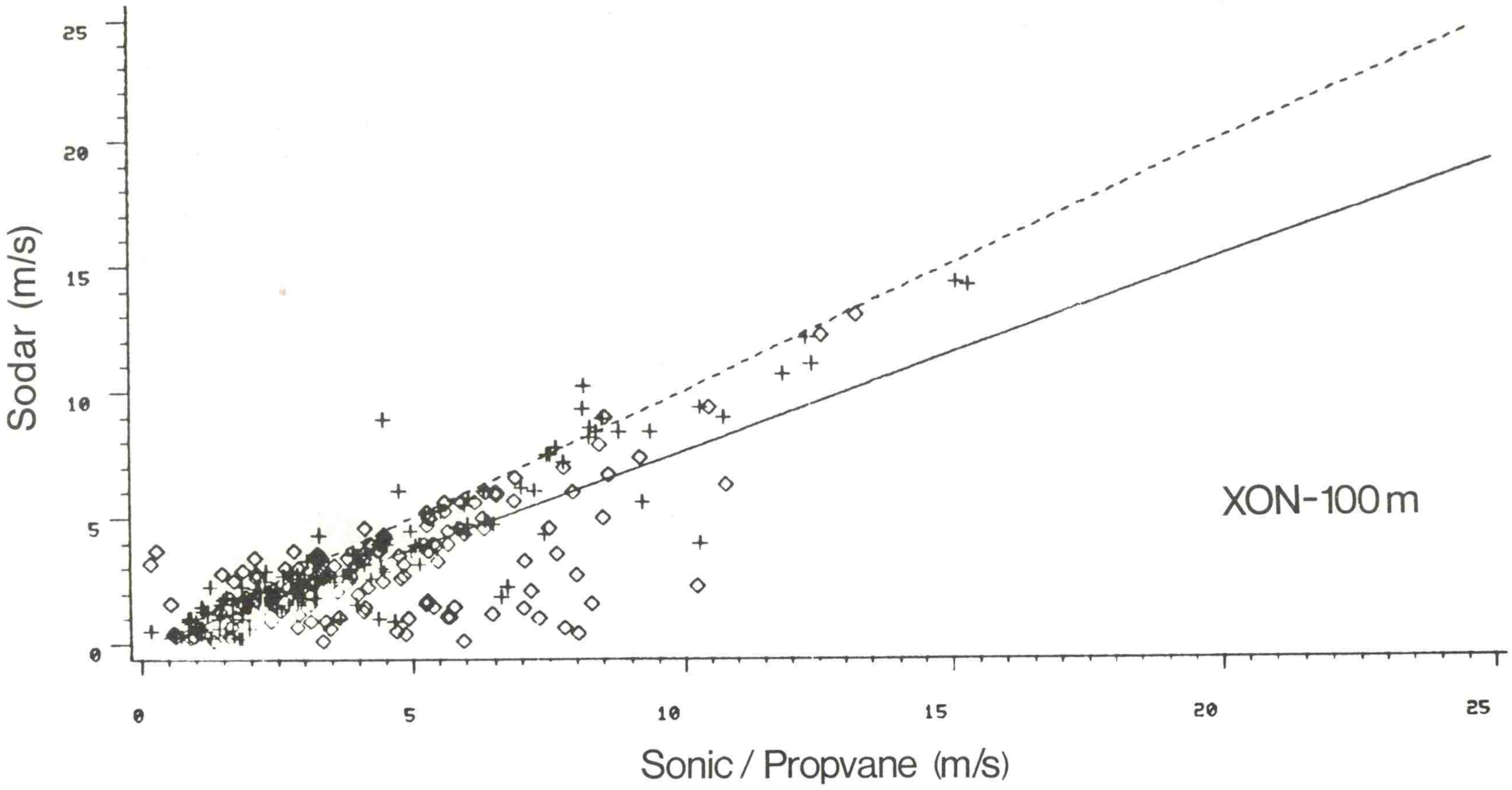

Figure 28. Comparison of 100 m wind speeds from XON sodar and BAO sensors.

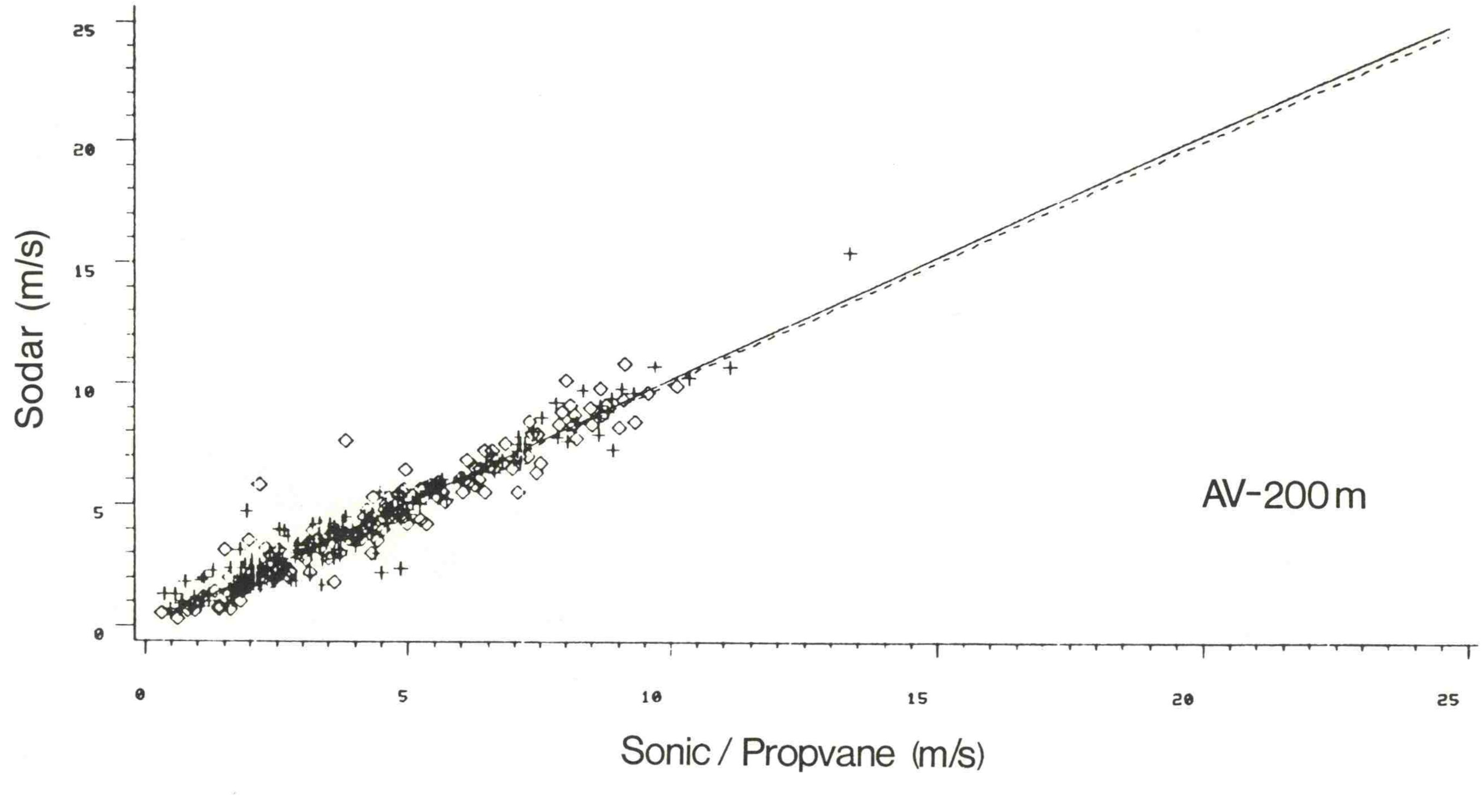

Figure 29. Comparison of 200 m wind speeds from AV sodar and BAO sensors.

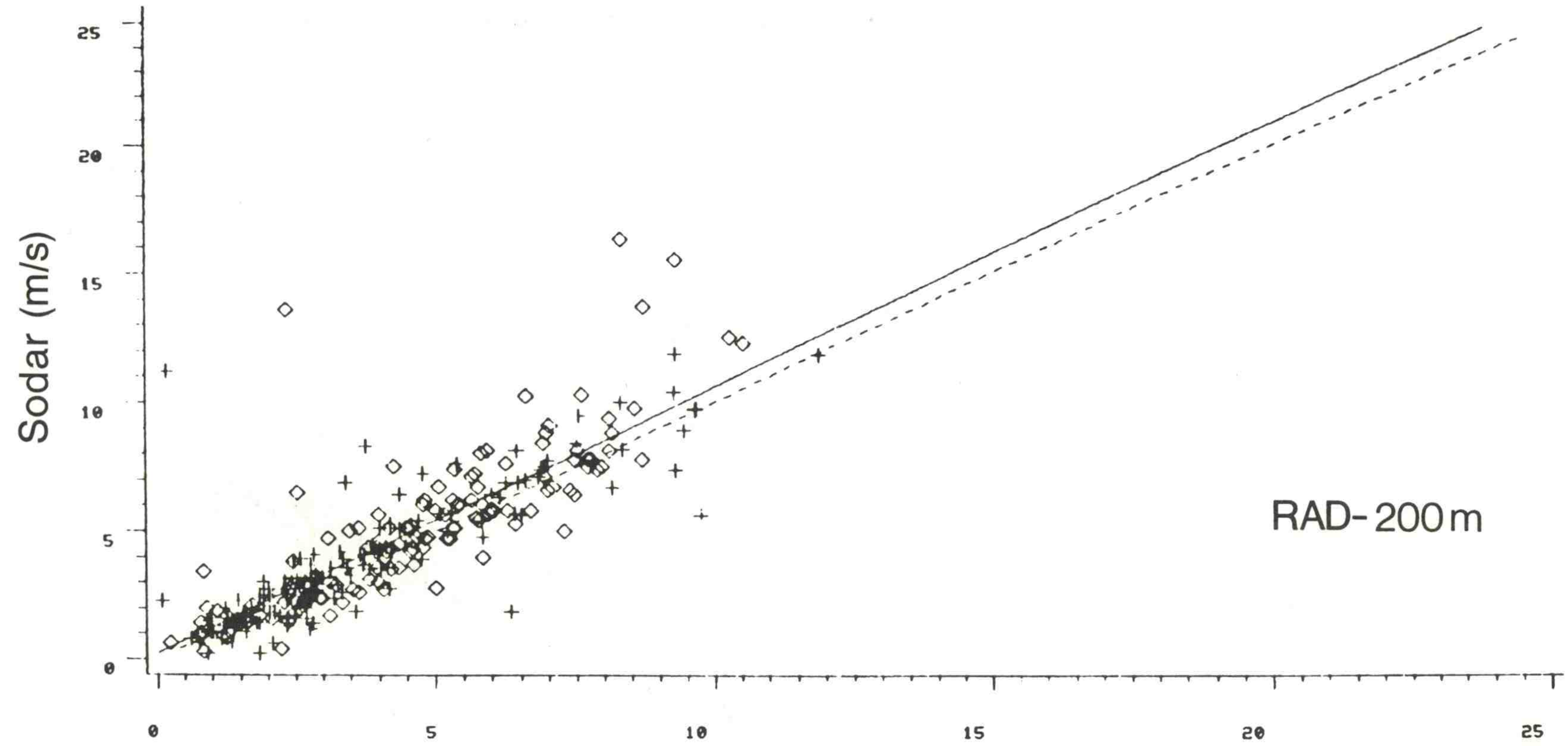

Figure 30. Comparison of 200 m wind speeds from RAD sodar and BAO sensors.

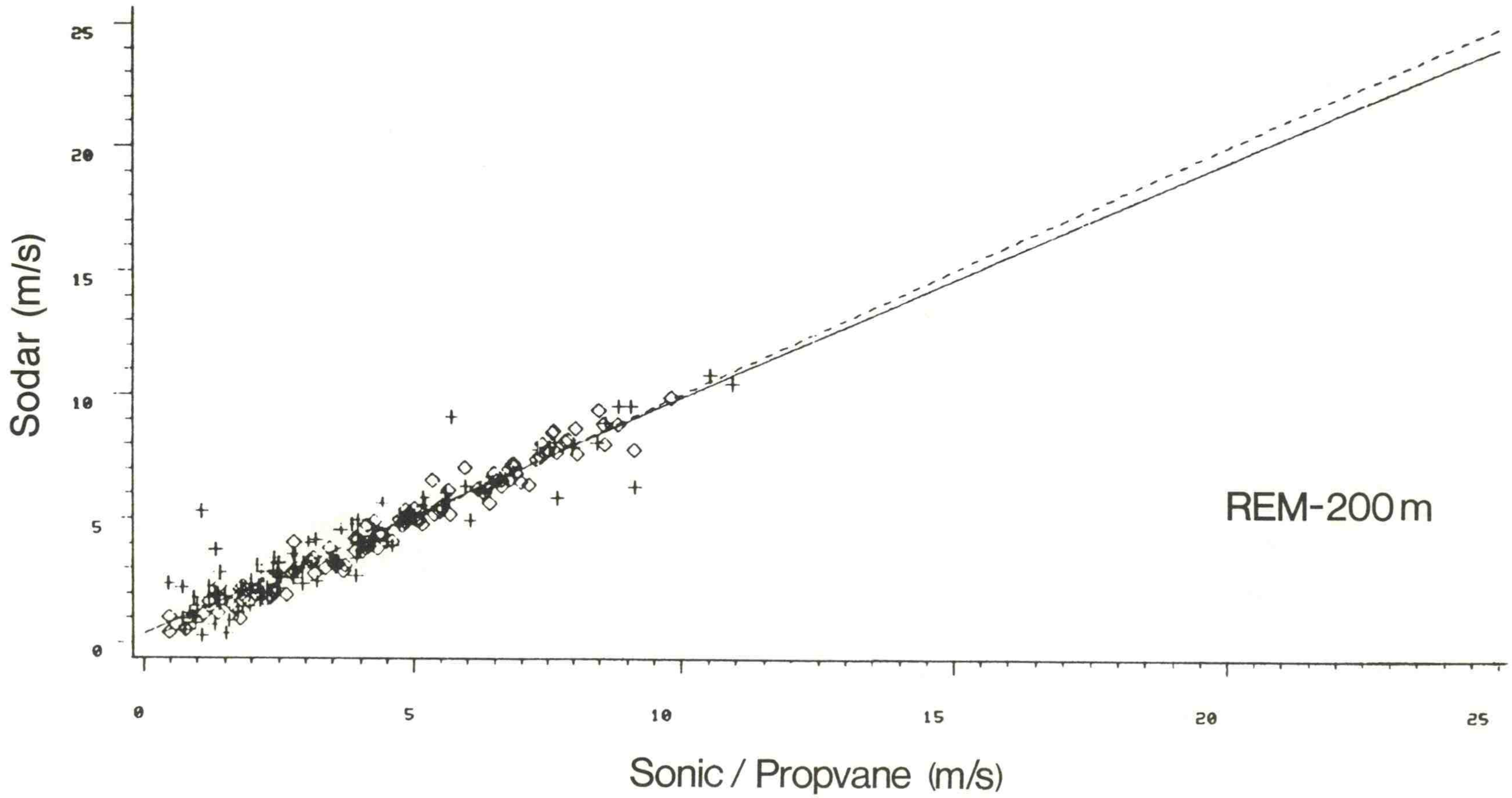

Figure 31. Comparison of 200 m wind speeds from REM sodar and BAO sensors.

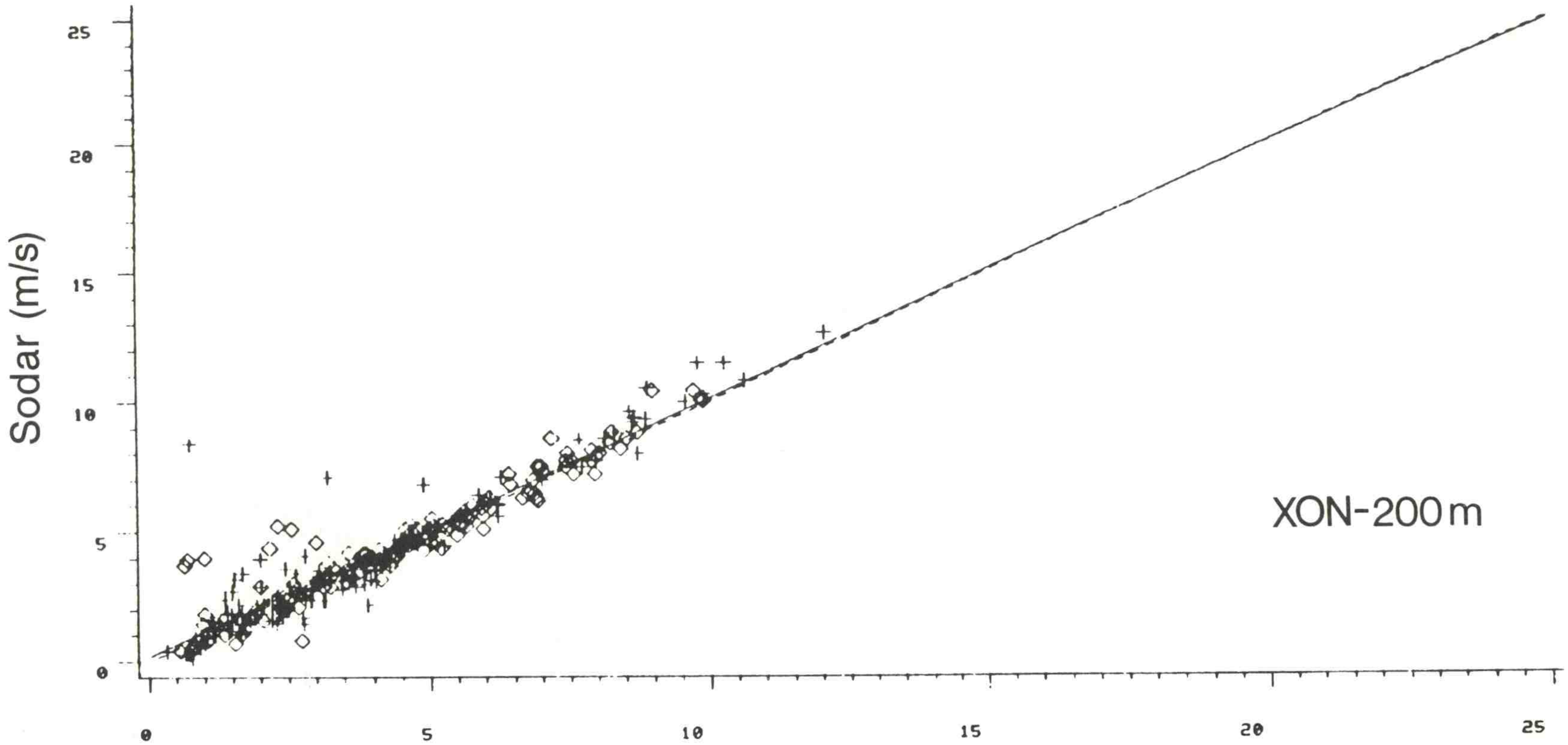

REGRESSION LINE ————————

DAY TIME OBSERVATIONS +

NIGHT TIME OBSERVATIONS ◇

INTERCEPT=0 AND SLOPE=1 (45° ANGLE) LINE -------

Figure 32. Comparison of 200 m wind speeds from XON sodar and BAO sensors.

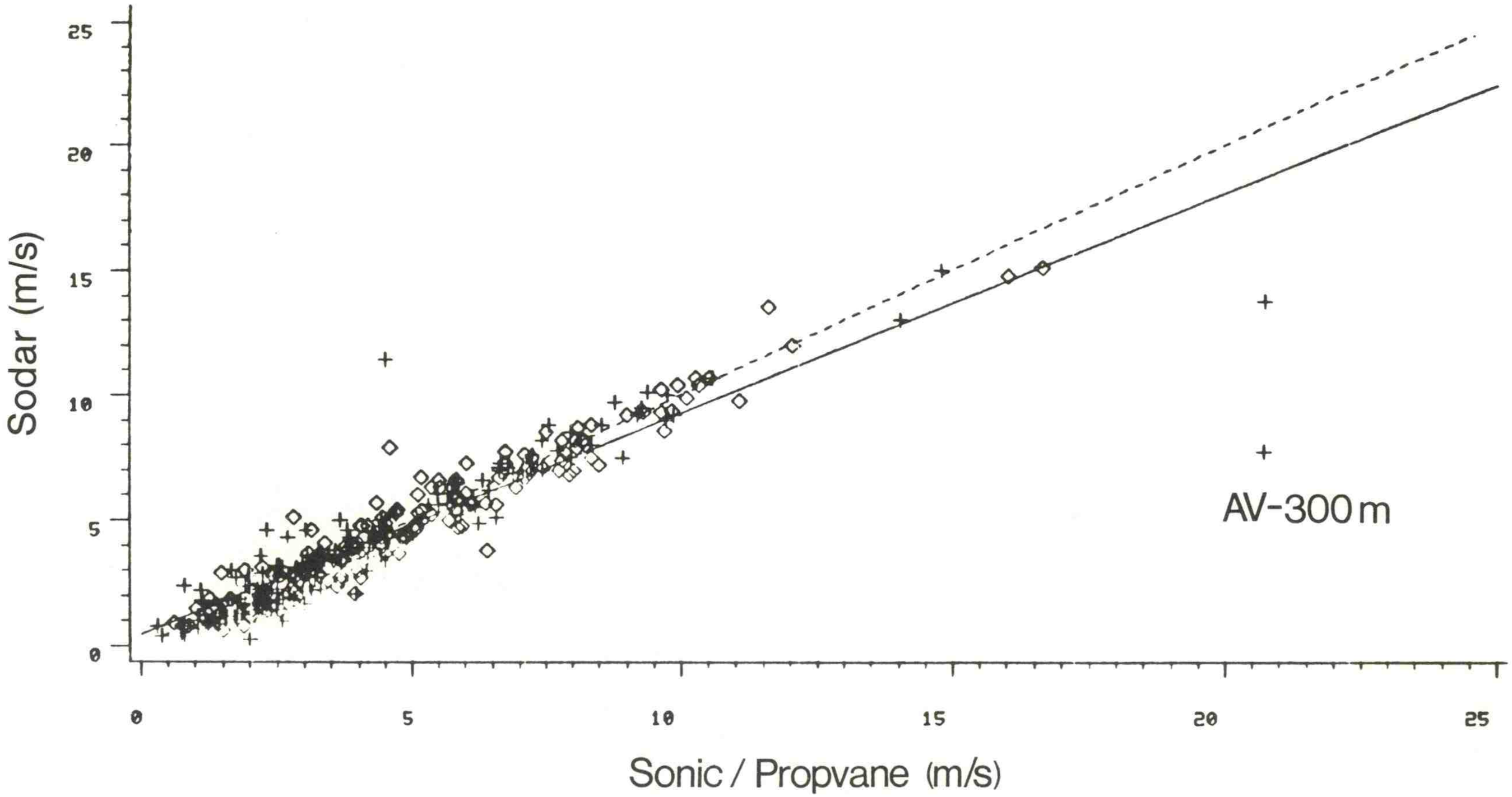

REGRESSION LINE ————————
DAY TIME OBSERVATIONS +
NIGHT TIME OBSERVATIONS ◇
INTERCEPT=0 AND SLOPE=1 (45 ANGLE) LINE -------

Figure 33. Comparison of 300 m wind speeds from AV sodar and BAO sensors.

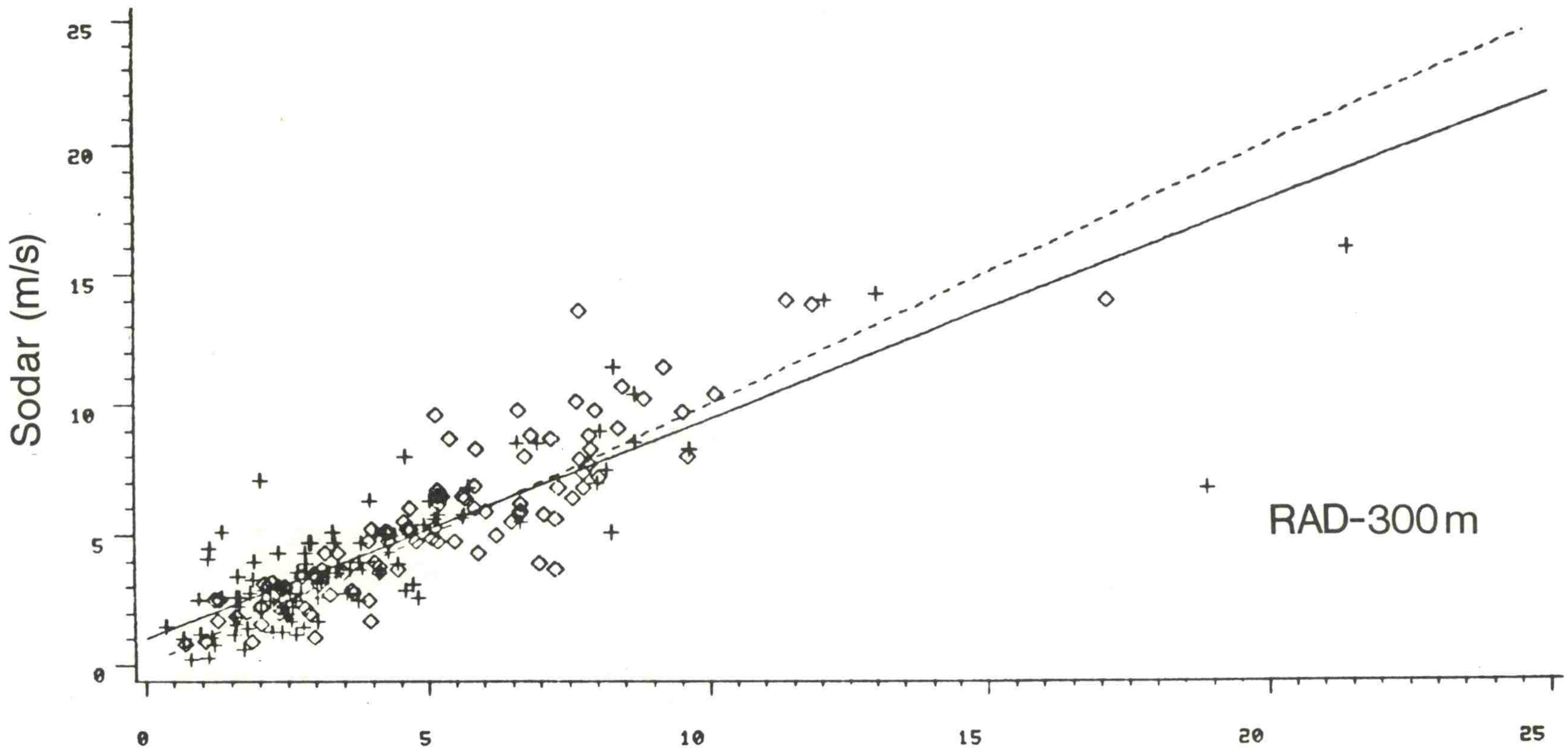

Figure 34. Comparison of 300 m wind speeds from RAD sodar and BAO sensors.

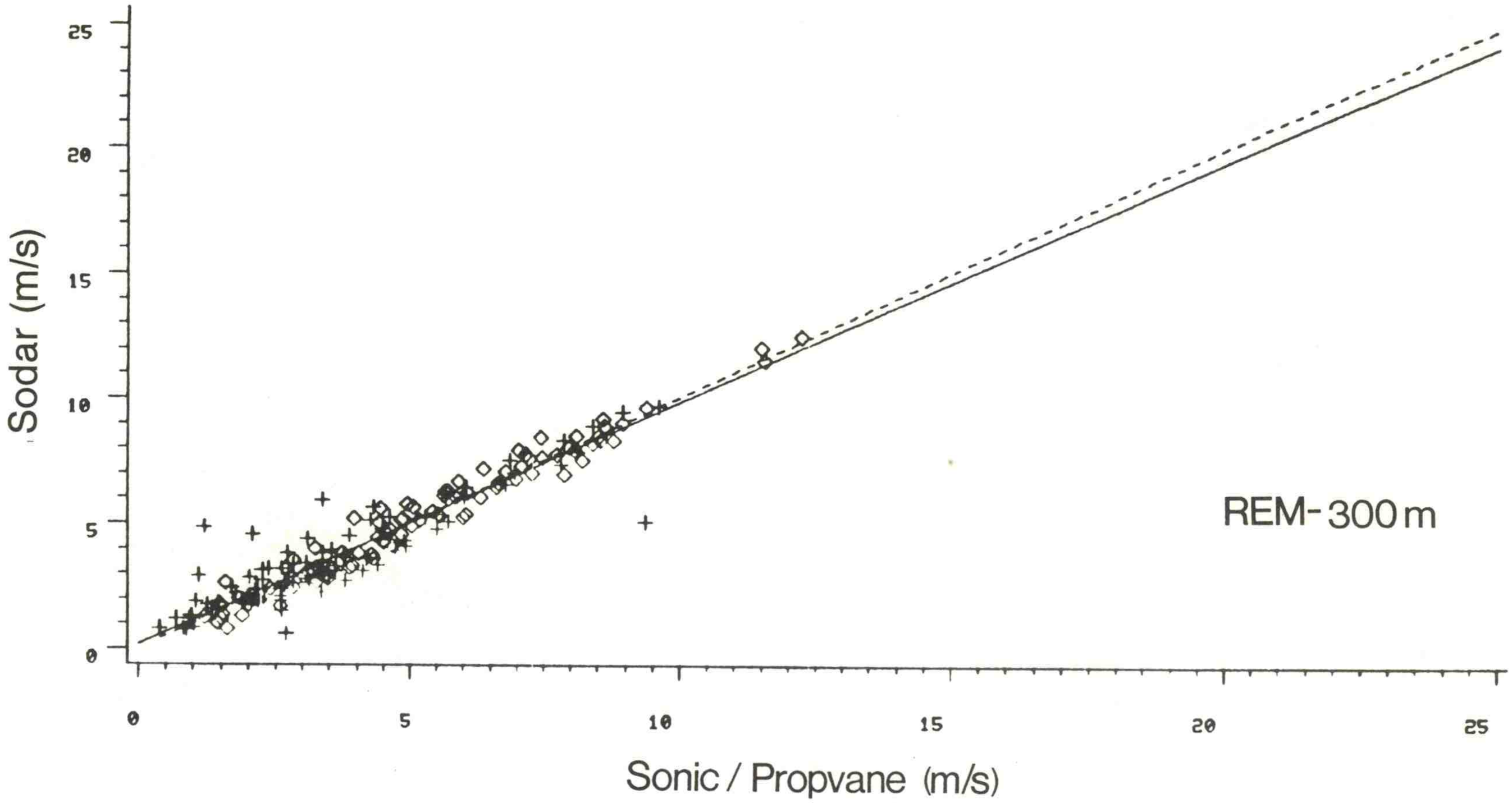

Figure 35. Comparison of 300 m wind speeds from REM sodar and BAO sensors.

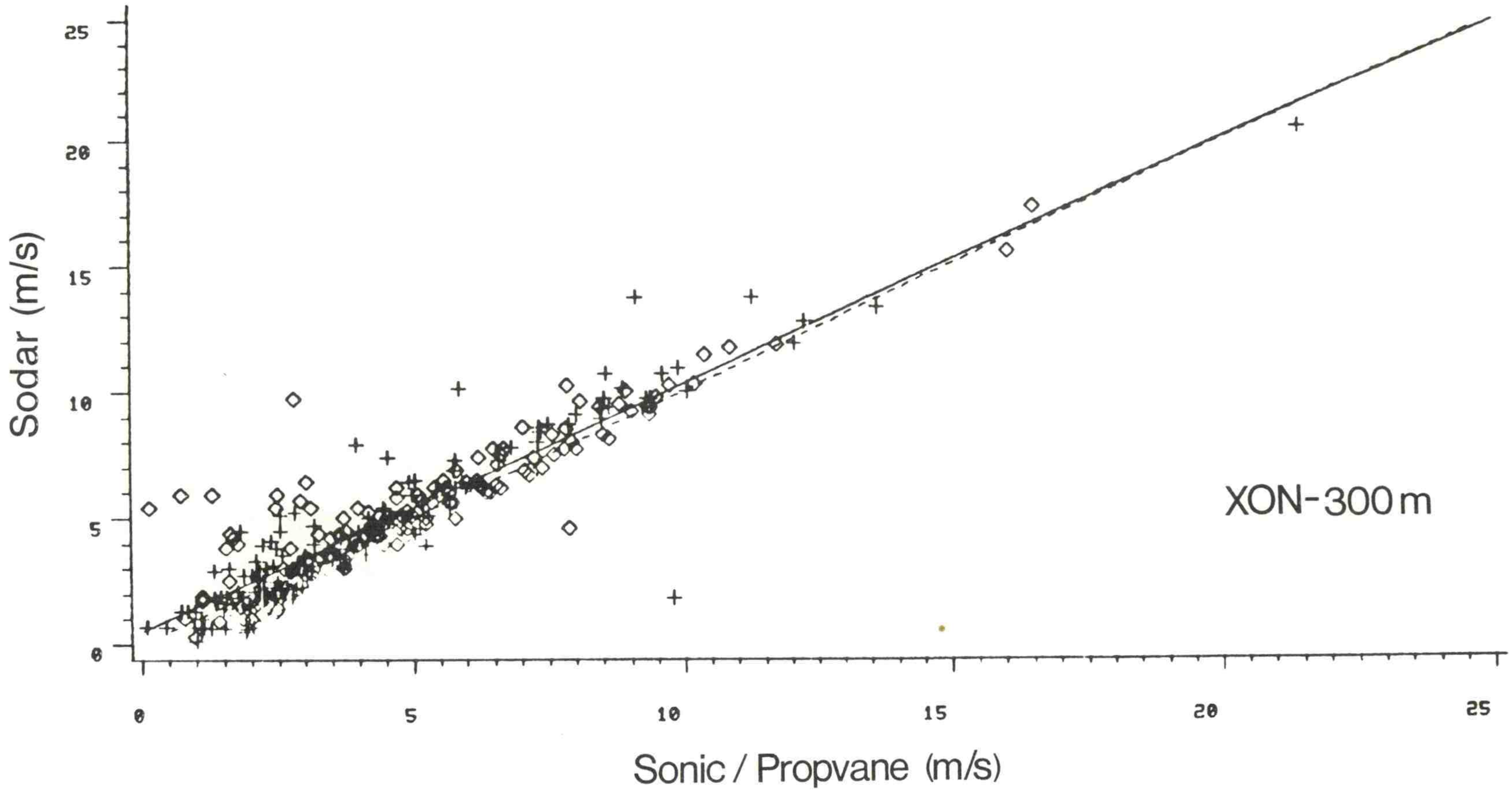

REGRESSION LINE ————————
DAY TIME OBSERVATIONS +
NIGHT TIME OBSERVATIONS ◇
INTERCEPT=0 AND SLOPE=1 (45 ANGLE) LINE -------

Figure 36. Comparison of 300 m wind speeds from XON sodar and BAO sensors.

6. MEASUREMENT OF WIND DIRECTION

All four sodar vendors reported wind direction (D). At the three heights under consideration (100 m, 200 m, 300 m), AV had complete data, and the other manufacturers ranged in completeness as follows: RAD, 60% to 96%; REM, 55% to 72%; XON, 91% to 92%. However, the wind shadow zone mentioned in Sec. 4 limited the amount of data that could be used. An investigation of the propeller-vane data indicated that they could not be substituted as reference values for wind direction. There were unexplained disparities between the propeller and sonic data that are still under investigation. Because sonic data showed more consistent behavior and we therefore believe them to be more reliable, only the sonic wind direction measurements are used as reference data, resulting in these completeness percentages for sodar/sonic differences: AV, 43% to 63%; RAD, 36% to 49%; REM, 31% to 39%; XON, 36% to 55%.

6.1 Sodar Reference Differences

Values of sample bias (b), comparability (c), and standard deviation (s) for the differences between sodar and sonic reference values are presented in Table 8 for combined sodar observations at each height as well as for the sodar record of each vendor.

The values of bias in Table 8 show negative values at 100 m and 200 m for all vendors, but positive values at 300 m for all vendors except for RAD. However, most of these values are not significantly different from zero, con-

sidering the variability of the wind direction and the number of cases included. Day and night biases given in Table 9 show some differences, but for the most part they are not statistically significant.

The comparability (c) of sodar wind direction with sonic reference values is also given in Table 8. The low values at 200 m may be due to the loss of data at that height during a storm on 13 September. Considering the scatter in data, it can be assumed that the vendors' measurements of wind directions are equivalent to each other.

6.2 Individual 20 Minute Averaged Values

Scatter diagrams of 20 min averaged sodar values plotted against reference values are given in Figs. 37-48. For the most part, each sodar datum agreed with the tower datum quite well. There were some notable exceptions, however, especially during the night. XON seems to have predicted many more north winds than actually occurred at 100 m and 300 m, but its agreement at 200 m is very good.

From the figures it seems that most of the vendors predicted more northerly winds at night at 100 m than actually occurred, especially when the tower measured winds from the east and south. This does not seem to be the case at 200 m or 300 m and may be due to local terrain effects, rather than instrument problems.

Correlation coefficients are given in Table 10, with intercepts and slopes of the linear regression lines. With two exceptions, ρ values are 0.9 or greater.

6.3 Sodar Modes

The three modes of operation for the RAD system showed no appreciable difference in their ability to measure wind direction.

Table 8. Sodar wind direction compared with sonic wind direction

Height	Vendor	b (deg)	c (deg)	s (deg)	N
100 m	All	-4.41	28.59	28.25	667
	AV	-3.87	26.70	26.41	187
	RAD	-6.76	27.06	26.20	177
	REM	-2.03	18.51	18.40	137
	XON	-4.49	37.85	37.58	166
200 m	All	-3.43	23.22	22.97	523
	AV	-0.79	19.47	19.45	155
	RAD	-7.86	25.67	24.43	128
	REM	-3.89	24.67	24.36	110
	XON	-1.85	23.80	23.73	130
300 m	All	0.75	29.59	29.58	697
	AV	0.26	28.56	28.56	227
	RAD	-3.25	29.98	29.80	131
	REM	0.62	19.70	19.69	142
	XON	4.05	35.96	35.73	197

b = bias (accuracy)
c = comparability
s = standard deviation of differences (precision)
N = number of observations

Table 9. Test of day versus night wind direction bias

Height	Vendor	b (day)	b (night)	N (day)	N (night)
100 m	All	-6.23	-2.11	373	294
	AV	-6.81	0.53	112	75
	RAD	-8.24	-5.20	91	86
	REM	-3.13	-0.66	76	61
	XON	-6.09	-2.41	94	72
200 m	All	-5.75	-0.84	94	72
	AV	-1.48	0.06	86	69
	RAD	-11.31	-4.19	66	62
	REM	-5.25	-2.43	57	53
	XON	-6.18	2.89	68	62
300 m	All	-0.44	2.24	388	309
	AV	-1.01	2.00	131	96
	RAD	-2.42	-4.20	70	61
	REM	-0.13	1.49	76	66
	XON	1.26	7.66	111	86

Table 10. Regression analysis for wind direction

Height	Vendor	ρ	β_0	β_1	N
100 m	AV	0.94	-0.25	0.98	187
	RAD	0.92	5.20	0.94	177
	REM	0.96	4.26	0.98	137
	XON	0.85	8.29	0.96	166
200 m	AV	0.97	8.15	0.95	155
	RAD	0.90	14.07	0.90	128
	REM	0.93	16.72	0.91	110
	XON	0.95	2.37	0.98	130
300 m	AV	0.93	-5.86	1.05	227
	RAD	0.93	-8.87	1.03	131
	REM	0.97	-4.64	1.03	142
	XON	0.89	-8.79	1.09	197

ρ = estimate of correlation coefficient

β_0 = intercept term

β_1 = slope term

N = number of observations

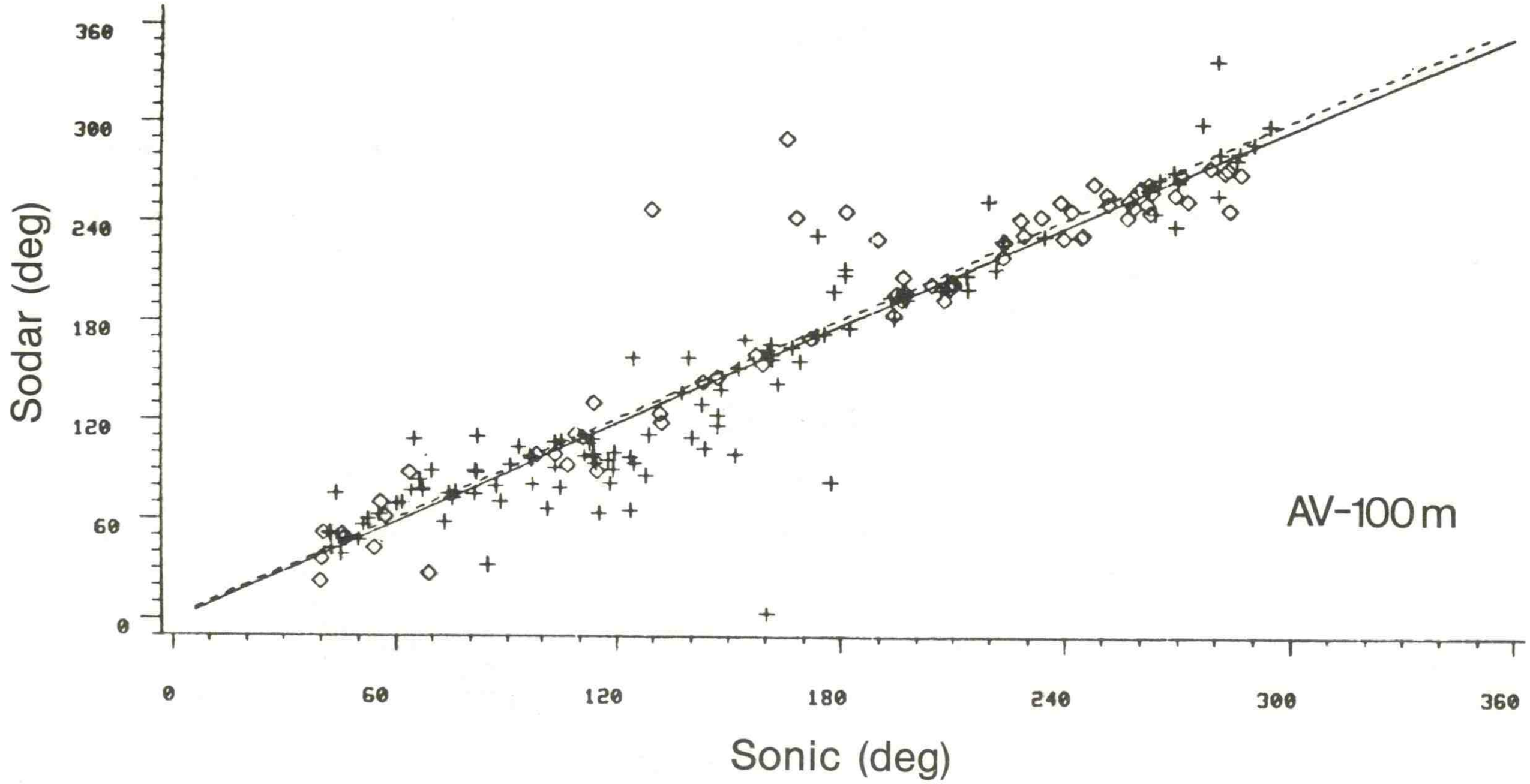

REGRESSION LINE ————————
DAY TIME OBSERVATIONS +
NIGHT TIME OBSERVATIONS ◇
INTERCEPT=0 AND SLOPE=1 (45° ANGLE) LINE -------

Figure 37. Comparison of 100 m wind directions from AV sodar and BAO sensors.

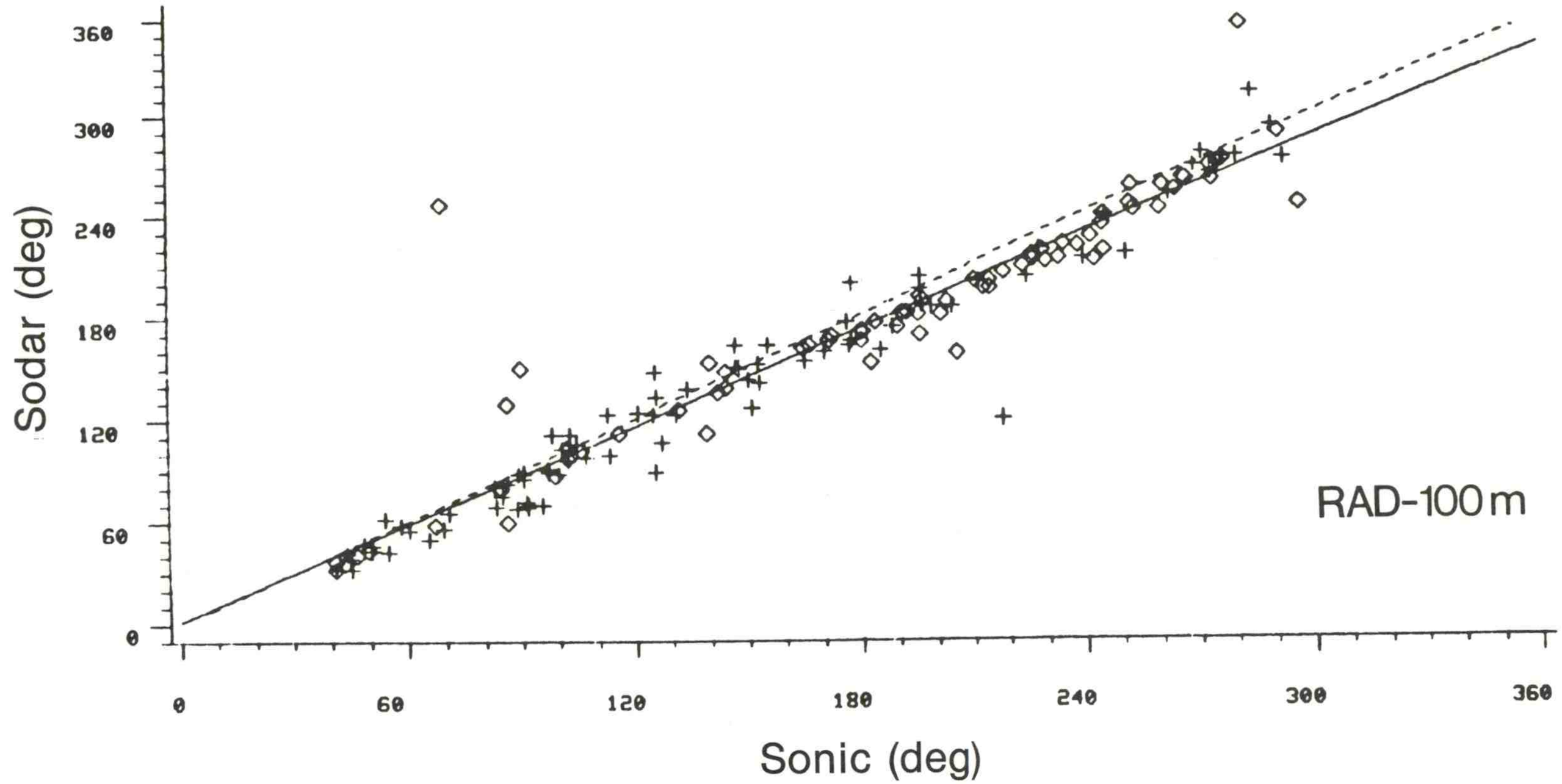

REGRESSION LINE ————————
DAY TIME OBSERVATIONS +
NIGHT TIME OBSERVATIONS ◇
INTERCEPT=0 AND SLOPE=1 (45° ANGLE) LINE -------

Figure 38. Comparison of 100 m wind directions from RAD sodar and BAO sensors.

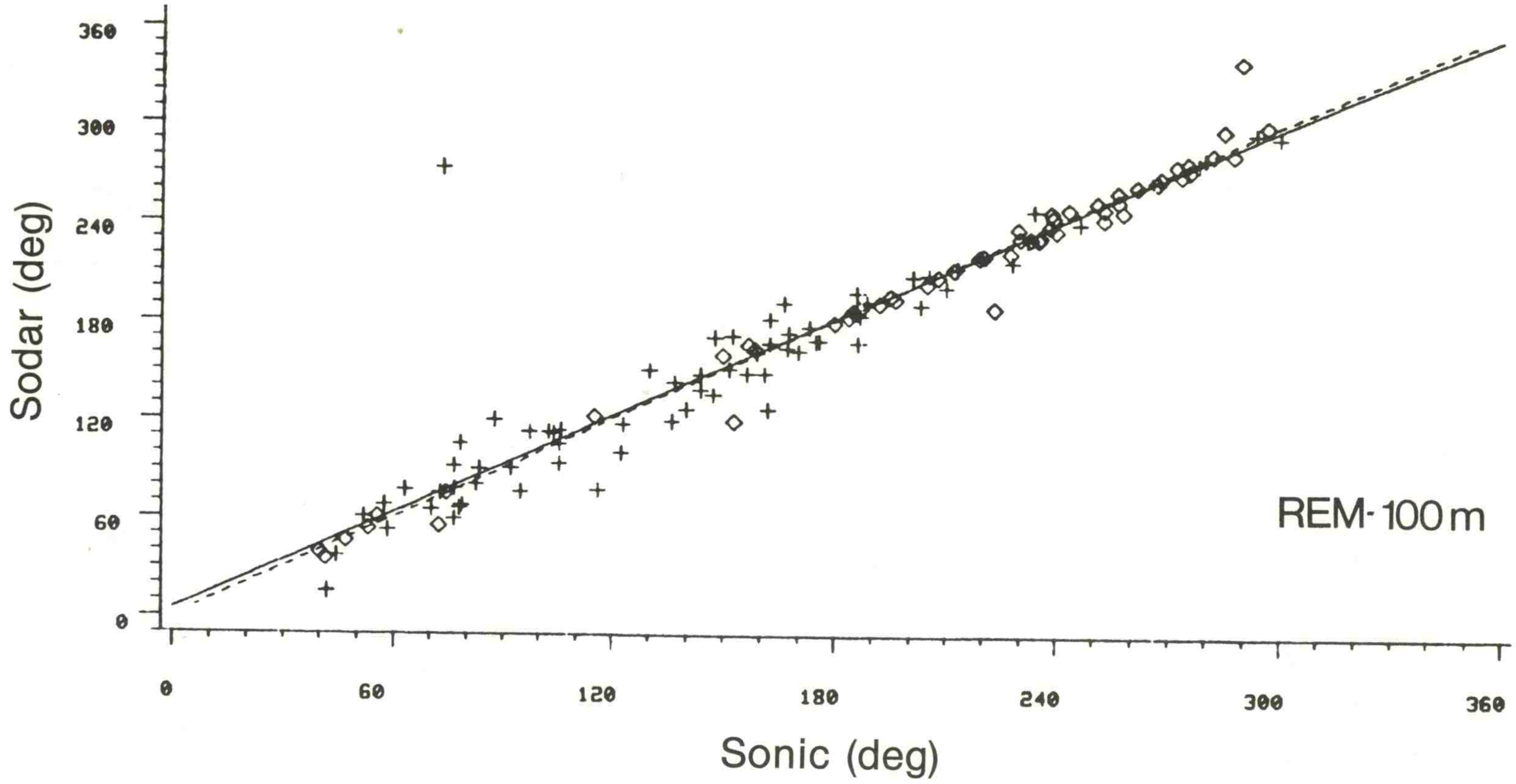

REGRESSION LINE ————————————

DAY TIME OBSERVATIONS +

NIGHT TIME OBSERVATIONS ◇

INTERCEPT=0 AND SLOPE=1 (45° ANGLE) LINE -------

Figure 39. Comparison of 100 m wind directions from REM sodar and BAO sensors.

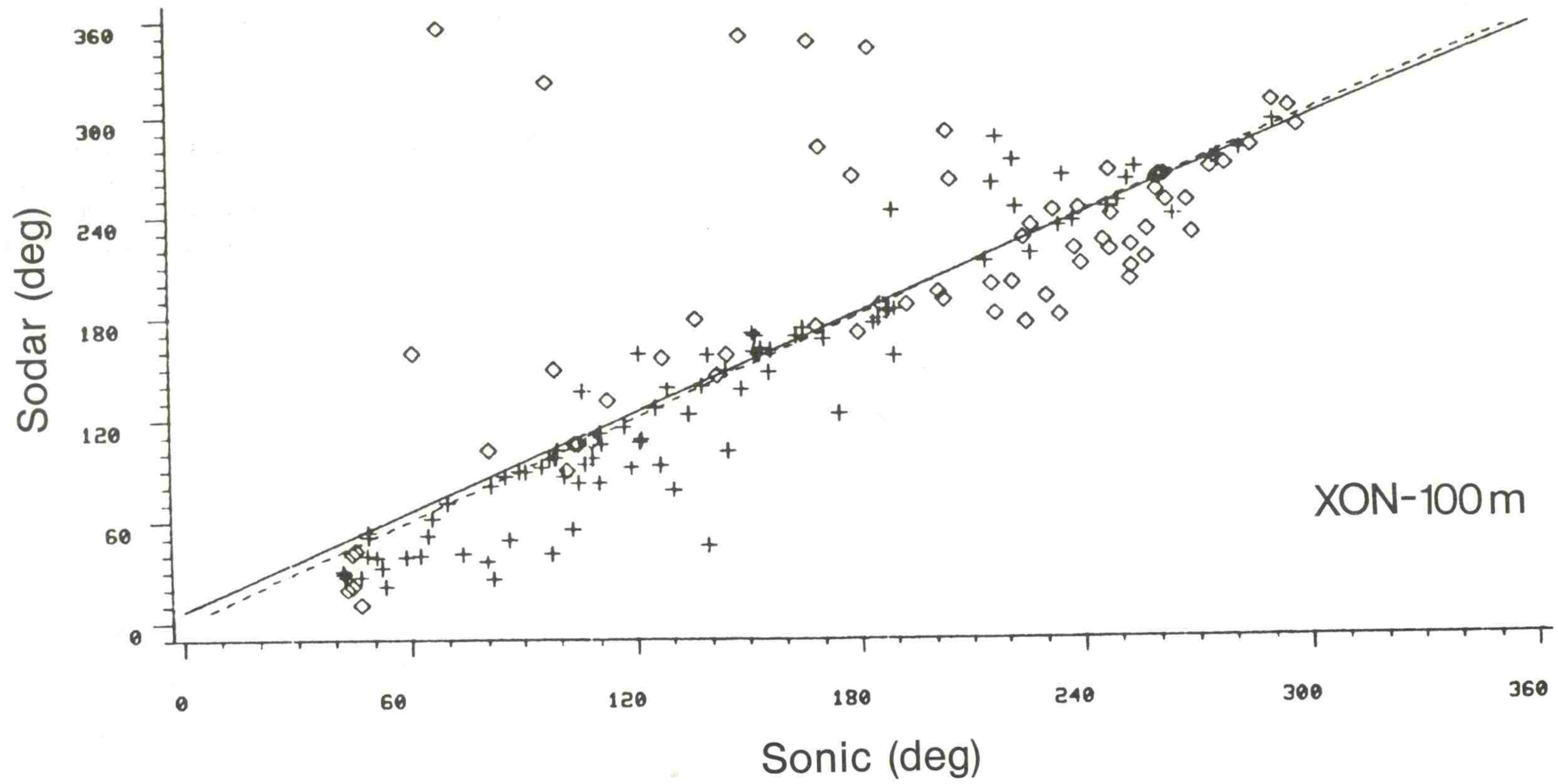

REGRESSION LINE ————————

DAY TIME OBSERVATIONS +

NIGHT TIME OBSERVATIONS ◇

INTERCEPT=0 AND SLOPE=1 (45° ANGLE) LINE --------

Figure 40. Comparison of 100 m wind directions from XON sodar and BAO sensors.

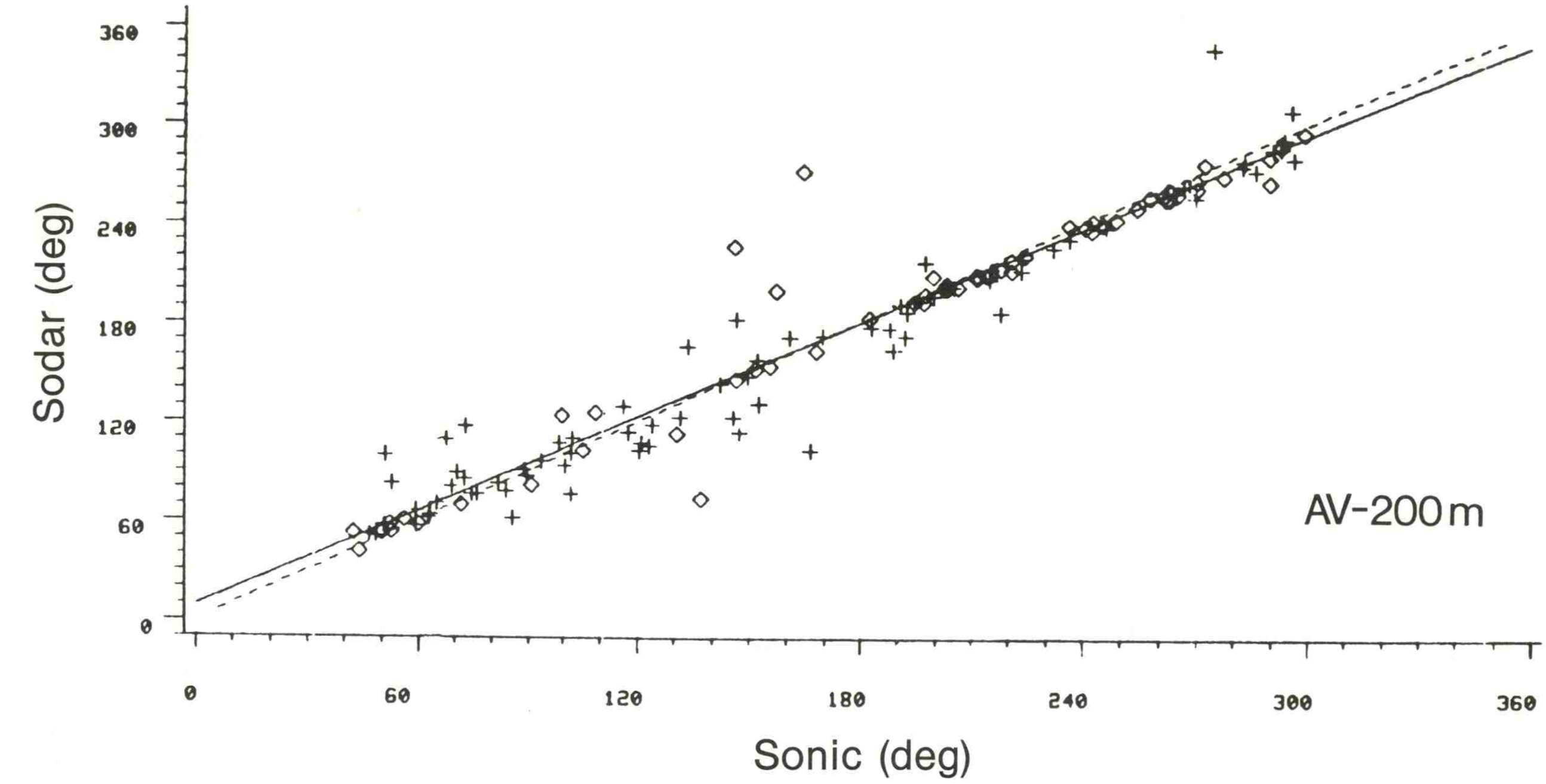

REGRESSION LINE ————————
DAY TIME OBSERVATIONS +
NIGHT TIME OBSERVATIONS ◇
INTERCEPT=0 AND SLOPE=1 (45° ANGLE) LINE -------

Figure 41. Comparison of 200 m wind directions from AV sodar and BAO sensors.

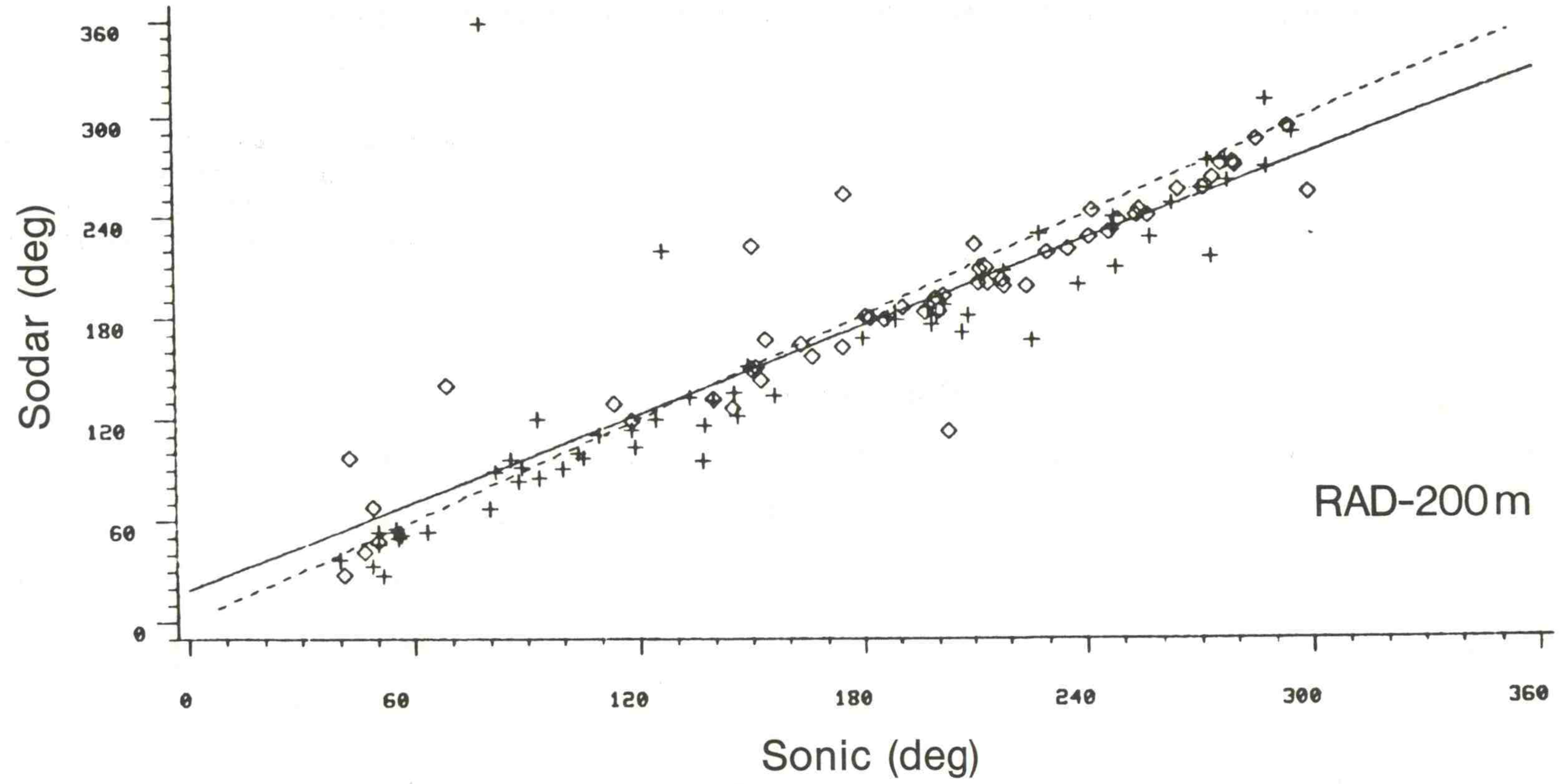

Figure 42. Comparison of 200 m wind directions from RAD sodar and BAO sensors.

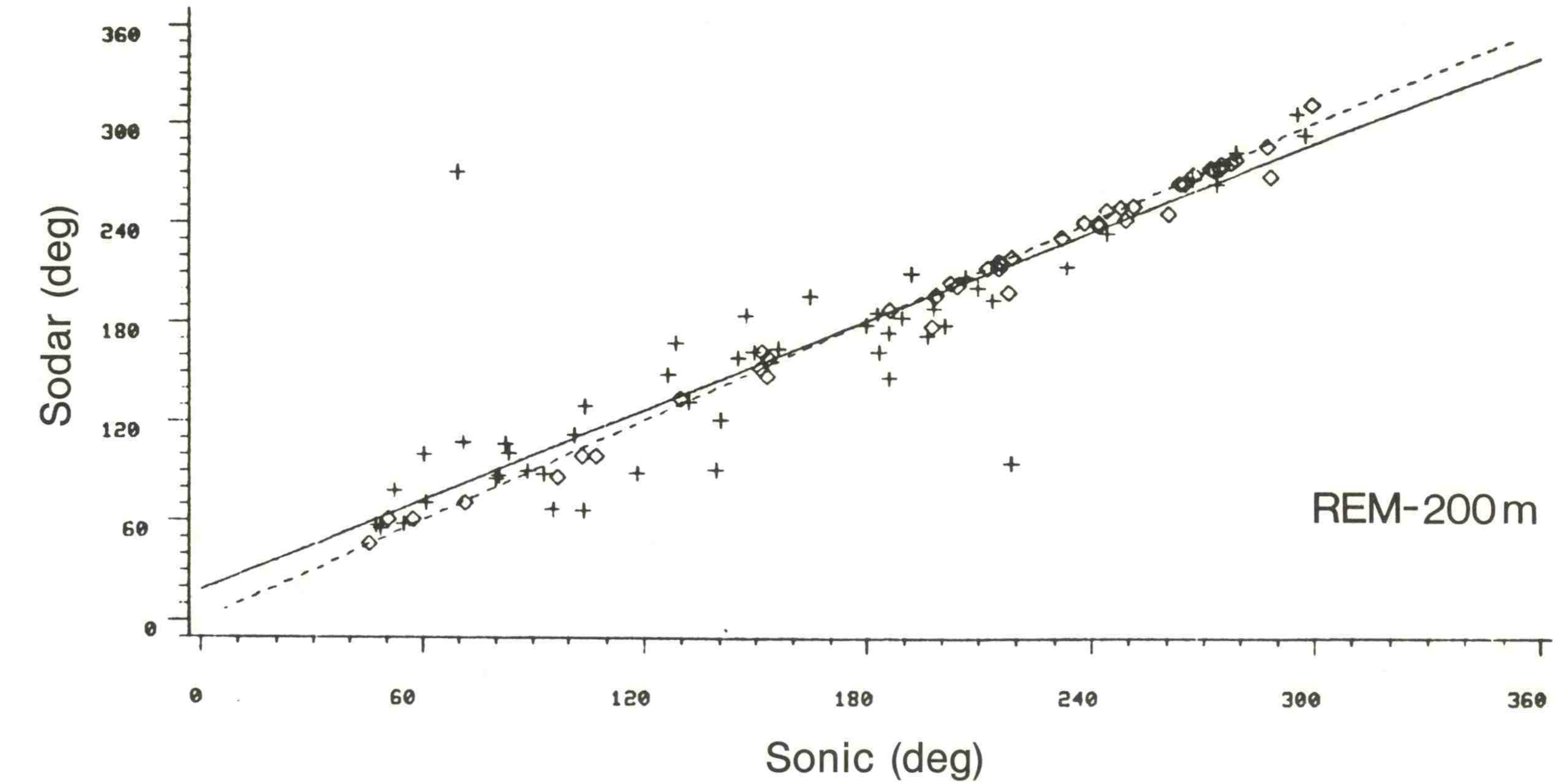

Figure 43. Comparison of 200 m wind directions from REM sodar and BAO sensors.

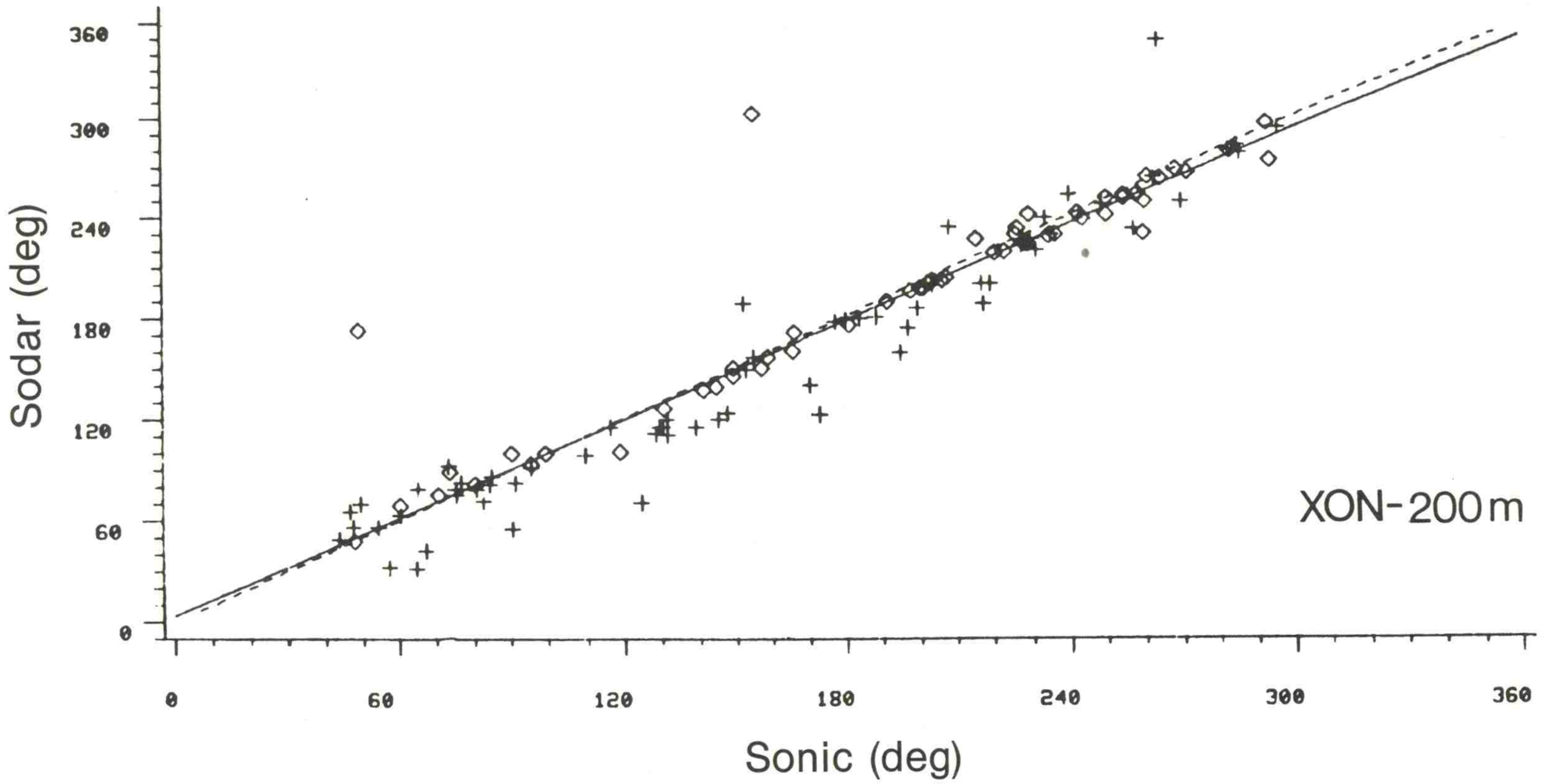

Figure 44. Comparison of 200 m wind directions from XON sodar and BAO sensors.

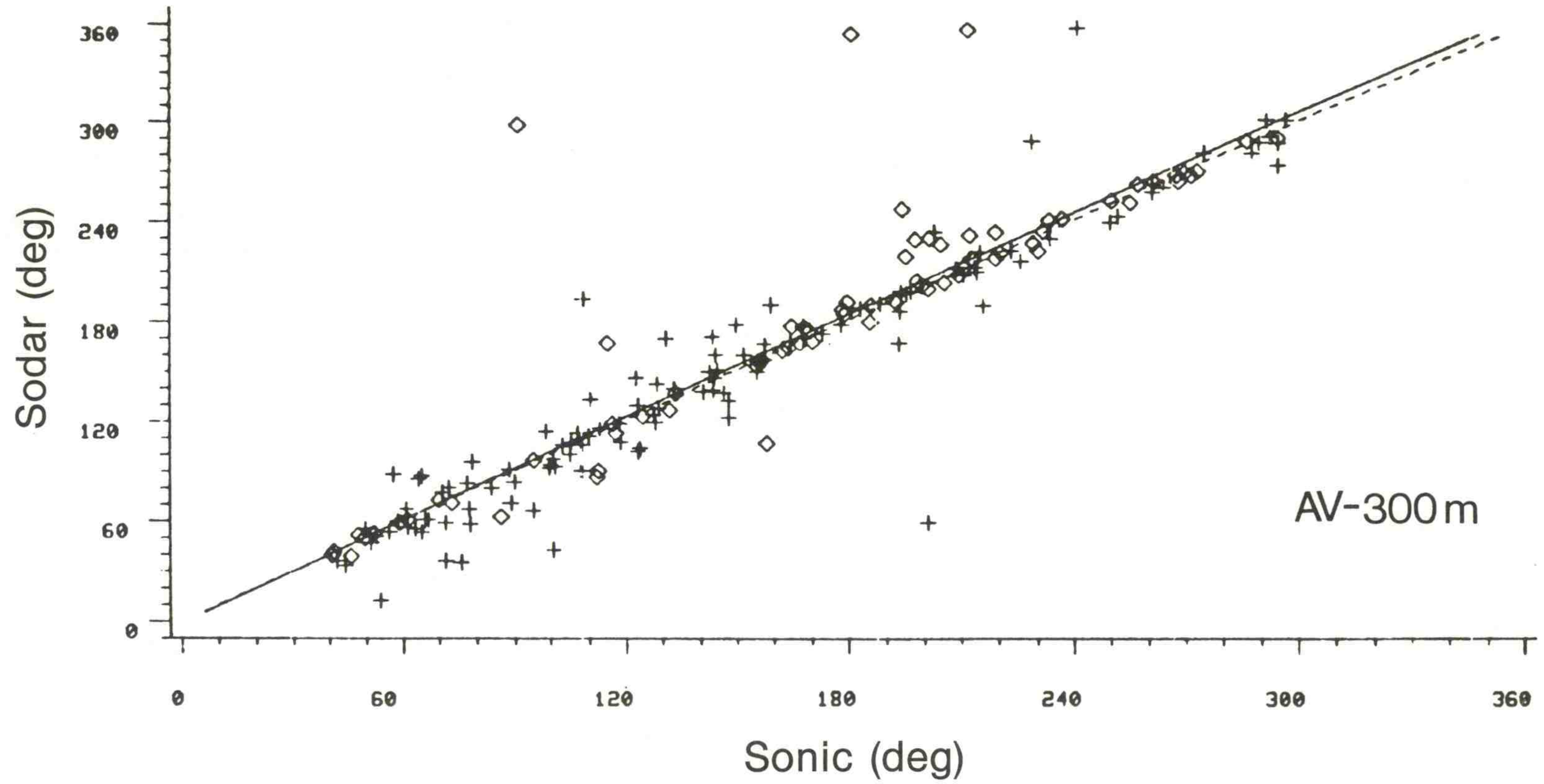

REGRESSION LINE ————————
DAY TIME OBSERVATIONS +
NIGHT TIME OBSERVATIONS ◇
INTERCEPT=0 AND SLOPE=1 (45° ANGLE) LINE -------

Figure 45. Comparison of 300 m wind directions from AV sodar and BAO sensors.

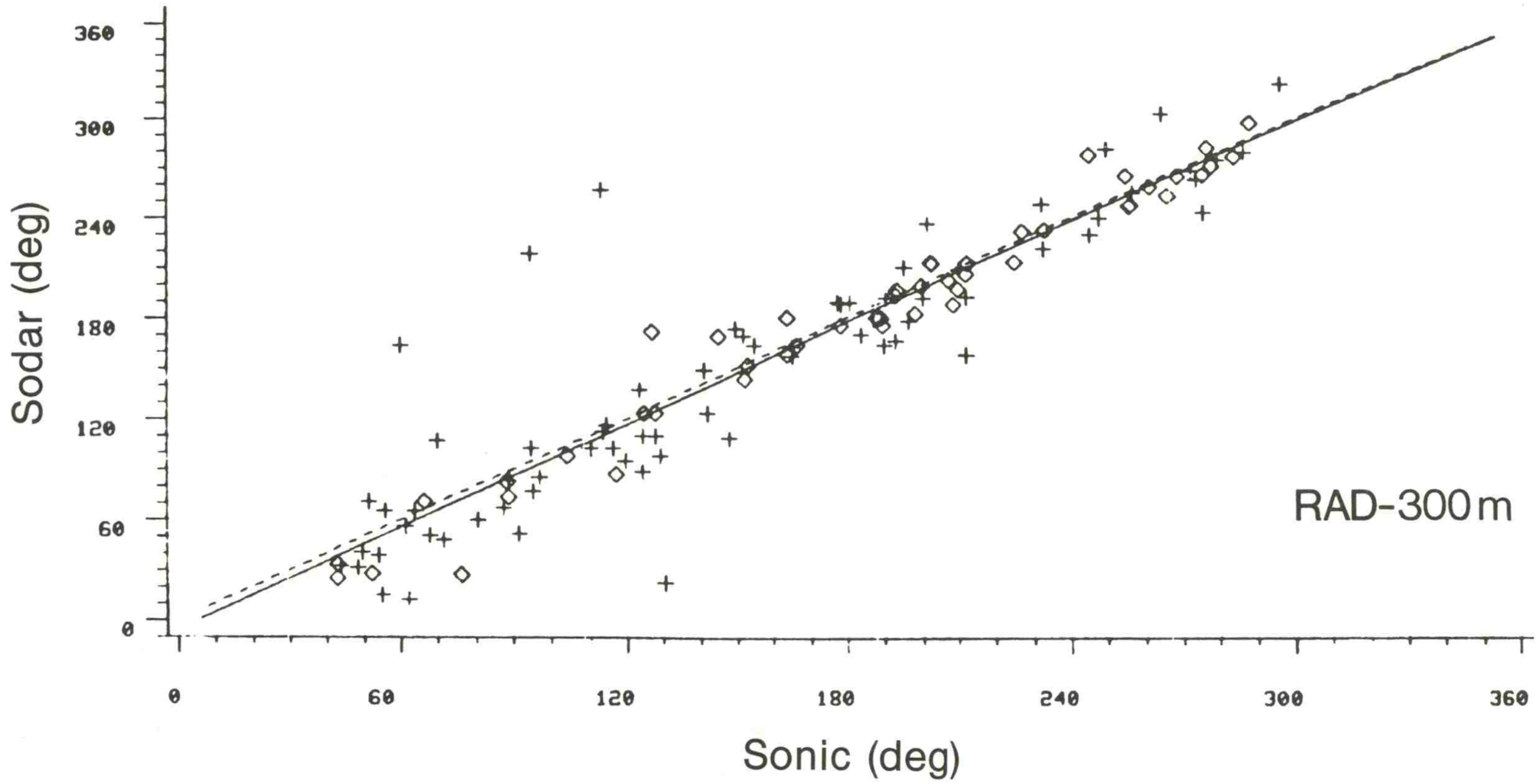

REGRESSION LINE ————————
DAY TIME OBSERVATIONS +
NIGHT TIME OBSERVATIONS ◇
INTERCEPT=0 AND SLOPE=1 (45° ANGLE) LINE -------

Figure 46. Comparison of 300 m wind directions from RAD sodar and BAO sensors.

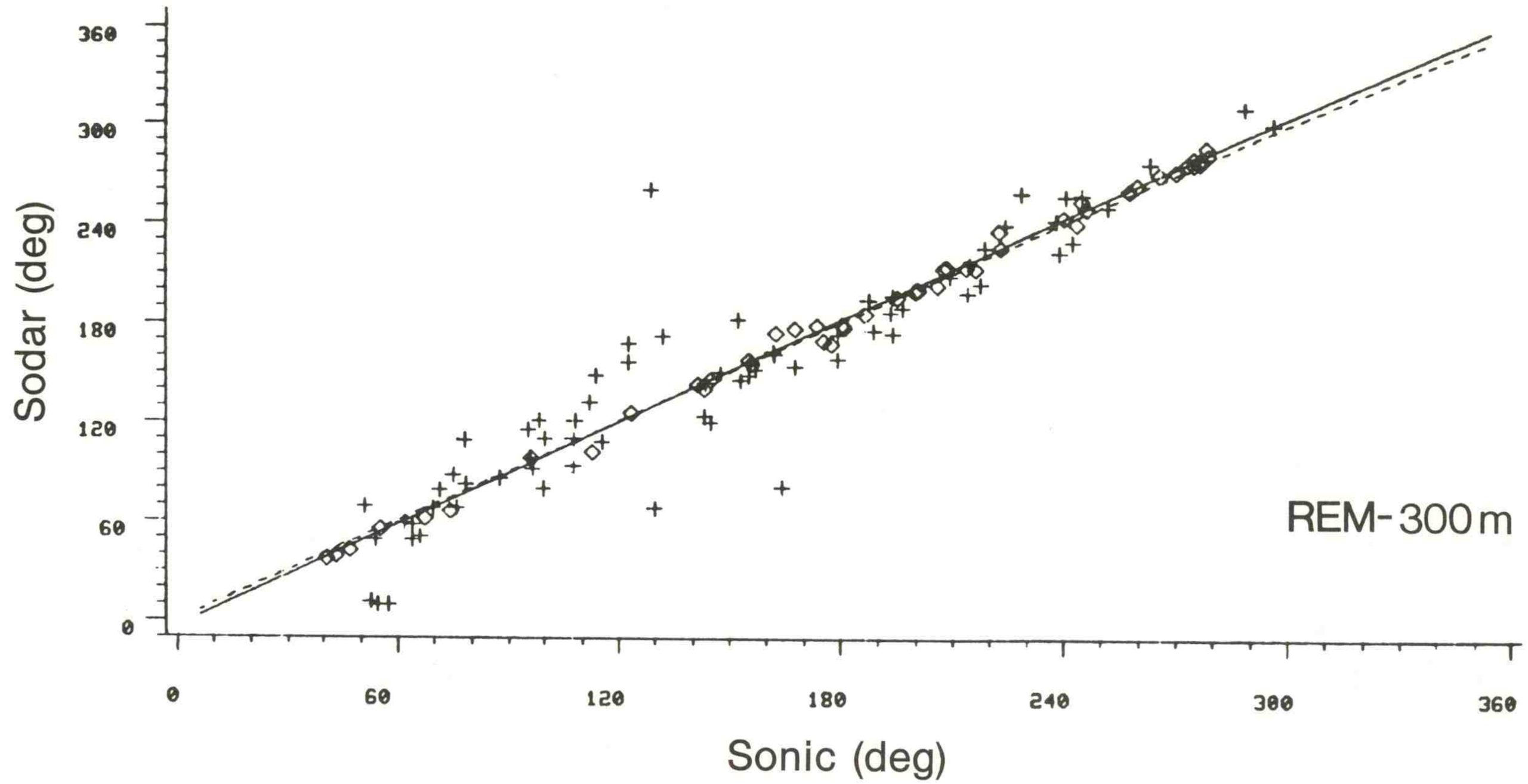

REGRESSION LINE ————————
DAY TIME OBSERVATIONS +
NIGHT TIME OBSERVATIONS ◇
INTERCEPT=0 AND SLOPE=1 (45° ANGLE) LINE -------

Figure 47. Comparison of 300 m wind directions from REM sodar and BAO sensors.

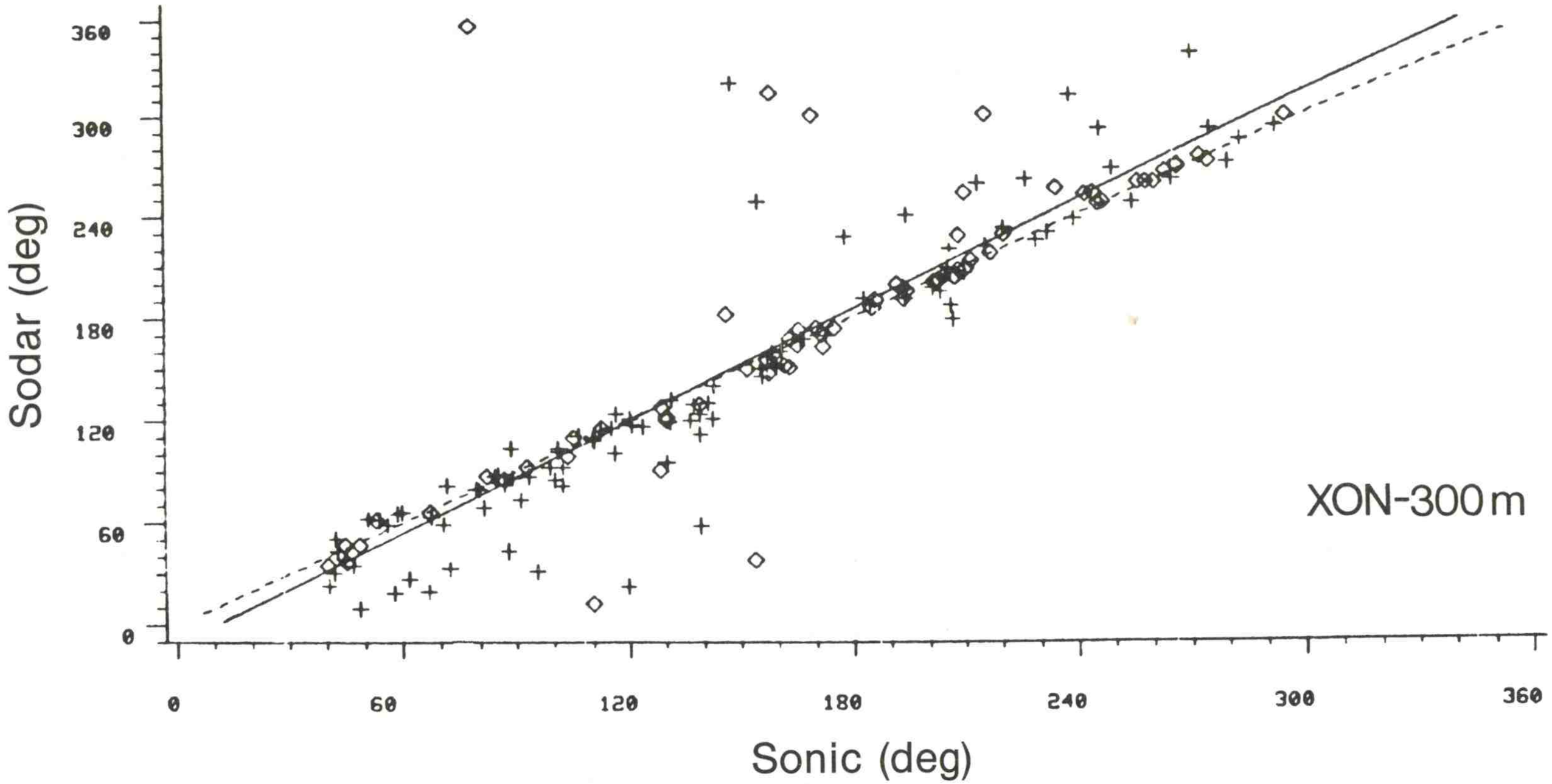

REGRESSION LINE ————————

DAY TIME OBSERVATIONS +

NIGHT TIME OBSERVATIONS ◇

INTERCEPT=0 AND SLOPE=1 (45° ANGLE) LINE -------

Figure 48. Comparison of 300 m wind directions from XON sodar and BAO sensors.

7. SODAR RAWINSONDE COMPARISONS

Although our formal evaluation of the sodars was limited to the three observing levels (100, 200 and 300 m) within the range of the tower instrumentation, the vendors submitted data from higher levels in the atmosphere on some occasions. These data were compared with the rawinsonde data obtained concurrently. Values of sample bias, comparability, and correlation for the measured wind speeds and wind directions for each sodar are given in Table 11. Only measurements at 200 m and above are included in the statistics because of the limitations in the rawinsonde's accuracy below that height. These comparisons serve two objectives: to assess at least in a qualitative sense the ability of sodars to track the broad features in the speed and direction profiles above 300 m; and to determine the magnitude and nature of the uncertainties encountered in comparing measurements from a single rawinsonde traverse with time-averaged (20 min) sodar measurements.

The numbers in Table 11 are of the same order as the numbers in earlier tables comparing sodar and tower measurements. Agreement with the rawinsonde is better for some sodars than for others. The differences are not considered significant, given the fact that this experiment was designed, and the antennas set up, for performance evaluation in the first 300 m.

Some idea of the agreement in the data can be obtained from the scatter diagram in Fig. 49. The wind speed and direction measurements from one of the sodars (AV) is plotted against the rawinsonde measurements. The scatter is

Table 11. Sodar wind speeds and directions for all heights compared with rawinsonde speeds and directions

Variable	Sensor	b	c	ρ	N
Speed (m/s)	AV	0.37	1.17	0.86	61
	RAD	-0.09	0.92	0.61	14
	REM	0.24	0.91	0.94	19
	XON	-1.25	2.34	0.38	31
Direction (deg)	AV	4	44	0.90	61
	RAD	18	40	0.89	14
	REM	- 8	37	0.95	19
	XON	15	39	0.96	31

b = bias
c = comparability
ρ = estimate of correlation coefficient
N = number of observations

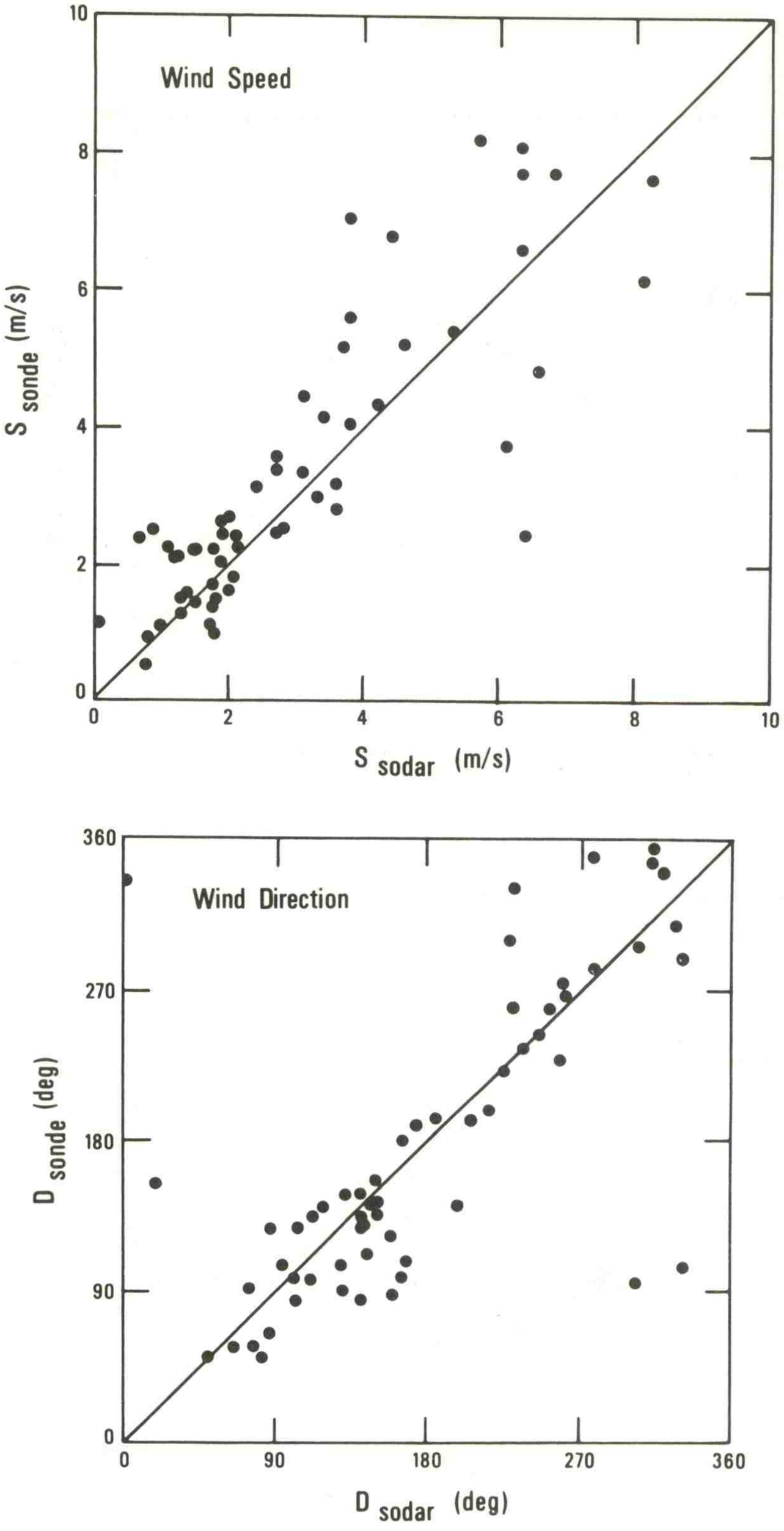

Figure 49. Comparison of wind speeds and wind directions from rawinsonde and sodar measurements.

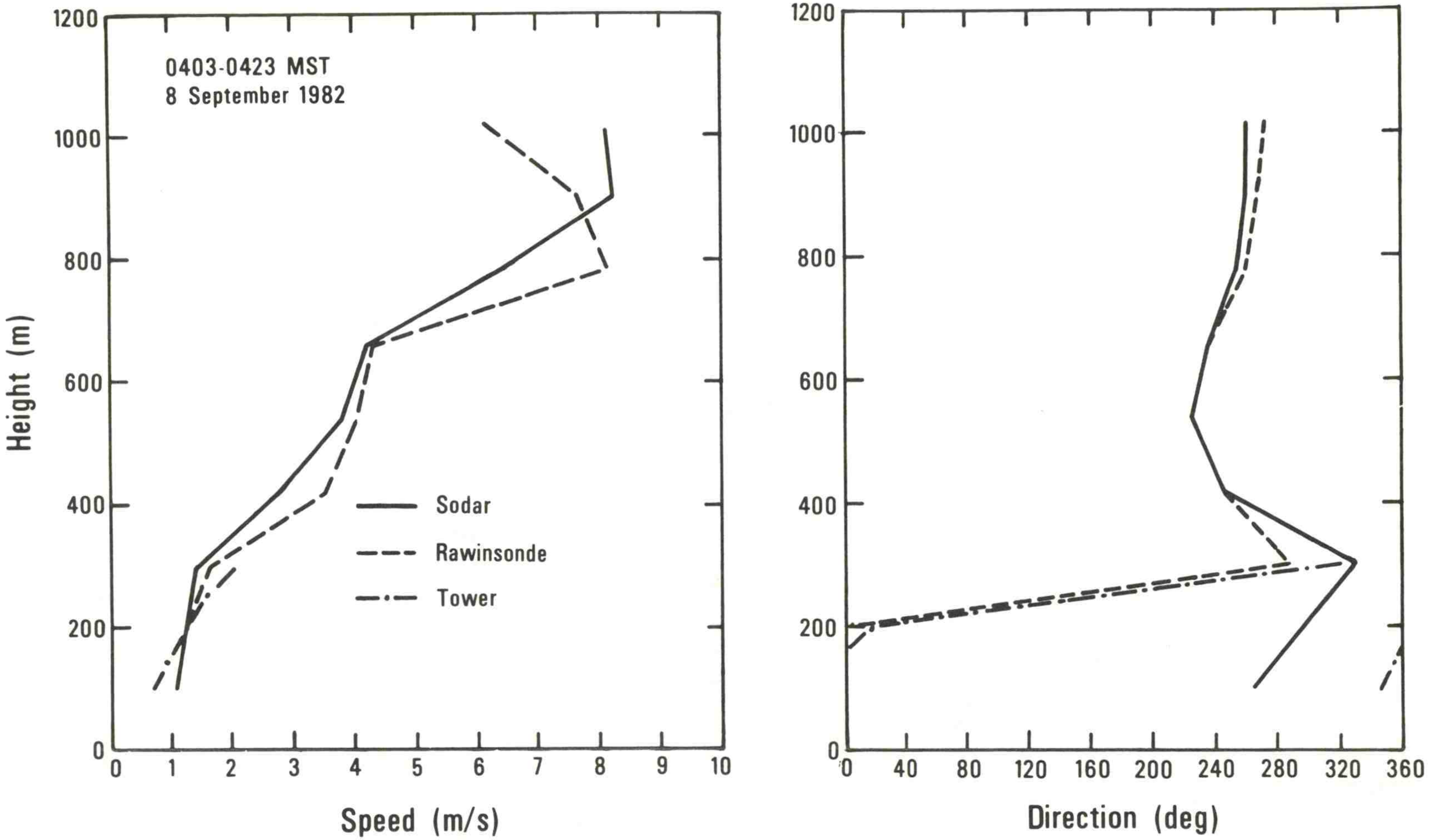

Figure 50. Wind speed and wind direction profiles from sodar (AV), rawinsonde, and tower measurements in a stable boundary layer.

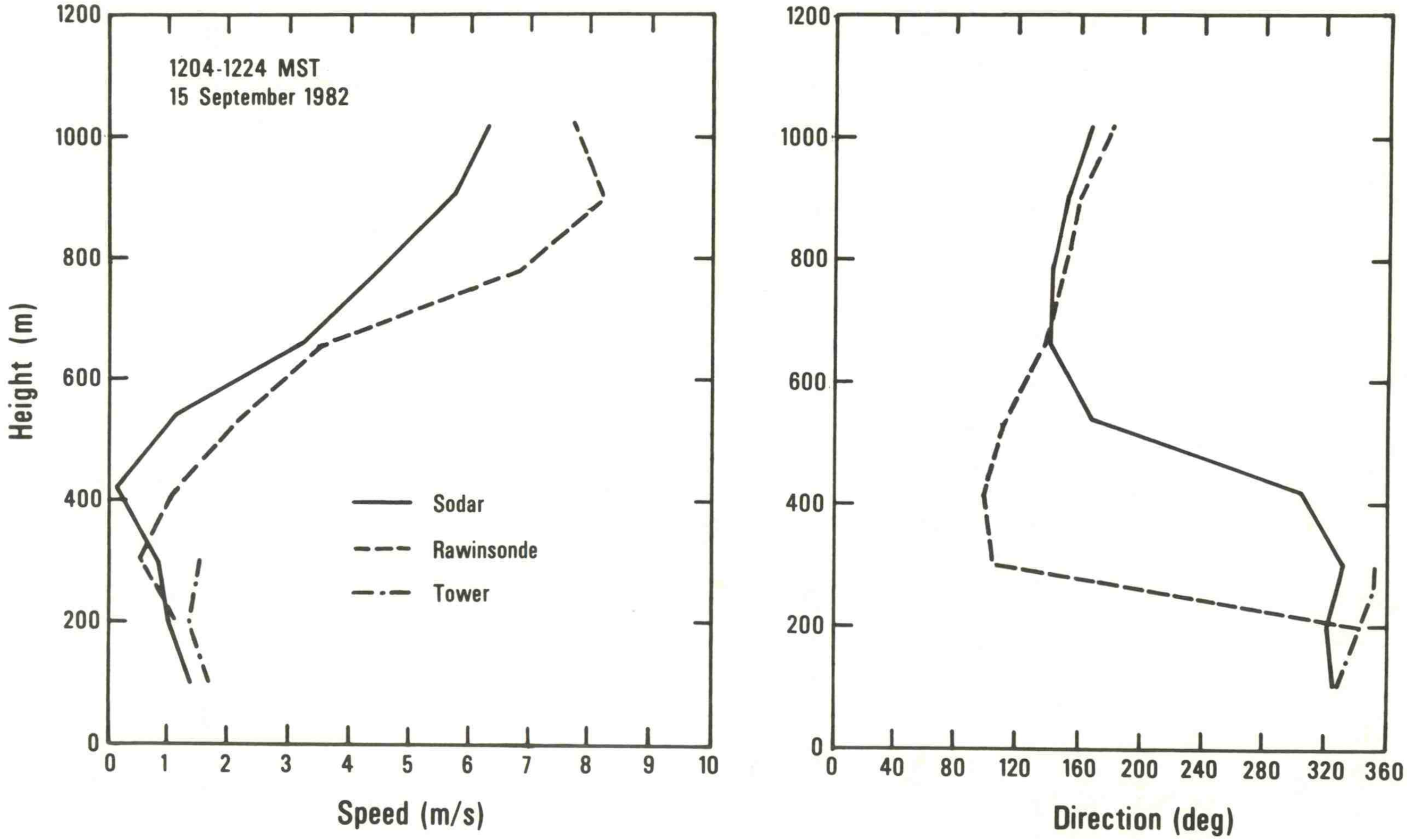

Figure 51. Wind speed and wind direction profiles from sodar (AV), rawinsonde and tower measurements in a convective boundary layer.

not significantly larger than in the plots against the tower measurements. It is apparent, however, that the wind speeds agree better when they are less than 4 m/s, although the percentage error is approximately the same. The increase in scatter above 4 m/s suggests that the larger spatial separation introduced between sensing volumes at the larger wind speeds (with the rawinsonde drifting farther away from the release point) is a factor to be recognized when rawinsondes are used for evaluating sodar performance. Another factor to be recognized (but not obvious in Fig. 49) is the possibility of large wind direction differences in sodar rawinsonde comparison under light wind conditions. Wind directions under such conditions tend to be highly variable both spatially and temporally. These conditions occur frequently at the BAO when the winds are from E to SE. One cannot expect good agreement between the near-instantaneous and the time-average measurements from the two systems during periods of light winds. This point is brought home very clearly in the speed and direction profiles of Figs. 50 and 51. When wind speeds drop below 2 m/s, wind direction differences become large regardless of stability. When the wind speeds are larger, the agreement between the rawinsonde and sodar profiles is good. The two cases presented here are perhaps more spectacular in terms of the wind speed effect on the comparison than most of the other cases examined. Over more complicated terrain, differences in speed and directions between sodars and rawinsondes could be much larger. Caution must be exercised, therefore, in interpreting data that compare sodars with rawinsondes. Nonetheless, this evaluation does indicate that, under proper conditions, reasonable agreement can be expected between the two sets of measurements as though both techniques measured bulk properties of the wind with reasonable accuracy.

8. CHARACTERISTICS OF SODAR w SPECTRA

The spectra of the vertical wind speed derived from sodar Doppler measurements should, in principle, correspond to spectra from the sonic anemometers, subject to the effects of spatial averaging and aliasing. Spatial averaging attenuates fluctuations with scales smaller than the dimensions of the sampling volume. Aliasing folds energy left over at frequencies above n_o, the Nyquist frequency (= 1/2 sampling rate), back into the available spectral bandwidth ($0 < n < n_o$). In the presence of spatial averaging, the energy folded back is reduced by the amount lost through averaging. A schematic representation of the distortions introduced on a typical w spectrum for two different sampling rates is given in Fig. 52(a). In this example, the attenuation from spatial averaging is assumed to commence at frequency n_1 = 0.02 Hz. The wavelength λ, corresponding to this frequency ($\lambda_1 \simeq U/n_1$, where U is the mean horizontal wind component) is roughly 2π times the longest dimension in the sampling volume. (A sampling volume 40 m diam × 40 m long is assumed here with U = 5 m/s.) Because of the sharp spectral attenuation above 0.02 Hz, aliasing is confined primarily to the first fold, which merely raises the energy near n_o by a factor of 2. For typical beamwidths used in most sodar operations, $n_o \approx n_1 \approx 0.02$ Hz at $100 < z < 300$ m for moderate wind speeds.

In the convective boundary layer the percentage of spectral energy contained in frequencies above n_o increases as height, Z, decreases. Consequently the uncertainties in the observed spectral forms and in the measured

variances also increase as the height decreases. Figure 52(b) shows the progression of the spectrum on a typical day. The frequency at the n $S_w(n)$ spectral maximum, n_m, is nearly constant above 0.25 Z_i, (where Z_i is the boundary layer depth) and varies inversely with height below that. Within the height range of most sodar systems, the wavelength at the spectral peak can be approximated by

$$\lambda_m = U/n_m = \begin{cases} 6Z, & (Z \leq 0.25\ Z_i) \\ 1.5Z_i, & (Z \geq 0.25\ Z_i)\ . \end{cases} \qquad (5)$$

Spectral energy in the observed bandwidth also drops with decreasing Z. The attendant decrease in signal-to-noise ratio in the sodar measurements serves to increase further the uncertainty in the spectral and variance (σ_w^2) estimates.

In the stable nocturnal atmosphere, the w spectral scales and intensities are more strongly controlled by stratification than by Z. Over flat terrain, within the stable boundary layer (Kaimal et al., 1972) one can approximate λ_m using

$$\begin{aligned} \lambda_m &\simeq Z(0.55 + Z/L)^{-1}\ , \\ &\approx L, \quad \text{for } L \ll Z\ , \end{aligned} \qquad (6)$$

where L is the Monin-Obukhov length. Within the height range of our comparisons, λ_m would be roughly an order of magnitude smaller than under unstable conditions. There is proportionally less energy within the spectral bandwidth, so one can expect to find larger uncertainties and errors in the nighttime spectra than in the daytime spectra. This may account for the increased scatter in the nighttime σ_w values in Sec. 4. An improvement in

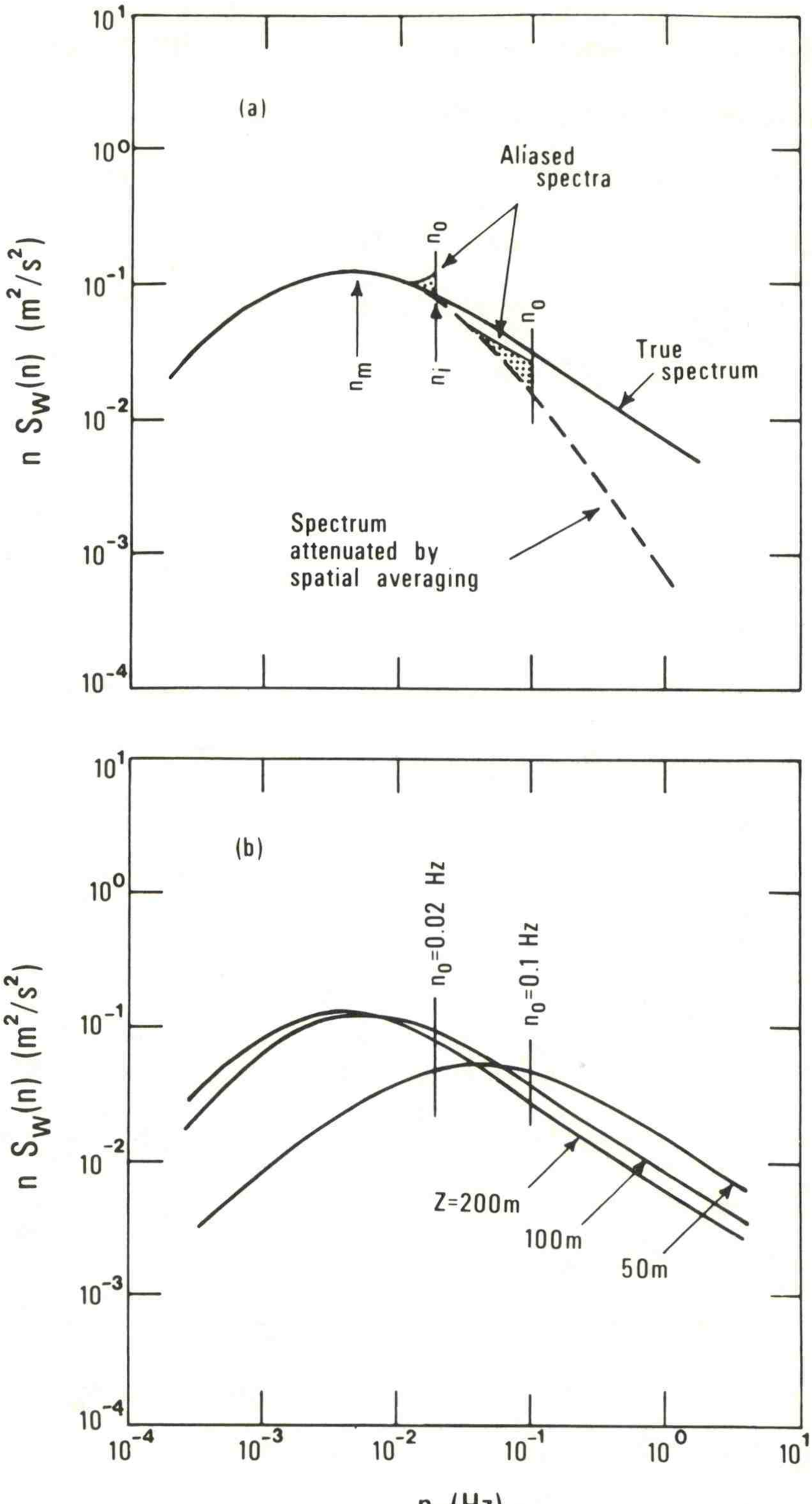

Figure 52. (a) Schematic representation of distortions introduced in the w spectrum from attenuation due to spatial averaging and from aliasing.
(b) Shift in spectral behavior with height and its implications for sampling and aliasing errors.

accuracy is possible in the presence of strong gravity waves because of its large contribution to variance at frequencies below n_o.

The spectra presented in Figs. 53 and 54 were computed from time series provided by AV. No significance is attached to the choice of AV. The outputs are treated as generic signals from a Doppler sodar. The absence of liftup at the high end implies extensive influence of spatial averaging at frequencies below n_o.

The sonic spectra in Fig. 54(a) and (b) illustrate the effect of stability on spectral wavelengths and intensities at the 300 m level. The sodar spectrum shows poor agreement with the sonic spectrum at night; spectral levels are greatly enhanced. The high σ_w levels at night in Sec. 4 can now be traced back to this distortion. To determine how much of this distortion comes from aliasing, the sonic time series was converted to grab samples every 24 s. The resulting spectrum, also shown in Fig. 54(b), has the same shape as the sodar spectrum, but one-half the energy.

More precise estimates of the contributions from aliasing and other factors, such as spatial averaging and noise, can be made from the variances listed in Table 12. Sonic anemometer variances estimated over two bandwidths, 0-5 Hz and 0-0.02 Hz, are listed alongside the sodar variances. Sodar variances appear to be 10% - 15% lower than the full range (5 Hz) sonic variances during the day but 15% - 20% higher than the sonic variances integrated to 0.02 Hz (see Table 12). From Table 13 (last column) we find the sonic anemometer variance in the band $0.02 < n < 5$ Hz to be between 20% and 25% of the total variance ($0 < n < 5$ Hz) under convective conditions. If all that variance were to be aliased back into the frequency range $0 < n < 0.02$ Hz, the ratio $(\sigma_w^2)_{sodar}/(\sigma_w^2)_{son(0<n<5\ Hz)}$ in Table 13 would be unity. In the

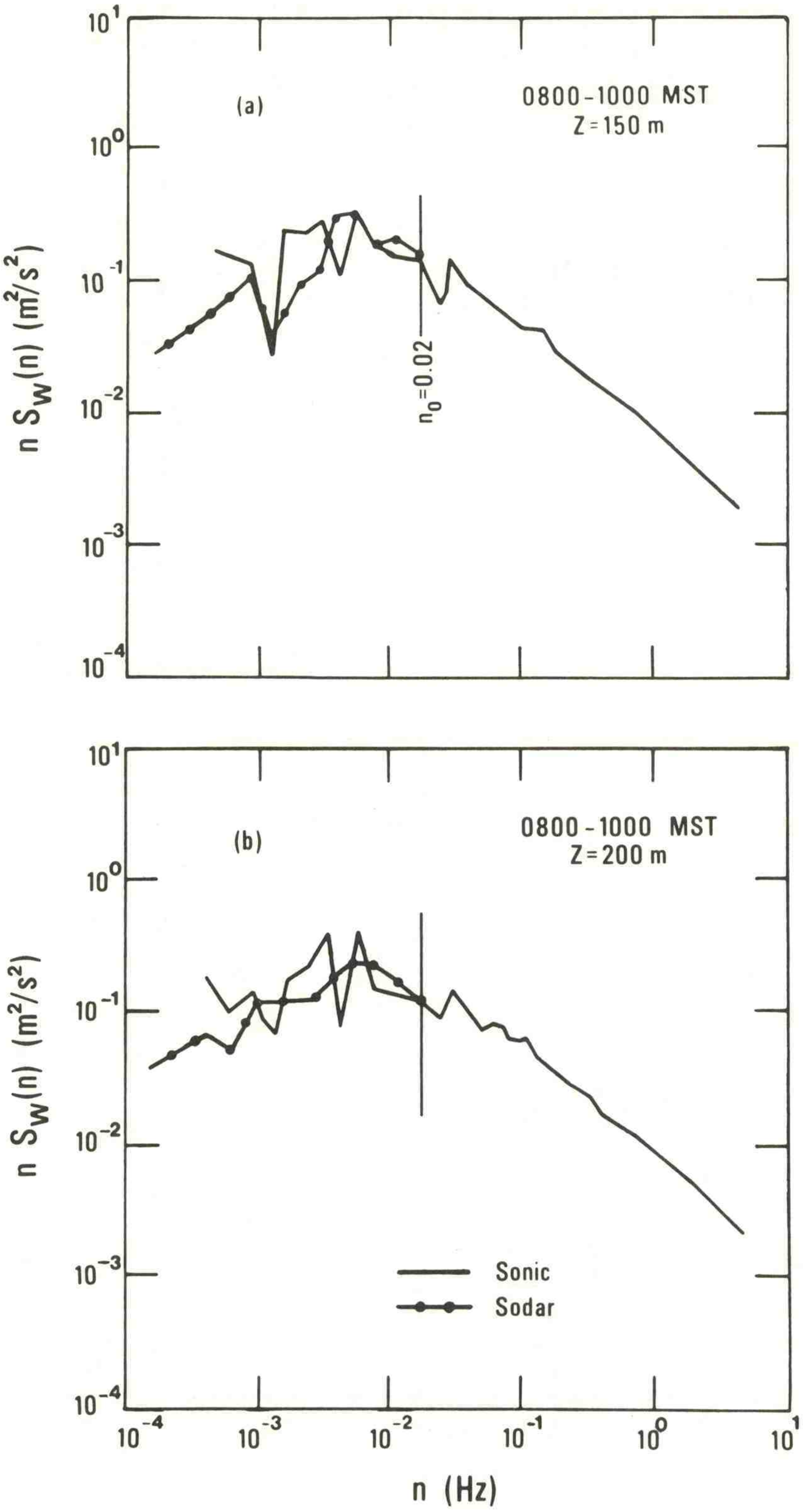

Figure 53. Sodar and sonic anemometer w spectra at (a) 150 m and (b) 200 m compared for morning conditions.

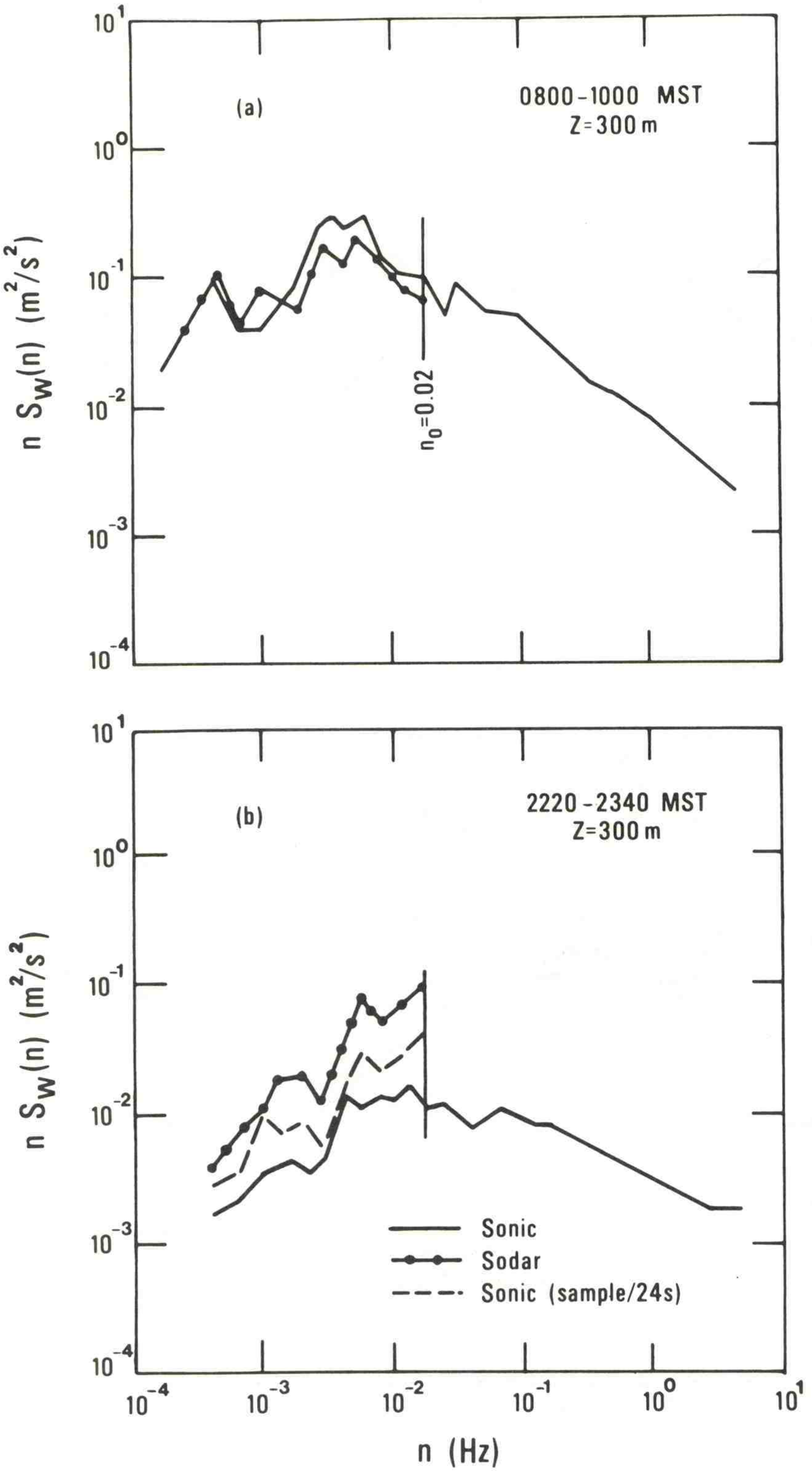

Figure 54. Sodar and sonic anemometer w spectra at 300 m compared for (a) morning and (b) nighttime conditions.

Table 12. Variances of w from the sodar and the sonic anemometers for the cases illustrated in Figs. 53 and 54

Time (MST)	Date	Height (m)	$(\sigma_w^2)_{sod}$ (0<n<0.02 Hz)	$(\sigma_w^2)_{son}$ (0<n<5 Hz)	$(\sigma_w^2)_{son}$ (0<n<0.02 Hz)
0800-1000	9 Sept	150	0.846	0.925	0.711
		200	0.822	0.951	0.716
		300	0.762	0.801	0.644
2220-2340	18 Sept	300	0.123	0.082	0.064

Table 13. Fraction of total variance sensed by the sodar and sonic anemometers over bandwidth 0 < n < 0.02 Hz

Time (MST)	Date	Height (m)	$\frac{(\sigma_w^2)_{sod}}{(\sigma_w^2)_{son(0<n<5\ Hz)}}$	$\frac{(\sigma_w^2)_{son(0<n<0.02\ Hz)}}{(\sigma_w^2)_{son(0<n<5\ Hz)}}$
0800-1000	9 Sept	150	0.91	0.76
		200	0.86	0.75
		300	0.95	0.80
2220-2340	18 Sept	300	1.50	0.78

unstable case, it is roughly 10% smaller at all three heights, which suggests that only half the variance above 0.02 Hz is aliased back. The other half represents the variance lost through spatial filtering. In the stable case at 300 m, that ratio is 50% higher than unity, implying contribution from sources other than the true w fluctuations in that spectral bandwidth.

The time series used for computing the spectra in Fig. 54(b) offer clues as to the cause for enhancement in the sodar spectrum. Shown from top to bottom in Fig. 55 are the fluctuations in w recorded by the sodar (~0.04 samples/s), the sonic anemometer sampling slowed down to the same rate (~0.04 samples/s), and the original sonic anemometer time series block-averaged over 10 s nonoverlapping blocks. These traces are counterparts of the spectra in the $0 < n < 0.02$ Hz range. Not surprisingly, the 0.04/s-sampled sonic traces show larger excursions than the block-averaged traces. In the sodar traces, the excursions are even larger, and the very large oscillation that occurred at about 2230 MST accounts for at least 25% of the excess over the variance in the 0.04/s-sampled sonic data. Whether this oscillation is real or an artifact of data processing cannot be determined now since the only other w measurements available to us are from the BAO tower 600 m away. The tower data show no such large amplitude oscillation. At this time one can only state that the w measurements in stable air have to be edited carefully before any σ_w value is accepted as correct.

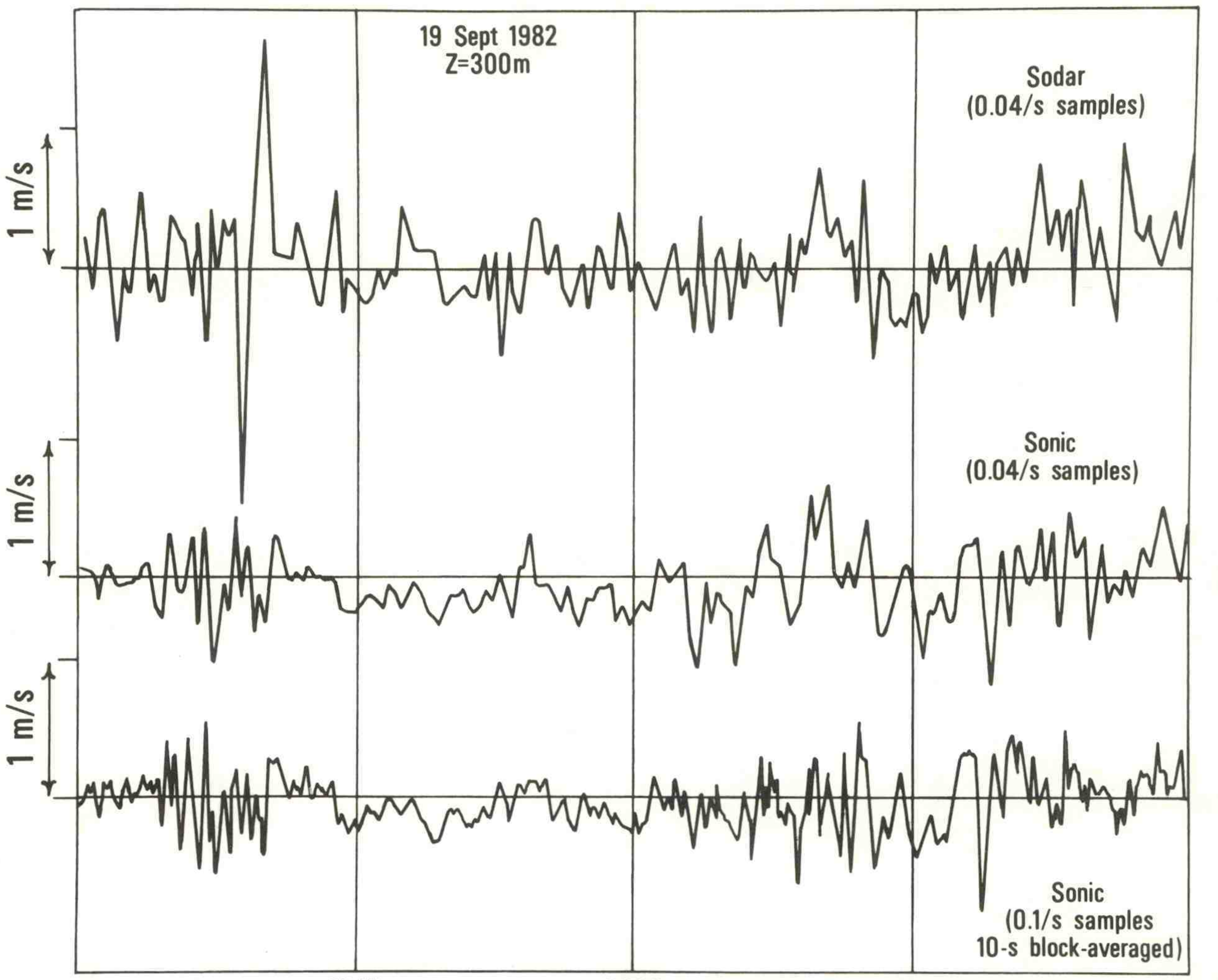

Figure 55. Time series of w corresponding to spectral forms shown in Fig. 54(b) in the frequency range 0<n<0.02 Hz.

9. CONCLUDING REMARKS

The wind measurements analyzed in this report represent the state of the art in wind sensing with commercially available Doppler sodars. Considering the requirements that the sodar operation be unattended except for maintenance and repair, and that the data be subjected to no editing by the vendors, the results obtained are reassuring. The scatter in the wind speed and wind direction data compare very well with scatter in past experiments (Kaimal et al., 1980; Gaynor and Korrell, 1981) when some of the same sodar systems were compared at the BAO, under more controlled conditions. In these data some vendors show more scatter than others, but much of that can be attributed to factors such as rain, high winds, cable damage (as in the case of REM), and transducer failures (as with XON). If data from these suspected periods were eliminated, the different systems would have more similar scatter.

The measurement of σ_w with sodars seems to show promise, at least for daytime conditions. Here too, vendor performance shows variations that can be attributed in some cases to weather and equipment failure, but individual differences in processing the data might also be a factor. The predictable behavior of sodar w spectra in the convective boundary layer leads us to believe that σ_w^2 measurements can be made to within 10% at heights above 100 m. However, the nighttime results are not so encouraging. More work is needed to ascertain the reasons for the large discrepancies in the w measurements at night.

REFERENCES

Balser, M., C. A. McNary, A. E. Nagy, R. Loveland, and D. Dickson (1976): Remote wind sensing by acoustic radar. J. Appl. Meteor., 15, 50-58.

Gaynor, J. E. and J. A. Korrell, 1981: Instrument intercomparisons at the Boulder Atmospheric Observatory during 1981. NOAA Tech. Memo. ERL-WPL-69, Boulder, CO.

Hoehne, W. E., 1971: Standardized functional tests. NOAA Tech. Memo. NWST&EL-12, Sterling, VA. U.S. Department of Commerce.

Hoehne, W. E., 1977: Progress and results of functional testing. NOAA Tech. Memo. NWST&EL-15, Sterling, VA. U.S. Department of Commerce.

Kaimal, J. C., and J. E. Gaynor, 1983: The Boulder Atmospheric Observatory. J. Appl. Meteor., 22, 863-880.

Kaimal, J. C., and D. A. Haugen, 1977: An acoustic Doppler sounder for measuring wind profiles in the lower boundary layer. J. Appl. Meteor., 16, 1298-1305.

Kaimal, J. C., R. A. Eversole, D. H. Lenschow, B. B. Stankov, P. H. Kahn and J. A. Businger, 1982: Spectral characteristics of the convective boundary layer over uneven terrain. J. Atmos. Sci., 39, 1098-1114.

Kaimal, J. C., J. C. Wyngaard, Y. Izumi and O. R. Cotè, 1972: Spectral characteristics of surface-layer turbulence. Quart. J. R. Meteor. Soc., 98, 563-589.

Kaimal, J. C., H. A. Baynton and J. E. Gaynor (Editors), 1980: Low-Level Intercomparison Experiment, Boulder, Colorado, U.S.A., August-September 1979. Instrument and Observing Methods Report No. 3. World Meteorological Organization, Geneva, Switzerland.

APPENDIX

DAILY WEATHER SUMMARIES

Date (September 1982)	Weather Conditions	Precipitation in inches	Peak 20 min , 10 m level wind speed in m/s (direction in deg)	Time of max. wind (MST)
1	Very weak, dry front passed mid-aftermoon. Mostly clear, E to SE winds, 1-3 m/s, turning NW later in the afternoon.	0	7 (310)	1540
2	Surface high moved in from W. Mostly clear day. Light ESE winds in the morning turning NE by late afternoon.	0	5 (10)	1700
3	Drainage winds at night, WSW at lower levels, NNW above. Surface high well established. Very weak winds after sunrise, became SE (2 m/s) by mid-morning, then NE (3 m/s) by mid-afternoon.	0	4.5 (220)	2220
4	Surface high moved eastward. Partly cloudy. SW drainage winds all night with SSW winds above. SSW surface winds (3-4 m/s) established a few hours after sunrise became WNW at about noon and N at 1440 owing to nearby weak thunderstorm. Back to W by 1600 (5-10 m/s), then SSW (5-8 m/s) by 1700.	0	9 (190)	1640

DAILY WEATHER SUMMARIES (Continued)

Date (September 1982)	Weather Conditions	Precipitation in inches	Peak 20 min , 10 m level wind speed in m/s (direction in deg)	Time of max. wind (MST)
5	Wind from SSW at low levels and NW at upper levels. Frontal passage in early morning, winds turning NE. By 0700, winds were E to SE; cloudy with light rain. By mid-morning, winds turned S to SW (4-6 m/s) changing to W. Rain increased by noon and stopped by 1700. Winds became SW and S by 1900.	0.10 (measurable between 1240 and 1400, fairly steady)	6 (260)	1240
6	Light and variable winds all night in lower half of tower. Early morning fog. SE winds at 6 m/s above fog layer. Fog burned off about 0900. Winds weak ESE all day until late afternoon when they increased to 5-8 m/s and turned through N all the way over to SW in 1 hour before 1940. A good SSE jet (10 m/s) developed before midnight at mid-tower height.	0	6 (170)	2320

DAILY WEATHER SUMMARIES (Continued)

Date (September 1982)	Weather Conditions	Precipitation in inches	Peak 20 min , 10 m level wind speed in m/s (direction in deg)	Time of max. wind (MST)
7	Winds SW, 5-8 m/s, in early morning, became NW and weaker at sunrise, then N by 0700, and NE by 0840. Light and variable between NW and NE for much of day. Clear and sunny until late afternoon. At about 1600, winds increased to 11 m/s from W at top of tower in response to a developing mountain lee trough, turning to NE at 1840, owing to thunderstorms in the area. About 2100, wind shifted to NW and became weaker.	0	6 (240)	1700
8	Winds light and variable in early morning; weak SW drainage flow in lower half of tower. Clear until afternoon. Winds light and generally SE at mid-morning. Shifted to NW at 8-11 m/s by 1340; thunderstorms in area. Winds dropped suddenly by 1700, became SSW by 1800 at 5-8 m/s and W by midnight in response to a mountain lee trough.	0	8 (300)	1340

DAILY WEATHER SUMMARIES (Continued)

Date (September 1982)	Weather Conditions	Precipitation in inches	Peak 20 min , 10 m level wind speed in m/s (direction in deg)	Time of max. wind (MST)
9	SW drainage winds; W winds above after midnight, turned W at all levels by mid-morning (4 m/s) and NNW by noon. Mostly clear day. E winds at 5 m/s by 1520 became SE by 1900 and increased while gradually turning WSW by 2100.	0	5.5 (210)	0120
10	Winds became light and variable in early morning; SW drainage at lower levels. Remained light after sunrise then became stronger (4 m/s) out of E just before noon. Mostly sunny day until afternoon. Slow shift to S in afternoon in response to frontal approach from NW. Sudden strong W winds at 1420 (up to 12 m/s) due to dry thunderstorms in area, then strong SW winds (up to 15 m/s) after 1700 as front approached. A jet at mid-tower levels from S 1900-2100. Frontal passage at about 2220, and N to NE winds followed.	0	10 (270)	1420

DAILY WEATHER SUMMARIES (Continued)

Date (September 1982)	Weather Conditions	Precipitation in inches	Peak 20 min , 10 m level wind speed in m/s (direction in deg)	Time of max. wind (MST)
11	Clouds through early morning. NNE winds 3-7 m/s, became more N by dawn. Rain began around 0800. Winds increased to 10 m/s out of N by 1400. Light to moderate rain through most of night. Winds decreased by midnight.	0.80 (May include some from early morning of 12 September, clock malfunction).	7 (20)	1240
12	Winds N at upper levels and NW near ground. Some rain within a few hours after midnight. Partly cloudy by early morning. By dawn, winds were (3-5 m/s) from S and skies remained partly cloudy most of day. Winds became SE by noon and gradually strengthened by late afternoon to 7-9 m/s. S winds by 1800, increased to 11 m/s at upper tower levels, but gradually decreased before midnight.	Unknown (see comment for 11 September).	7 (150)	1520

DAILY WEATHER SUMMARIES (Continued)

Date (September 1982)	Weather Conditions	Precipitation in inches	Peak 20 min , 10 m level wind speed in m/s (direction in deg)	Time of max. wind (MST)
13	Upper level system deepened to the W of Colorado causing S winds. By early morning (0700) winds were easterly (3-4 m/s at upper tower levels) indicating that surface system moved through. Skies became cloudy and winds remained light from E to SE until mid-morning when they began to increase gradually from E and rain began. By 1540, E winds approached 20 m/s near tower top and rain became heavier. Hail fell about 2040, and winds became briefly W and NW. By 2120, NE winds prevailed and a 10 m/s jet near center of tower persisted until just before midnight. Rain stopped before midnight, and skies became partly cloudy.	0.72 (measurable between 1430 and 2300, particularly heavy between 1500 and 1600 (0.1) and 2040 and 2200 (0.6))	12 (100)	1640

DAILY WEATHER SUMMARIES (Continued)

Date (September 1982)	Weather Conditions	Precipitation in inches	Peak 20 min , 10 m level wind speed in m/s (direction in deg)	Time of max. wind (MST)
14	Through early morning, weak NW winds at lower levels and moderate N winds above. By sunrise, winds light NNE at all levels and skies mostly clear. Winds from E by early afternoon at 3 m/s. Clouds increased again by late afternoon. Winds became NE after 1920 and increased to 6 m/s as another weak system with moderate rain moved through in late evening. Winds weakened and became NW just before midnight.	0.41 (clock did not work but all rain occurred between about 2000 and 2400)	6 (50)	2120
15	By 0600, winds 3-5 m/s from W, low clouds, fog, and drizzle. Fog dissipated soon after 0800 but remained partly cloudy through rest of day; winds SW and light. By late morning all levels showed NW winds, which gradually increased to 3-4 m/s by late afternoon. Winds became 1-2 m/s after 2100.	0.01 (in early morning)	5 (320)	0440

DAILY WEATHER SUMMARIES (Continued)

Date (September 1982)	Weather Conditions	Precipitation in inches	Peak 20 min , 10 m level wind speed in m/s (direction in deg)	Time of max. wind (MST)
16	Fog and light winds through early morning. Weak drainage flow from WSW at lower levels. By 0900, winds E on lower half of tower at 3 m/s otherwise light and variable. Sun appeared through fog. Fog dissipated after 0940, and day became mostly clear. At 1200, winds NE, 3-4 m/s, gradually increasing through afternoon. NNW winds by 1740 turning gradually back to NE by 2100. Wind speeds increased to 12 m/s near tower top at 2140 as still another weak front came down from N. Clouds increased before midnight but winds decreased and became more N.	0	5.5 (360)	2240
17	Winds gradually became more NE at 3-7 m/s; light drizzle and fog in early morning. Winds decreased to 3-4 m/s from NE in later morning, becoming E by noon. Fog decreased in mid-morning, but cloudy all day with drizzle. Skies remained cloudy during night.	0.03 (Drizzled through much of day)	5.5 (30)	0700

DAILY WEATHER SUMMARIES (Continued)

Date (September 1982)	Weather Conditions	Precipitation in inches	Peak 20 min , 10 m level wind speed in m/s (direction in deg)	Time of max. wind (MST)
18	Early morning drizzle. Winds weakened and became SW and W by early morning. Skies became partly cloudy by sunrise. Very weak S winds until noon, then increased to 2-3 m/s; gradually turned E through SE by 1400 and gradually back to SE by 1500 and to S by 1720 at 6-8 m/s. Winds SW by 1740 at 10 m/s in a jet near 100 m. By 2000, winds turned N and decreased to 3-5 m/s but increased slightly before midnight.	0.02 (midnight to 0600)	7 (180)	1740
19	N to NE winds (6-8 m/s) most of morning but gradually decreased after 0700 down to 1-3 m/s by 1000. Mostly sunny day. Winds unchanged until about 1940 when they became light and variable, then back to ENE (3-5 m/s) just before midnight.	0	4 (340)	0000

*U.S. GOVERNMENT PRINTING OFFICE: 1984-0-776-001/4113

DAILY WEATHER SUMMARIES (Continued)

Date (September 1982)	Weather Conditions	Precipitation in inches	Peak 20 min , 10 m level wind speed in m/s (direction in deg)	Time of max. wind (MST)
20	After midnight, winds more ESE at 3-6 m/s, becoming light and variable by 0300 and N (3-6 m/s) after 0400. Clear day. Winds gradually became lighter through mid-morning and turned slightly to NE. Winds light and easterly until about 1620 when they became NW and strengthened to 3-5 m/s. Winds very light near ground by late evening, and became more N at upper tower before midnight.	0	4.5 (360)	0520
21	Light and variable winds in early morning with N component above first two tower levels. Clear day. Turned NE after 0800 but still light, becoming E by noon and SE, but light through afternoon.	0	2.5 (250)	0200

OBAOBAO